DOI:10.15774/PPKE.ITK.2022.004

Investigation of drug absorption through physiological barriers

Zsófia Varga-Medveczky

Supervisor:
Franciska Vidáné Dr. Erdő, PhD

Pázmány Péter Catholic University
Roska Tamás Doctoral School of Sciences and Technology

A thesis submitted for the degree of *Doctor of Philosophy*

Budapest, 2022

DOI:10.15774/PPKE.ITK.2022.004

DOI:10.15774/PPKE.ITK.2022.004

Abstract (in English)

My dissertation focuses on the study of effective drug delivery methods across physiological barriers. The new results on the properties of the nasal and dermal barriers are presented in two separate sections.

Nowadays, more and more people in aging societies are being diagnosed with some form of neurodegenerative disease (e.g. Alzheimer's disease, Parkinson's disease, amyotrophic lateral sclerosis etc.), of which the pathomechanism are extensively investigated, however they are not yet curable. The use of effective therapeutic treatments is hindered by the blood-brain barrier, which prevents successful drug delivery directly to the central nervous system. The nose-to-brain drug delivery route offers a promising pathway for targeting the brain directly by circumventing the blood-brain barrier. The brain penetration of a well-known P-glycoprotein model drug, quinidine, was investigated following intranasal treatment by *in vivo* microdialysis in two transgenic mouse strains modeling the properties of vascular disease and Alzheimer's dementia. Furthermore, changes in the levels of cerebral inflammatory markers generated by the processes of pathological and physiological aging were examined by studying various cerebral cytokine levels. Brain morphological changes caused by pathological processes were investigated by magnetic resonance imaging.

There is a growing demand to develop various artificial skin substituents for both medical and cosmetic purposes in which the physiological and pathological processes of skin can be studied, but this is difficult due to the anatomical complexity of the skin. The similarity of drug absorption following the application of caffeine, as a model drug used in a cream formulation was examined in human abdominal skin and in artificial skin equivalent. Finally, the properties of psoriasis were investigated. Psoriasis is a chronic, immune-mediated inflammatory skin disease of unknown origin that affects a high number of patients all over the world. There is no cure for the disease yet, but there are many treatments available to relieve the symptoms. Although many patients use some topical therapy, only a few data are yet available on the skin permeability properties altered by the disease. In an acute mouse model of psoriasis, the changing skin permeability was monitored as a function of time. Different mouse strains were examined through the measurement of caffeine penetration across the dorsal skin samples excised at different time points after the induction of the disease.

DOI:10.15774/PPKE.ITK.2022.004

Abstract (in Hungarian)

A dolgozat középpontjában a fiziológiai barriereken történő hatékony gyógyszerbeviteli módszerek vizsgálata áll. Két, elkülönült részben kerülnek bemutatásra a nazális, illetve a dermális barrier tulajdonságainak vizsgálata során elért új eredmények.

Napjainkban az elöregedő társadalmakban egyre több embert diagnosztizálnak valamilyen neurodegeneratív betegséggel (pl.: Alzheimer-kór, Parkinson-kór, amyotrophiás lateralsclerosis stb.), amelyek patomechanizmusáról bár egyre többet tudunk, jelenleg azonban még nem gyógyíthatók. Jelentős akadályt jelent a hatékony terápiás kezelések alkalmazásában a vér-agy gát, amely megakadályozza a gyógyszerek közvetlen, azonnali központi idegrendszerbe történő sikeres bejuttatását. Az orr-agy gyógyszerbeviteli útvonal lehetőséget kínál a gyógyszermolekulák közvetlen agyi hatóanyag-felszívódására a vér-agy gát megkerülésével. Egy jól ismert P-glikoprotein szubsztrát modellhatóanyag, a kinidin intranazális kezelést követő agyi penetrációját vizsgáltam vascularis és Alzheimer-típusú neurodegeneráció tulajdonságait modellező transzgenikus egértörzsekben *in vivo* mikrodialízissel. Továbbá a különböző agyi citokinszintek tanulmányozásával nyomonkövettem a patológiás és fiziológiás öregedés folyamatainak eredményeképpen létrejövő agyi gyulladási markerek szintjének változását, illetve mágneses rezonancia képalkotással vizsgáltam a patológiás folyamatok okozta agyi morfológiai elváltozásokat.

Egyre nagyobb igény mutatkozik mind gyógyászati, mind kozmetikai célból olyan mesterséges bőrszubsztituensek létrehozására, amelyekben a bőrben lejátszódó fiziológiás és patológiás folyamatokat tanulmányozni lehet, azonban ezt a bőr anatómiai komplexitása jelentősen megnehezíti. Humán hasi bőrben és egy mesterséges bőrekvivalensben vizsgáltam a hatóanyagfelszívódás hasonlóságát egy krém formulációban alkalmazott modellhatóanyag, a koffein felvitelét követően. Végül egy sokakat érintő, ismeretlen eredetű, immunmediált gyulladásos bőrbetegség, a pikkelysömör (psoriasis) tulajdonságait tanulmányoztam. A betegség egyelőre nem gyógyítható, a dermatológiai tünetek enyhítésére azonban már számos kezelési lehetőség elérhető. Bár igen sok beteg esetében alkalmaznak valamilyen topikális terápiát, egyelőre csak kevés adat áll rendelkezésre a betegség hatására megváltozott bőrpermeabilitási tulajdonságokról. A psoriasis egy akut egérmodelljében a betegség indukciójának különböző időpontjaiban kimetszett háti bőrminták koffein-penetrációs vizsgálatával követtem nyomon a betegség kialakulásának következtében megváltozó permeabilitást különböző genetikai hátterű egértörzsekben.

DOI:10.15774/PPKE.ITK.2022.004

Table of contents

DOI:10.15774/PPKE.ITK.2022.004

DOI:10.15774/PPKE.ITK.2022.004

DOI:10.15774/PPKE.ITK.2022.004

List of abbreviations

ABC	ATP-binding cassette
aCSF	Artificial cerebrospinal fluid
AD	Alzheimer's disease
AIDS	Acquired immune deficiency syndrome
AJ	Adherens junction
ALS	Amyotrophic lateral sclerosis
AMP	Antimicrobial peptid
APC	Antigen presenting cell
ApoB-100	Apolipoprotein B-100
APOB-100	Human Apolipoprotein B-100 overexpressing transgenic mice
APP	Amyloid precursor protein
APP-PSEN1	Amyloid precursor protein - presenilin 1 expressing transgenic animals
aPPF	Artificial peripheral fluid
ATP	Adenosine triphosphate
AUC	Area under the curve
Aβ	Amyloid β-peptide
BBB	Blood-brain barrier
BCRP	Breast cancer resistance protein, ABCG2
BEC	Brain endothelial cell
BM	Basement membrane
BSA	Body surface area
CBF	Cerebral blood flow
CNS	Central nervous system
COX-2	Cyclooxygenase-2
CSF	Cerebrospinal fluid
DC	Dendritic cell
DMEM	Dulbecco's Modified Eagle Medium
DNA	Deoxyribonucleic acid
EC	Endothelial cell
ECM	Extracellular matrix
EDTA	Ethylenediaminetetraacetic acid
EGF	Epidermal growth factor
ELISA	Enzyme linked immunosorbent assay
ETL	Echo train length
FBS	Fetal bovine serum
FGF-β	Fibroblast growth factor β
FOV	Field of view
FSEMS	Fast Spin-Echo Multi-Slice
G-CSF	Granulocyte colony-stimulating factor
GI	Gastrointestinal
GLUT-1	Glucose transporter 1
GM-CSF	Granulocyte-macrophage colony-stimulating factor
HPLC	High-performance liquid chromatography
HSPG2	Heparan sulfate proteoglycan 2, perlecan
IFN	Interferon
IFN-α	Interferon-α

IFN-β	Interferon-β
IFN-γ	Interferon-γ
IGF-1	Insulin-like growth factor-1
IL-1α	Interleukin-1α
IL-2	Interleukin-2
IL-4	Interleukin-4
IL-6	Interleukin-6
IL-10	Interleukin-10
IL-12	Interleukin-12
IL-17A	Interleukin-17A
IL-22	Interleukin-22
IMQ	Imiquimod
IN	Intranasal
IP	Intraperitoneal
IV	Intravenous
JAM	Junctional adhesion molecule
KO	Knockout
LIR	Luminescence intensity ratio
LL-37	Cathelicidin
LRP	Lipoprotein receptor-related protein
MCC	Mucociliary clearance
MCP-1	Monocyte chemoattractant protein 1
MD	Microdialysis
mDC	Myeloid dendritic cell
MIP-1α	Macrophage inflammatory protein-1α
MMP	Matrix metalloproteinase
MRI	Magnetic resonance imaging
MRM	Multiple reaction monitoring
MRP	Multidrug resistance protein
MS	Multiple sclerosis
MSC	Mesenchymal stromal cell
MyD88	Myeloid differentiation primary response 88
NALP3	NLR family pyrin domain containing 3
NF-κB	Nuclear factor-κB
NO	Nitric oxide
NVU	Neurovascular unit
OAT	Organic anion transporter
OATP	Organic anion transporting polypeptide
OCT	Organic cation transporting polypeptide
P-gp	P-glycoprotein, MDR1
PBS	Phosphate-buffered saline
PCL	Polycaprolactone
PD	Parkinson's disease
pDC	Plazmacitoid dendritic cell
PDGF-B	Platelet-derived growth factor subunit B
PDGF-BB	Platelet-derived growth factor-BB

DOI:10.15774/PPKE.ITK.2022.004

PDMS	Polydimethylsiloxane
PECAM-1	Platelet endothelial cell adhesion molecule-1, CD31
PET	Positron emission tomography
PLA	Polylactic acid
PsA	Psoriatic arthritis
PSEN1	Presenilin 1
QND	Quinidine
RAGE	Receptor for advanced glycation end products
Rantes	Regulated on activation normal T cell expressed and secreted, CCL5
RNA	Ribonucleic acid
ROI	Region of interest
ROS	Reactive oxygen species
RP	Reversed-phase
RTX	Resiniferatoxin
SCF	Stem cell factor
SEM	Standard error of mean
SOD1	Superoxide dismutase-1
SPECT	Single-photon emission computerized tomography
TE	Echo time
TGFβ	Transforming growth factor β
Th1	T helper 1 cell
Th17	T helper 17 cell
Th22	T helper 22 cell
TJ	Tight junction
TLR	Toll-like receptor
TNF-α	Tumor necrosis factor-α
TR	Repetition time
TRP	Transient receptor potential
TRPA	Transient receptor potential ankyrin
TRPA1	Transient receptor potential ankyrin 1
TRPC	Transient receptor potential canonical
TRPM	Transient receptor potential melastatin
TRPML	Transient receptor potential mucolipin
TRPP	Transient receptor potential polycystin
TRPV	Transient potential receptor vanilloid
TRPV1	Transient receptor potential vanilloid 1
UV	Ultraviolet radiation
V1	Ophthalmic nerve, nervous ophthalmicus
V2	Maxillary nerve
VEGF	Vascular endothelial growth factor
VNO	Vomeronasal organ

DOI:10.15774/PPKE.ITK.2022.004

VSMC	Vascular smooth muscle cell
WMH	White matter hyperintensity
WT	Wild type
ZO	Zonula occludens protein
2D	Two-dimensional
3D	Three-dimensional
3Rs rule	Reduction, Replacement and Refinement

DOI:10.15774/PPKE.ITK.2022.004

Introduction - Motivation and a brief overview

The main scope of my experimental work is the investigation of the properties of two different physiological barriers, the nasal and the dermal barrier. As the biological background and research methodologies of the two research areas are well separable, I also discuss the results in two separate parts.

In the first part of the dissertation, the results related to the investigation of the nasal barrier are presented. Previously, our research group has successfully investigated various P-glycoprotein (P-gp) model drugs crossing the blood-brain barrier in a rat model by *in vivo* microdialysis (MD). Both young and middle-aged animals were studied, so that by comparing the results, they were able to successfully investigate the changes on the drug absorption and elimination caused by physiological aging [1]. Bors et al. developed an intranasal administration method in which the brain uptake of a P-gp substrate, quinidine (QND) could be examined in rats in the presence or absence of a P-gp inhibitor or a sympathomimetic drug [2]. Based on these previous results, we posed the question of how pathological aging (e.g. Alzheimer's disease (AD), atherosclerosis etc.) affects the absorption of different model drugs through the blood-brain barrier (BBB). The previously used intranasal administration procedure was further developed for mice, thus the alterations in the nasal barrier function caused by pathological aging using two age-related neurodegenerative disease models, in APOB-100 and in APP-PSEN1 mice could be examined. By comparing the levels of different cerebral cytokines in the two transgenic models compared with age-matched wild type (WT) mice, we could further characterize the differences between physiological and pathological aging. We also investigated the cerebro-morphological status of the animals by magnetic resonance imaging (MRI).

In the second part of the dissertation, the results of two research topics related to the dermal barrier are presented. Nowadays, there is a growing demand to develop various human skin substituents that could mimic appropriately the physiological and pathological processes that take place in the skin. However, the complex anatomical structure and the wide variety of macrostructures present in the skin make this a difficult task. The first research topic was the investigation of the permeability of human abdominal skin and a human skin substituent with a topically applied caffeine cream in a skin-on-a-chip device.

The second research topic is connected to the altered properties of the dermal barrier due to psoriasis, which is a chronic, inflammatory skin disease of unknown origin. In the development of this disease, in addition to genetic factors, environmental triggers also play an

DOI:10.15774/PPKE.ITK.2022.004

important role. Psoriasis severely disintegrated the dermal barrier, resulting in a significant increase in skin permeability. Various therapeutic approaches are available for the treatment and relief of symptoms, which can be used either as monotherapy or in combination [3], but in most cases some topical treatments are also applied [4]. The involvement of Transient receptor potential ankyrin 1 (TRPA1) and Transient receptor potential vanilloid 1 (TRPV1) ion channels in psoriasis has been confirmed recently [5–7], therefore the examination of the effect of the genetic deletion of these cation channels on the permeability was aimed in a mouse model of Aldara-induced psoriasis-like inflammation using topically applied caffeine cream in a skin-on-a-chip device.

The structure of both parts of the dissertation is the same, the theoretical introduction is followed by the presentation of the experimental work, which is divided into three main parts (Materials and methods, Results and Discussion). At the final part of the dissertation, new scientific results are presented as thesis points in a joint summary.

DOI:10.15774/PPKE.ITK.2022.004

Part 1 – Investigation of the nasal barrier barrier function, the cerebro-morphological status and the cerebral levels of different inflammatory cytokines in APOB-100 and APP-PSEN1 mice

1.1. Theoretical background – Blood-brain barrier

In this chapter, in addition to presenting the structure and maintenance of the blood-brain barrier, I summarize briefly the possible pathways of drug molecules and other substances crossing this highly specialized multicellular vascular structure and the consequences of malfunction of this complex system. At the end of this chapter, the main features of the most common neurodegenerative diseases associated with blood-brain barrier dysfunction are also discussed briefly.

1.1.1. Structure and the function of the blood-brain barrier – the role of cellular and non-cellular elements in blood-brain barrier regulation

The blood-brain barrier is a multicellular vascular system that structure based on the close interaction of cellular (such as brain endothelial cells (BECs), pericytes, astrocytes, vascular smooth muscle cells (VSMCs), neurons and immune cells) and non-cellular elements (e.g. basal lamina). Due to its unique cellular structure, it performs several functions simultaneously [8]. In addition to separating the cerebral and systemic circulation, it maintains the cerebral homeostasis for proper brain and synaptic function, which requires the maintenance of a stable, well-controlled microenvironment, because the neuronal tissue is very sensitive to hypoxia and lack of other essential nutrients [9].

BBB acts as bidirectional mediator, which strictly controls the efflux and influx processes passing through it. The passage of different molecules allows the central nervous system (CNS) to be properly supplied with nutrients, energy metabolites, essential molecules and oxygen as well as to remove from the brain the metabolic waste products and the different substances that are no longer needed. Moreover, the blood-brain interface also has a protective function by preventing blood-borne xenobiotics and other molecules (e.g. environmental toxins, drugs, pathogens, different plasma components, blood cells etc.) that are harmful and potentially neurotoxic to the central nervous system from entering [8–11]. On the other hand, this neuroprotective property of this selective physiological barrier also carries a number of difficulties, as it significantly impedes the delivery of drugs targeting the central nervous system [2,12,13].

DOI:10.15774/PPKE.ITK.2022.004

Vascular network of the central nervous system shows a special barrier function, which is based on that the cerebral blood microvessels are structurally and functionally different from those on the periphery [14,15]. The expression of its specialized properties already appears at the level of endothelial cells (ECs), which differ from non-CNS endothelial cells in that they are highly polarized [9,15]. The core anatomical basis of BBB is based on this cell type [8,15], because they form the wall of the vascular network, which is held together by tight junctions (TJs) with two types of tight junctional connections. Intraendothelial junctions, where the cerebrovascular endothelial cells are joined into themselves and interendothelial junctions, when these TJs are formed between adjacent endothelial cells [15]. They play an important role in the regulation of transport processes on the BBB, prevent the paracellular permeability of different molecules [8,12,15,16], and also perform a kind of fence function by separating and restricting the flow the apical and basal cell membrane domains [12,17]. TJs are composed of various transmembrane proteins, of which claudin (claudin 1, claudin 3, claudin 5 and claudin 12 as most significant members), occludin, and junctional adhesion molecules (junctional adhesion molecules (JAMs): JAM-A, JAM-B and JAM-C) have been extensively studied [10,12,17]. In addition, several cytoplasmic TJ proteins have been identified, including individual zonula occludens (ZO: ZO-1, ZO-2 and ZO-3) and jacop proteins [12,16]. In addition to TJs, adherens junctions (AJs) are also involved in maintaining connections between cerebrovascular endothelial cells. These connections are also made up of different proteins, mostly vascular endothelial-cadherin (cadherin-5) and Platelet endothelial cell adhesion molecule-1 (PECAM-1), which bind to the cytoskeleton via catenin molecules [10,12,16,17].

The luminal surface of the vascular endothelium is covered by a special carbohydrate-based layer, glycocalyx. This layer provides a kind of line of defense for endothelial cells because it regulates the interaction between the brain endothelial cells and different molecules and other cells [15]. Abluminal surface of vascular cells in the central nervous system and in the periphery are also anchored by integrin to the basement membrane (BM), which is made up of different extracellular matrix (ECM) components (e.g. collagen IV, laminin, heparan sulfate proteoglycans (agrin and perlecan (HSPG2)), nidogen) [10,15,18]. The basement membrane consists of two separate layers [15,18]. The inner membrane, called the endothelial basement membrane, is made up of endothelial cells and pericytes. The second, outer layer is called the parenchymal basement membrane, which is secreted by astrocytes and to which the astrocyte end-feets are attached due to various molecular interactions [15,18,19].

The two main cell types that surround cerebral microvessels and help develop and maintain blood-brain barrier functions are pericytes and astrocytes [8,10]. Pericytes cover the

DOI:10.15774/PPKE.ITK.2022.004

abluminal surface of the cerebral vasculature and bind to the basement membrane, which is shared with endothelial cells. Although the discovery of pericytes dates back a long time, the description of their properties and function in the neurovascular unit (NVU) has only recently begun, as it is significantly complicated by the fact that no pericyte-specific markers have been known so far [8,20]. Numerous studies suggest the use of platelet-derived growth factor B (PDGF-B) as an indicator for this cell type, as a pathological process of angiogenesis has been found in PDGF-B-deficient mice, associated with a lack of pericytes in the CNS, cerebral hemorrhage and embryonic lethality [8,11,21]. Despite this signaling pathway, there are other important signal transduction cascades, which take part in the crosstalk between the ECs and pericytes (eg. Transforming growth factor-β (TGF-β) and the associated receptors). This cell type play multiple role, because it is involved in the regulation of many different neurovascular functions, such as in the angiogenesis, in the development and maintenance of the blood-brain properties and integrity, and in the regulation of the cerebral blood flow (CBF) by contraction and relaxation of the vessels [8,10,11,20,22]. Astrocytes are thought to appear only postnatally and play a very important role in establishing and maintaining the specific properties of the blood-brain barrier [23]. These cells are located in the parenchymal facing of the cerebral blood vessels, which are encircled by astrocyte end-feets, through which many complex cellular processes take place. Astrocytes are involved in the regulation of the water and ion homeostasis of the brain and therefore it is hypothesized that its dysfunction or any change in their properties may play a role in the development or progression of pathological processes [8,12,15,24].

1.1.2. Transport systems of the blood-brain barrier

Blood-brain barrier has a highly specialized multicellular structure, which strictly regulates transport of molecules, ions, peptides and proteins (exceptions are O_2, CO_2 and the small lipophilic molecules, which can freely cross the BBB) [12]. Due to the special properties of the endothelium and the presence of the tight junctions, the paracellular pathway is inhibited for hydrophilic molecules and thus they pass through the BBB via the transcellular pathway, of which has several possible ways [11,22].

One transcellular pathway is carrier-mediated transport, which plays a role in the transport of monocarboxylic acids, different neutral amino acids, nucleosides and certain vitamins etc. in addition to the most important, essential nutrients, like glucose. These processes are primarily controlled and regulated by the needs of CNS for maintaining the proper homeostasis, but the serum concentration of each molecule is also a determining factor.

DOI:10.15774/PPKE.ITK.2022.004

Molecules can be transported at the BBB via several efflux transporters (such as the ATP-binding cassette (ABC) transporters), which are located mainly on the luminal side of the continuous monolayer of endothelial cells. One of the best known ABC transporters is the P-glycoprotein efflux transporter, which is a multidrug resistance transporter, and it plays an important role in the removal of putative neurotoxic molecules. This efflux transporter can appear in both the luminal and abluminal membranes, and Bendayan and his coworker showed that it is expressed even in astrocytes and pericytes. Its expression causes serious difficulties in the delivery of various drug molecules to the CNS [25]. In addition to P-gp, a number of other transporter proteins (multidrug resistance proteins (MRPs), such as organic cation transporters (OCTs), organic anion transporters (OATs), organic anion transporting polypeptides (OATPs), breast cancer receptor proteins (BCRPs) etc.) are present in the cerebrovascular network, which work together to significantly reduce the rate of absorption of xenobiotics and on the other hand to mediate the uptake of essential nutrients for the brain [22].

In addition, it is important to note that there are other pathways via which molecules can pass through the BBB. Ion transporters are responsible for maintaining the ion balance and pH of the brain, individual peptides and proteins can cross this barrier thanks to different transport systems. Besides these, caveolae-mediated transport may be another efficient pathway for non-lipophilic molecules [22].

1.1.3. Methods for investigation of the consequences of altered barrier function of the BBB

The unique properties of the blood-brain barrier ensured the required environment for proper neuronal function. Impairment of the BBB can be caused by a number of factors (eg. oxidative stress, reactive oxygen species (ROS), activation of matrix metalloproteinases (MMPs), leukocyte trafficking etc.), which usually affect the proper function of both cellular and non-cellular elements of this selective barrier, as a result of which the structure and the functionality of the blood-brain barrier is significantly impaired and its permeability is increased. Finally these processes lead to impaired neurovascular and neuronal function, neuroinflammation and neurodegeneration [8,10,16,22,26].

The altered structural and functional properties of the blood-brain barrier can be investigated by a number of different experimental methods (e.g. positron emission tomography (PET), single-photon emission computerized tomography (SPECT), immunohistochemistry etc.). In the following subsections, only the most closely related methods for my experimental work are presented briefly.

DOI:10.15774/PPKE.ITK.2022.004

1.1.3.1. *In vivo* microdialysis

Microdialysis allows the study of unbound drug molecules as well as various metabolites *in vivo*. One field of application of MD is the study of transport processes into the central nervous system, through the blood-brain barrier. Adequate surgical knowledge and skills are required to apply this method, as one or more probes could be implanted in parallel in the target organ(s) or fluid. Many different types and geometries of probes are now available. Some of them have in common a needle-shaped, concentric structure with semipermeable membrane at the tip through which diffusion can occur, and thus the molecular environment of the target tissue can be monitored even for a long time in awake or anesthetized animals [27,28].

The great advantage of this technique is that many experimental data can be extracted from a single experiment, thanks to which animal consumption can be significantly reduced („3Rs rule"- Reduction, Replacement and Refinement [29]). Due to the continuous perfusion, the data points show the concentration-time curve of the unbound molecule in the tissue and/or blood. A further advantage of the method is that only molecules of a certain size can pass through the membrane of the probes (it is characterized by the cut-off value of the membrane), so that the dialysate samples are protein-free and therefore no special analytical sample preparation is needed.

The applicability of this invasive method is hampered by the relatively small volume and low concentration of samples, which require highly sensitive analytical methods. However, the physicochemical properties of the investigated molecules must be taken into account, as lipophilic molecules may bind specifically to certain elements of the microdialysis setup, making it difficult or even impossible to measure them [27,28,30].

1.1.3.2. Enzyme linked immunosorbent assay (ELISA)

There is a growing interest in understanding the possible link between inflammatory processes and neurodegenerative diseases, aging and age-related changes in the human body. Cytokine-ELISA plate array is a validated method with high sensitivity and specificity for the detection and measurement of several inflammatory cytokines at the same time in different biological samples (e.g. supernatants obtained from homogenization of different tissues (brain, skin or body fluids etc.)). The ELISA was first introduced in the 1970s [31–33], and since then several ELISA systems have been developed. In general, the consecutive, "double sandwich" ELISA technique is widely used, where the bottom of the well is sensitized with antibodies. An appropriately diluted sample (containing the antigen to be measured) is placed in these wells

DOI:10.15774/PPKE.ITK.2022.004

and the enzyme-labeled antibody (second antibody) is then added. As a final step, the substrate is added to the wells, as a result of which the colour change caused by the enzyme-substrate reaction that takes place is measured [31,33]. Nowadays, ELISA kits are becoming more and more common, where several cytokines can be measured from the same sample at the same time [31].

1.1.3.3. Magnetic resonance imaging

Magnetic resonance imaging is an useful technique for detecting and examining multiple structural changes (such brain atrophy, (multiple) microhemorrhages, calcification, white matter hyperintensity (WMH), white matter lesion, dilated perivascular space etc.) in the brain [34–36]. In clinical practice, it is routinely used to examine the brains of elderly patients in order to visualize the pathological processes associated with aging and neurodegeneration, brain tumors or cerebral ischemic attacks [34]. White matter hyperintensities are easily identifiable brain lesions on MRI scans that may be associated with dementia. The technique plays a particularly important role in Alzheimer's disease (AD) research, as WMH plays a role in the development of the disease [35,36].

1.1.3.4. Transgenic animal models

Animal models provide an opportunity to investigate a characteristic feature of neurodegenerative diseases in more detail, thereby discovering valuable information about the pathological processes, which could help to develop new therapeutic approaches. Evaluating the human relevance of the results measured in these models is often difficult due to significantly different physiological conditions between humans and animals [37]. Several animal models have been developed to study vascular dementia and Alzheimer's disease, however, in this study, during the experimental work only the human apolipoprotein B-100 (ApoB-100) overexpressing and APP-PSEN1 transgenic mouse strains were used, thus only these two transgenic mouse strains are described in more details.

More and more results support that hyperlipidemia caused cardio- and cerebrovascular abnormalities (e.g. atherosclerosis, increased vascular wall thickness, decreased elasticity and diameter of the microvessels) can be associated with neurodegeneration [38]. APOB-100 animals generated in a laboratory led by Sánta Miklós show the characteristic signs of neurodegeneration, which is caused by vascular origin (eg. tau hyperphosphorylation, oxidative stress, neuronal death etc.) [26,39]. Apolipoprotein B-100 is a large glycoprotein whose

DOI:10.15774/PPKE.ITK.2022.004

elevated serum level has been observed in Alzheimer's disease [26,40,41]. ApoB-100 takes part in the formation and deposition of amyloid β (Aβ) plaques. Moreover cholesterol takes part in processing amyloid precursor protein (APP), which also shows elevated serum level in patients affected in AD. Therefore it is presumably that cholesterol metabolism is also involved in the development and progression of AD. Another used transgenic mouse strain is the double-humanized mouse model of AD, APP-PSEN1 mice, in which APP and presenilin 1 (PSEN1) gen are expressed, and which shows the main characteristics of this progressive disease from 7 months after the birth [42,43].

1.1.4. Relationship between the blood-brain barrier dysfunction and different CNS diseases

The structural or functional failure of the blood-brain barrier plays a role in many diseases affecting the central nervous systems. In the next subsection, a disease related to one of the research topics of the dissertation, Alzheimer's disease, is presented in detail, followed by a brief presentation on the role of the blood-brain barrier in other chronic neurodegenerative diseases.

1.1.4.1. Alzheimer’s disease

Alzheimer's disease is a severe neurodegenerative disease with cognitive decline characterized by neurovascular dysfunction and neuronal loss in the brain [10,16,22,44,45]. In addition, other features of AD include the accumulation of neurotoxic amyloid β peptide,, mainly a large deposit of Aβ40 and Aβ42 is characteristic [22,46]) and neurofibrillary tangles built up from aggregated hyperphosphorylated Tau [10,16,22,44,45]. Due to the neurovascular nature of the disease, cerebral vascular abnormalities (e.g. decreased cerebral blood flow, reduced microvascular density and diameters of brain microvessels, silent brain infarcts etc.) are thought to increase the likelihood of developing AD [10,22,44,45].

The role of the blood-brain barrier in Alzheimer's disease is related to faulty amyloid β clearance, which causes Aβ accumulation in the brain. The elevated level of amyloid β peptide in the brain as well as on the blood vessels initiates a series of deleterious processes associated with neurodegeneration, according to the amyloid hypothesis. In contrast, the two-hit vascular hypothesis for Alzheimer’s disease states that amyloid β accumulation is only a second factor in the development of the disease in addition to vascular problems because cerebral hypoperfusion as well as cerebrovascular damage also affect accumulation processes. These two interconnected processes contribute to neurodegeneration and development of AD [44,45].

DOI:10.15774/PPKE.ITK.2022.004

Several transporters (e.g. glucose transporter 1 (GLUT-1), receptor for advanced glycation end products (RAGE), low density lipoprotein receptor-related protein 1 and 2 (LRP1, LRP2), multidrug resistance 1 (MDR1) etc.) of the blood-brain barrier are affected in Alzheimer's disease. RAGE and LRP1 play key roles in the accumulation processes, because RAGE is implicated in the transport of the amyloid β peptide across the blood-brain barrier and LRP1 is responsible for the clearance of Aβ [10,16,22,44].

1.1.4.2. Other CNS diseases

In addition to Alzheimer's disease presented previously, changes in the integrity and permeability of the blood-brain barrier and its structural elements may play a role in the pathomechanism of many other severe neurodegenerative diseases (e.g. Parkisons's disease (PD), Amyotrophic lateral sclerosis (ALS), Multiple sclerosis (MS), epilepsy, stroke, neuromyelitis optica or acquired immune deficiency syndrome (AIDS) dementia etc.) [8,22]. The breakdown of the blood-brain barrier in Parkinson's disease (PD) is characterized by an increase in the permeability of this physiological barrier. In addition, in parallel a decreased number of different transport processes through the BBB can be seen, as the elimination of individual PD toxins is inadequate by P-gp efflux transporter [8,22,47]. In the case of ALS, it appears that all elements of the neurovascular unit may be involved in disease progression [22,48]. In experiments with superoxide dismutase-1 (SOD1) mutant animals, changes in the permeability and integrity of the blood-brain barrier and changes in both cellular and non-cellular elements have been observed [8,22,44,49]. In addition, the possible role of angiogenic factors (vascular endothelial growth factor (VEGF) and angiogenin) in the development of the disease has also been investigated in several experiments to shed light on the possible role of blood vessels [8,22,44,50,51]. The role of blood-brain barrier failure is also known in MS, which is characterized by chronic neuroinflammatory processes. These processes significantly damage the integrity of BBB, increase its permeability, and adversely affect TJs and basement membrane structure [22,52–55].

Exploring the pathomechanisms of these diseases in more detail, as well as understanding the relationship between the blood-brain barrier disruption and the development or progression of these diseases, may bring us closer to develop new therapeutic approaches (e.g. intravenous (IV) administration of mesenchymal stromal cells (MSCs) was proposed to induce regeneration of the stroke-damaged cerebrovascular network) [8,22].

DOI:10.15774/PPKE.ITK.2022.004

1.1.5. Effective methods to circumvent the BBB – Nose-to-brain route

Successful therapeutic treatment of diseases affecting the central nervous system requires delivery of the drug across the blood-brain barrier. However, this is inhibited in many cases due to the known structural and functional properties of this highly selective barrier [8,13,56]. Intranasal administration may offer an appropriate solution for circumventing the BBB and thus directly targeting the brain, as drugs absorbed through the nasal mucosa can enter the brain directly through the trigeminal and olfactory pathways (Figure 1.) [13,57,58].

The two main functions of the nose are respiration and olfaction. The nasal cavity is divided into two symmetrical halves by the nasal septum, which could be subdivided into three further parts (the nasal vestibule, the respiratory and olfactory region). The small vestibular region of just a few tenths of a cm^2 is located immediately at the entrance of the nostril openings, which is not optimal for drug absorption due to its cellular structure or small size. The major site of absorption of nasally administered drugs is the respiratory region, which is rich in vascular network. The region is made up of several cell types, the ciliated and non-ciliated columnar cells are responsible for increasing the surface area through the cilia and microvilli, while the basal cells are responsible for binding to the basement membrane, and the goblet cells are responsible for producing the mucus for the nasal mucosa which covers the walls of the nasal cavity and that the drug molecules have to pass through [13,57,59]. Rich vascularization and a large surface area are mainly conducive to absorption into the systemic circulation, however, the maxillary and ophthalmic branch of the trigeminal nerve (V1, V2) runs in this region, allowing the absorption of the drug molecules directly into the central nervous system [13,57,60]. The olfactory region has a significantly smaller surface area than the respiratory region. It is composed of several cells, and responsible for sensing different odorants [57,59]. Another alternative pathway to the CNS may be the vomeronasal-terminalis nerve, which binds the vomeronasal organ (VNO) to the brain through anatomical connections. The existence and properties of VNO have been demonstrated and described primarily in non-human primates, little is known yet about the human VNO. This organ can be found in the nasal cavity, and it is responsible for sensing external chemical signals (e.g. pheromone reception, regulating the sexual and social behavior) [13,60–63].

Intranasally administered molecules can enter the brain via the trigeminal and olfactory nerves with two different transport mechanisms, the intracellular or the extracellular pathway. During the intracellular transport mechanism, first the drug molecules are endocytosed into an olfactory neuron followed by the trafficking of the endosomes through the cell and the axon,

DOI:10.15774/PPKE.ITK.2022.004

while finally the process ends with the exocytosis of the endocytic vesicle. The extracellular pathway begins with the passage of drugs through the nasal mucosa and then the nasal epithelium through the paracellular cleft toward the lamina propria. In this translocation process, TJs play an important regulatory role, because these connections are responsible for the permeability of nasal barrier. From the lamina propria the molecules can be transported further mainly by fluid movement but there are some other, less significant pathways (lymphatic or perineural pathways) [13,57].

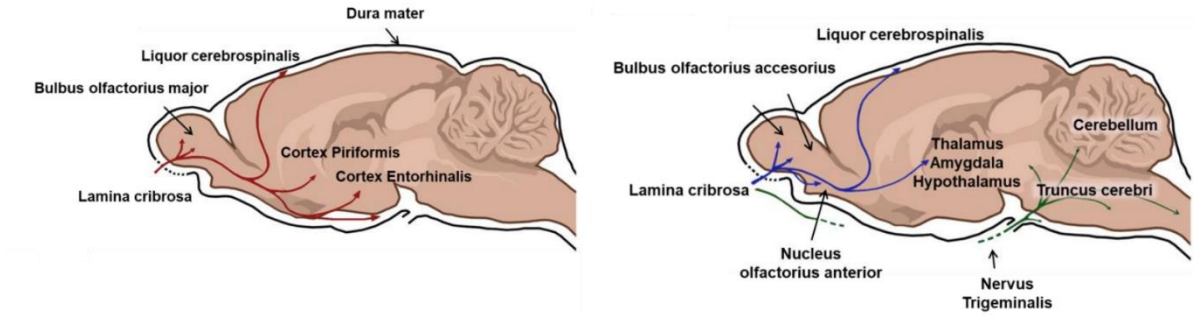

Figure 1. Presentation of nose-to-brain absorption routes of intranasal drugs [64]

The intranasal route allows rapid absorption of the active substances and the administration of lower than oral dosage, as the drug is delivered immediately after absorption to the site of action, which thus avoids the gastrointestinal (GI) tract and hepatic first-pass effect, furthermore the number of possible unpleasant side effects is less. Nevertheless it is a non-invasive delivery route, its popularity is further enhanced by its easy access to simple self-administration. [13,65,66]. While there are undoubtedly many and significant advantages to this drug administration route, the limitations must also be considered. One of these is the short drug residence time due to the mucociliary clearance (MCC) system, which may cause decreased or insufficient drug absorption [58,59,65]. The active substances are absorbed through the mucosa interwoven with a rich vascular network, so the effect of each administered drug on the vascular network (dilation, contraction) must be taken into account, because the blood flow can change significantly, which may affect the effectivity of the drug absorption. However, nasal degradation enzymes present in the nasal cavity as well as P-gp efflux transporters can negatively influence the absorption of the molecules. In addition, the volume of the nasal cavity as well as the individual anatomical properties and environmental factors that may affect the blood supply and the absorption through the mucosa, should be taken into account [58].

DOI:10.15774/PPKE.ITK.2022.004

1.2. Materials and methods

1.2.1. Materials and drug formulations

During the microdialysis experiment and before brain homogenization, animals were anesthetized with chloral hydrate (Sigma-Aldrich, St. Louis, MO, United States). Mice received the anesthetic intraperitoneally (IP) at a dose of 450 mg/kg, which was prepared by the dissolution of crystalline chloral hydrate in physiological saline. During the preparation of physiological saline, NaCl (Sigma-Aldrich, St. Louis, MO, United States) was dissolved in sterile Milli-Q water.

For *in vivo* microdialysis experiments for perfusion of peripheral and brain probe, aPPF (artificial peripheral perfusion fluid, 147 mmol/l NaCl, 4 mmol/l KCl, and 2.3 mmol/l $CaCl_2$) and aCSF (artificial cerebrospinal fluid, 147 mmol/l NaCl, 2.7 mmol/l KCl, 1.2 mmol/l $CaCl_2$, and 0.5 mmol/l $MgCl_2$) were prepared with sterile Milli-Q water. Each chemical was purchased from Sigma-Aldrich (St. Louis, MO, United States).

Quinidine (QND; Sigma-Aldrich, St. Louis, MO, United States) gel was used at a concentration of 50 mg/mL for intranasal treatment. Quinidine was dissolved in an oleogel matrix (which was a kind gift from Heinrich Heine University Düsseldorf, Germany, proprietary formulation MetP Pharma, AG, Emmetten, Switzerland [2]). Dissolution was improved by a few minutes of sonication or by manual stirring. After the preparation, this drug formulation was stored in a refrigerator (at 2-8 °C) for a maximum of 2 days.

1.2.2. Animals

APOB-100, APP-PSEN1 mice and their wild type littermates were used for *in vivo* dual-probe microdialysis experiments. The APOB-100 animals were bred at the Biological Research Centre in Szeged, where a transgenic mouse strain overexpressing the human APOB-100 protein had previously been successfully generated in a research group led by Miklós Sántha as described earlier [67]. B6C3-Tg(APPswe/PS1dE9)85Dbo/Mmjax mice were purchased from The Jackson Laboratory (Bar Harbor, ME, United States) [68]. Both transgenic mouse strains had the same C57BL/6 genetic background in a hemizygous form. Breeding of the transgenic mouse strains were approved by the regional Station for Animal Health and Food Control (Csongrád County, Hungary; project licenses: XVI./2724/2017 for APOB-100 mouse strain and XVI./1248/2017 for APP/PSEN1 mouse strain) (Appendix Table 1.) [68].

For ELISA cytokine microplate array and magnetic resonance imaging studies, 8–11 months old APOB-100, APP-PSEN1 and WT mice were used. For microdialysis experiments,

DOI:10.15774/PPKE.ITK.2022.004

male APOB-100 mice, both male and female APP–PSEN1 and male WT animals were used (Appendix Table 1. and Table 2.).

Animals were kept in groups of two to three in one cage, in a temperature controlled room with a 12-hour dark/light cycle. Mice had free access to food and water available *ad libitum*. During the whole surgical procedures of the microdialysis probe insertion, MRI experiments and brain dissection, all efforts were made to minimize pain and suffering of the animals.

1.2.3. *In vivo* microdialysis

1.2.3.1. Surgical procedures, drug administration and sampling during *in vivo* microdialysis experiments

Mice were anesthetized with chloral hydrate (450 mg/kg intraperitoneally). The anesthesia was regularly controlled and maintained throughout the experiment by re-administration IP of the anesthetic as needed. The hair from the area of the pectoralis muscle and the skull of the mice was removed by a hair clipper, after which the animals were fixed in a supine position on a heated operating bench. The right jugular vein was exposed, and the Microbiotech MAB1.4.3. (Appendix Table 4.) a peripheral microdialysis probe was inserted into the prepared vein. The probe was fixed on the pectoralis muscle with some surgical threads. Flow through the peripheral probe was checked, and the tubings of the microdialysis probe were exteriorized under the right scapula. Then, the animal's skin where the implantation was performed was closed with a few stitches. For implanting the second probe, mice were placed in a Stoelting stereotaxic instrument. Microbiotech MAB8.4.3. (Appendix Table 5.) brain probe was implanted into the left striatum using the following coordinates with respect to the bregma: anterior–posterior = +0.2 mm; medio-lateral = −2.2 mm and dorso-ventral = −3.2 mm. Flow through the brain probe was also checked. Both microdialysis probes were connected to a CMA/102 microdialysis pump. During all the experiments, 1.0 µl/min flow rate was applied. The peripheral probe was perfused with artificial peripheral perfusion fluid, and the brain probe was perfused with artificial cerebrospinal fluid. Animals were treated intranasally (IN) into their left nostril with 10 µL of 50 mg/mL quinidin containing gel by a 30G needle syringe under a microscope after 30 minutes equilibration period following the surgical insertion of the microdialysis probes. Although intranasal treatment of animals is often performed in the supine position for more effective treatment [13], this was not possible in this case due to the fixed position of cerebral microdialysis probe. After the intranasal administration, the sample

DOI:10.15774/PPKE.ITK.2022.004

collection was continued for 3 h. The microdialysate samples were collected every 30 min and placed on dry ice until the end of the experiment. Then the frozen dialysates were stored in a deep freezer at −80°C until the bioanalytical investigation.

1.2.3.2. Bioanalysis of dialysates

Quantitative analysis of the quinidine containing microdialysate samples was performed on a Sciex 6500 QTrap hybrid tandem mass spectrometer coupled to an Agilent 1100 High-performance liquid chromatography (HPLC) system. Electrospray ionization was applied in positive ion detection mode with multiple reaction monitoring (MRM) transitions of 325.2/307.2 (quantifier) and 325.2/172 (qualifier) with a collision energy of 31 and 45 V, respectively. The dwell time of the transitions was 300 ms. Source conditions were: curtain gas: 45 arbitrary unit (au), spray voltage: 5000 V, source temperature: 450°C, nebulizer gas: 40 au, drying gas: 40 au, and declustering potential: 171 V. The samples were introduced to the system via an HPLC system consisting of a binary pump, an autosampler, and a column compartment unit. A Phenomenex Synergi Fusion Reversed-phase (RP) column (length × diameter: 50 mm × 2 mm, particle size: 4 µm, pore size: 80 Å, Gen-Lab Kft., Budapest, Hungary) column was applied for the separation using 0.1% formic acid (VWR International Kft. Debrecen, Hungary) in water as eluent A and 0.1% formic acid containing acetonitrile (VWR International Kft. Debrecen, Hungary) as eluent B in gradient elution mode. The gradient started at 90% of eluent A, and the eluent B was increased to 95% by 3 min and kept at that concentration for 0.5 min then decreased to the initial composition by 0.3 min and kept there for 2.2 min, thus the overall analysis time was 6 min. Then, 10 µl of samples were injected. The column was kept at ambient temperature. A 5-point calibration curve was used in the range of 0.1–100 ng/ml.

1.2.4. Investigation of cerebral cytokine levels

1.2.4.1. Brain homogenate preparation

Mice were overanesthetized with chloral hydrate (450 mg/kg intraperitoneally) and decapitated. Then, the brain was quickly removed, divided to two separate hemispheres by a midline cut, which was followed by the quick removal of the cerebellum and bulbus olfactorius, and only the left hemisphere was weighed (Appendix Table 2.). Then, the volume of the 1x lysis buffer (EA-0001, Signosis, Inc., Santa Clara, CA, USA), which was previously prepared according to the instructions of the manufacturer's, was calculated according the weight of the brain samples (1 mL of 1x lysis buffer to 100 mg of brain sample). The precisely calculated

DOI:10.15774/PPKE.ITK.2022.004

amount was added to the weighted brain samples, which were placed into ice until homogenization began. This step was then repeated on all 5 animals in the group, and then the five left hemispheres were homogenized by a tissue homogenizer (Ultra-Turrax TP 18/10; Staufen, Germany) on ice for 60 seconds until a homogenous sample was obtained. The lysates were centrifuged at 10 000 rpm for 5 min at 4°C, which was followed by the collection of the supernatants. The removed supernatant was divided to 400 µL aliquots in Eppendorf tubes and was placed on ice. The aliquots were stored in a deep freezer at −80°C until determination of the protein content. Pooled samples were prepared for both transgenic mouse strains as well as wild type animals (n = 5).

1.2.4.2. Protein Assay

For determination of the protein content of aliquots Pierce^{TM} BCA Protein Assay Kit (Thermo Fisher Scientific, Waltham, MA, United States) was used according to the instruction of the manufacturer. As a first step, samples were prepared for the calibration curve (working range: 20-2000 µg/mL) from an albumin standard with a dilution series, then each aliquots were diluted to 1:10. The standards and the unknown diluted samples were placed into a 96-well plate, and then the freshly mixed reagents were added. The plate was covered, gently shaken for 30 s, and incubated for 30 min at 37°C. After the incubation period, plated cooled down to room temperature, was placed into the plate reader (Tecan Spark 20M, Männedorf, Switzerland), and the absorbance was measured at 562 nm. A calibration curve was prepared from the measured absorbance values of the standards and the protein content of each unknown sample was determined (Appendix Table 2.).

1.2.4.3. Cytokine ELISA plate arrays

Signosis Mouse Cytokine ELISA Plate Array I (EA-4003, Signosis Inc., Santa Clara, CA, USA) was used for determination of cerebral cytokine expression in pooled mouse brain homogenates, which were performed according to the manufacturer's protocol. Each aliquot was diluted to 1000 µg/ml of total protein. The dilution ratio was determined based on the instruction of the ELISA assay. More than 20 different cerebral cytokines were investigated (Table 1.), and luminescence was compared measured with 1 second integration time. Pooled samples (n = 5) of APOB-100 mice and APP–PSEN1 mice were compared to the group of WT mice. A 96-well plate was divided into four sections, and the sections included two parallels for each mouse strain, respectively. Two sections were used for the pool of five wild type mice

DOI:10.15774/PPKE.ITK.2022.004

as control, while the other two were used to investigate the level of different cerebral cytokines of the transgenic mice.

1.2.5. Comparative MRI in APOB-100, APP-SEN1 and WT animals

T2-weighted anatomical scans were performed on a 1T preclinical nanoScan MRI scanner (Mediso Ltd., Budapest, Hungary). The instrument was equipped with 450 mT/m gradients and a diameter of 20 mm transmit/receive volume coil. During the experimental period, mice were anesthetized with 1.5% isoflurane in medical oxygen and placed in a prone position on the MRI bed. A three-dimensional Fast Spin Echo Multi-Slice (FSEMS) was acquired with the following parameters: repetition time (TR) = 2 s, effective echo time (TE) = 75.8 ms, echo train length (ETL) = 16, number of excitations = 3, matrix size = 120 × 96 × 64, and field of view (FOV) = 30 mm × 30 mm × 19.2 mm [68].

In VivoQuant software (inviCRO) was applied for the semi-automatic segmentation in order to delineate the ventricles. An approximate region of interest (ROI) was selected manually, from which ventricles were segmented by connecting thresholding algorithms with thresholds calculated by Otsu's method [68].

1.2.6. Data analysis

The analytical results of the dual-probe *in vivo* microdialysis experiments and the results of the cytokine ELISA plate array assay, which were obtained from a pooled sample of 5 mice (both APOB-100, APP-PSEN1 and WT animals) were analyzed using Microsoft Excel 2016 Software (Microsoft Corporation) and OriginPro 2022 Software (OriginLab Corporation). The area under the curve (AUC) values were calculated from QND concentration-time curves measured in brain and in the circulation by *in vivo* microdialysis experiments was performed by OriginPro 2022 Software (OriginLab Corporation), and Microsoft Excel 2016 Software was used for the statistical analysis. In case of comparison of two groups of mice, Student's t-test was performed. The graphs of all experimental results, which are presented in this thesis were made in OriginPro 2022 Software (OriginLab Corporation). VivoQuant program was used to evaluate the MRI results, and the results were averaged similarly to *in vivo* microdialysis and ELISA experiments.

DOI:10.15774/PPKE.ITK.2022.004

1.3. Results

1.3.1. Comparison of brain penetration of intranasally administered quinidine in APOB-100, APP-PSEN1 and WT animals

The absorption pattern of a well-known P-gp substrate, quinidine [69,70] in two transgenic mouse strains, APOB-100 and APP-PSEN1 compared to wild type mice treated intranasally was investigated by *in vivo* dual-probe microdialysis (Appendix Table 1.). From the two investigated transgenic models, APOB-100 mice show the characteristics of atherosclerosis, while APP-PSEN1 mice are animal models of Alzheimer's disease [26,39,42]. In order to bypass the blood-brain barrier, nasal administration was chosen. Through this drug delivery route molecules can be absorbed directly into the central nervous system via trigeminal and olfactory pathways [13,57,59]. Animals were treated with a quinidine containing gelous vehicle, because the gel formulation has several advantages compared to other formulations. It could remain on the surface of the nasal mucosa for an elongated time, thus allowing a continuous drug release and absorption [2].

Similar concentration-time profiles of the QND were observed for APOB-100, APP-PSEN1 and wild type mice based on the results of the microdialysis experiments. After the IN treatment, a rapid absorption peak can be seen, followed by a long-lasting plateau phase due to prolonged release and absorption of QND from the gel formulation (Figure 2.). The concentration maximum (C_{max}) of quinidine (Figure 3.), AUC values (Figure 4. A and B) and the AUC_{brain}/AUC_{blood} ratio (Figure 4. C and D) has similar results in all three groups of mice. Analysis of the results revealed that in all cases a higher quinidine level can be measured in the brain, than in the blood. These results indicate that the P-gp efflux transporter does not significantly affect the absorption of quinidine in the nasal mucosa, furthermore no remarkable difference in nasal barrier function of diseased mice compared to the control animals can be detected.

DOI:10.15774/PPKE.ITK.2022.004

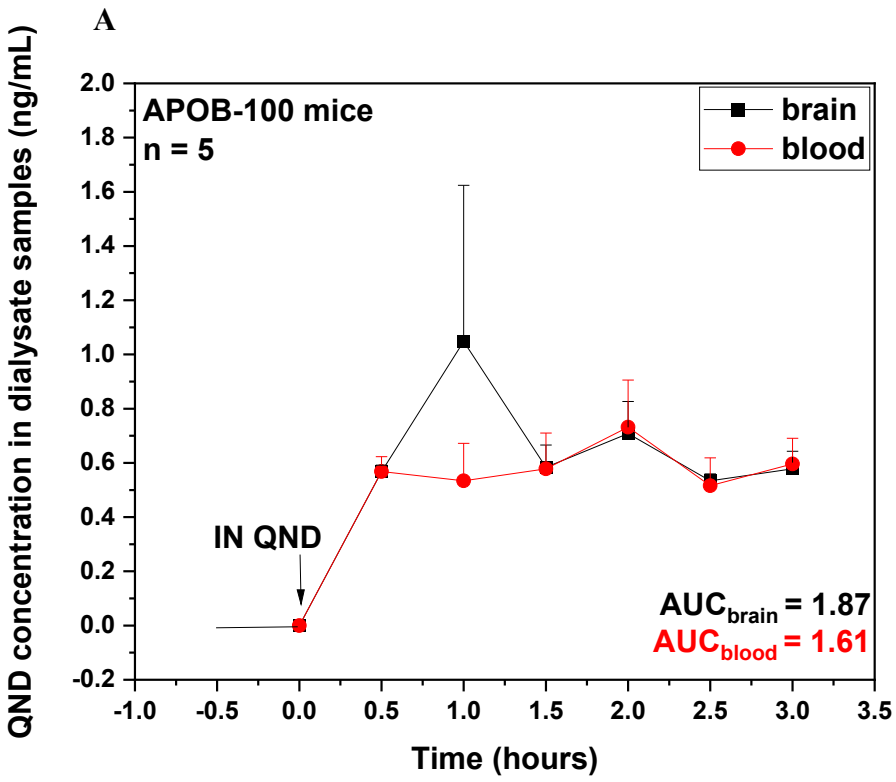

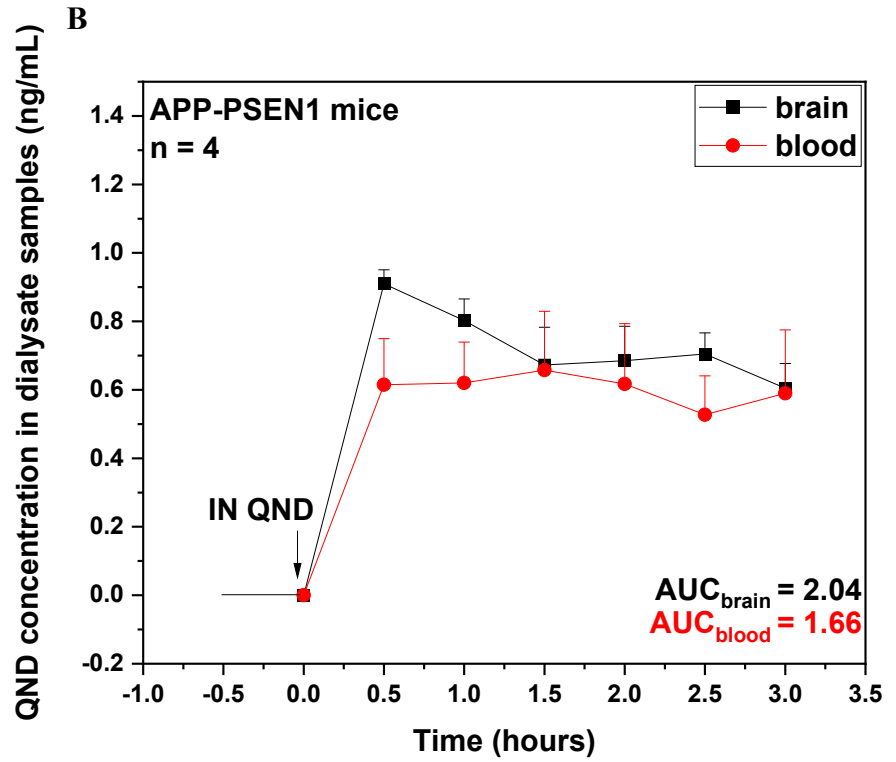

DOI:10.15774/PPKE.ITK.2022.004

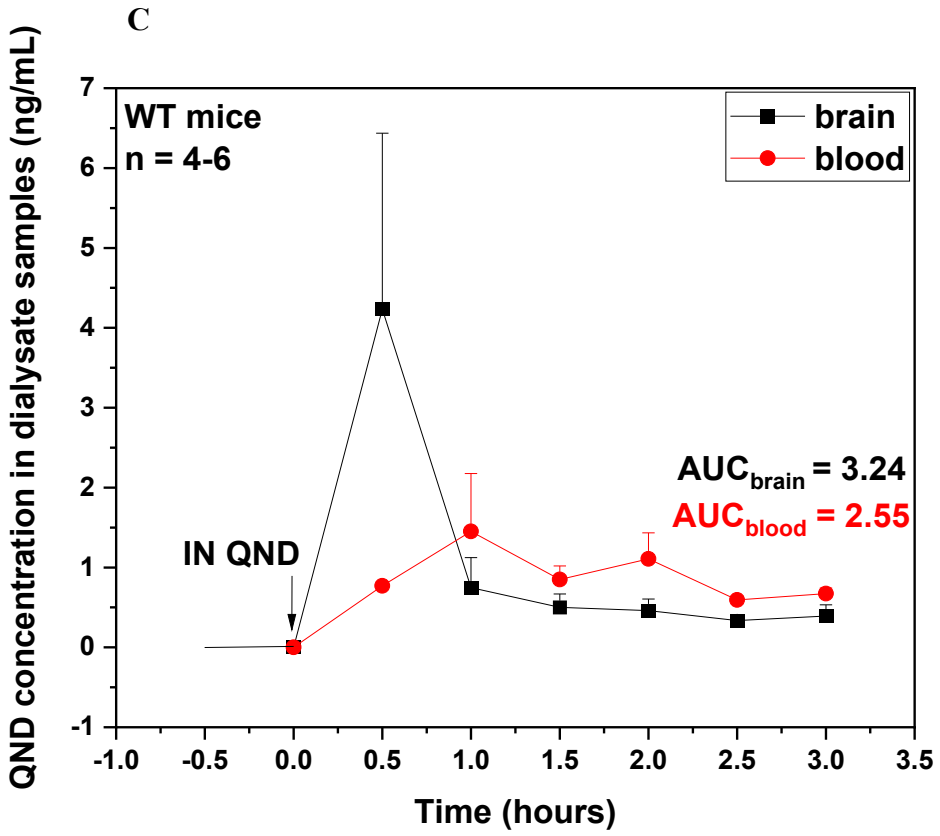

Figure 2. Investigation of the temporal characteristics of the absorption of quinidine following intranasal treatment (A) in APOB-100 and (B) in APP-PSEN1 mice compare to (C) wild type (WT) animals measured by dual-probe *in vivo* microdialysis. Intranasal administration was performed at $t = 0$. Black and red symbols represent the quinidine mean concentration in the brain and in the systemic circulation (plasma). Data shown as means ± SEM. (IN QND: intranasally administered quinidine; AUC: area under the curve)

DOI:10.15774/PPKE.ITK.2022.004

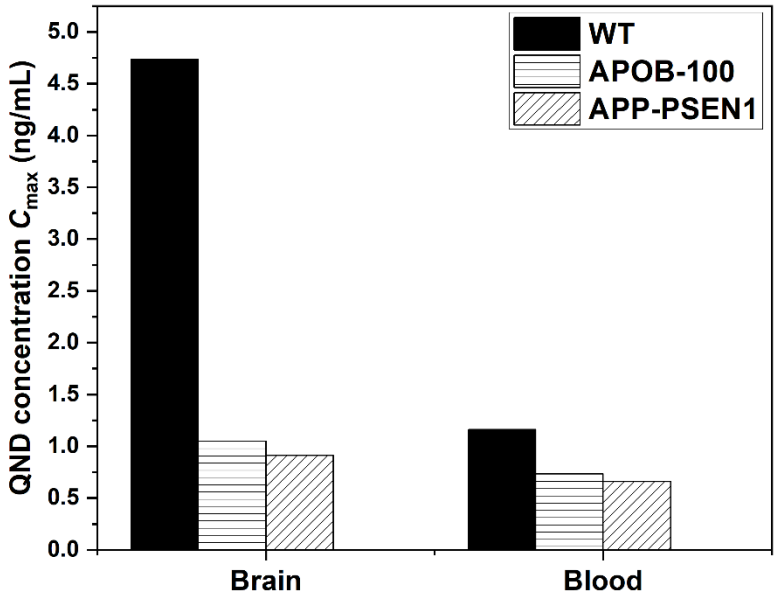

Figure 3. Comparison of brain and blood C_{max} values between groups of transgenic animals and control animals based on the result of *in vivo* microdialysis experiments (C_{max}: concentration maximum)

A

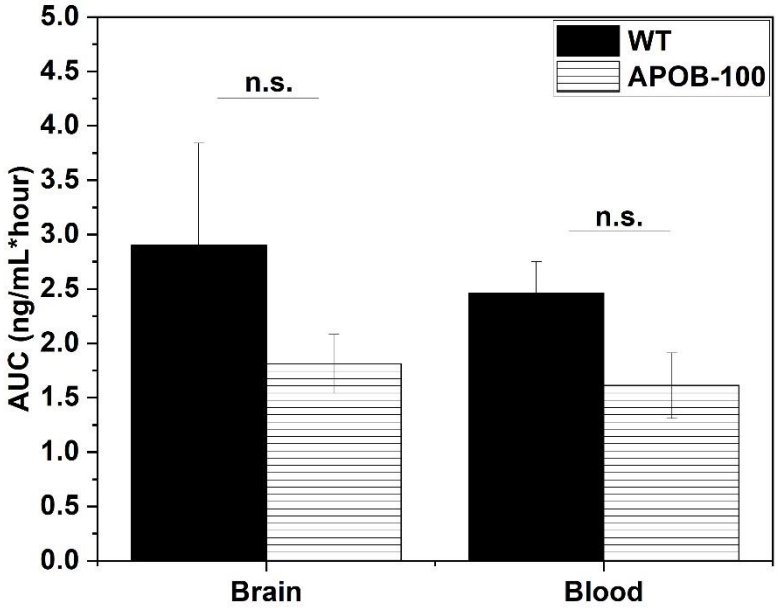

DOI:10.15774/PPKE.ITK.2022.004

B

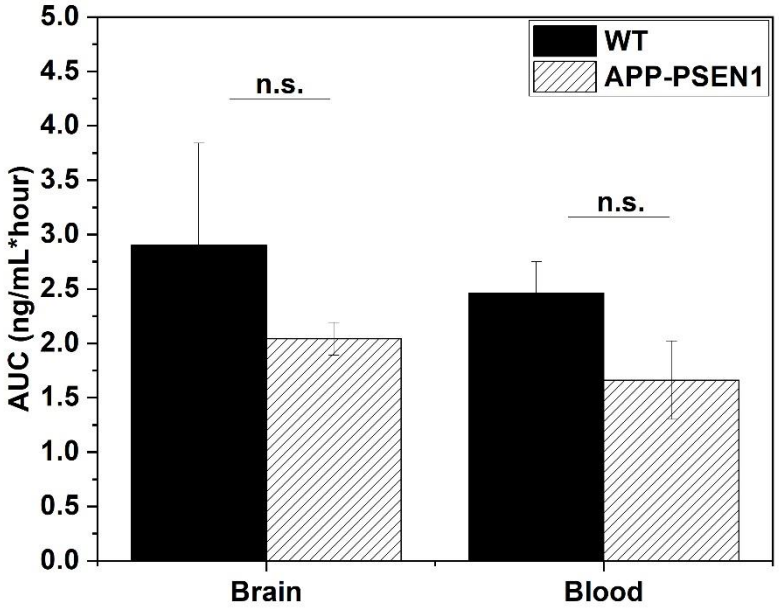

C

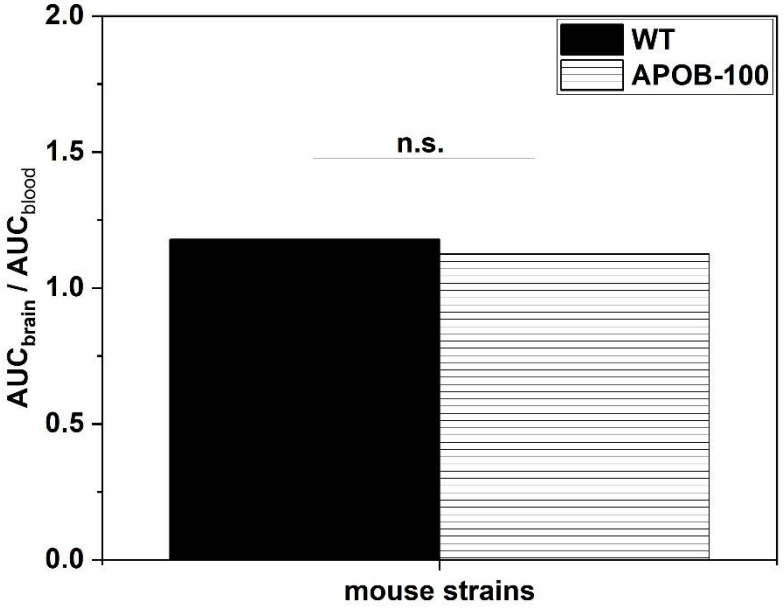

DOI:10.15774/PPKE.ITK.2022.004

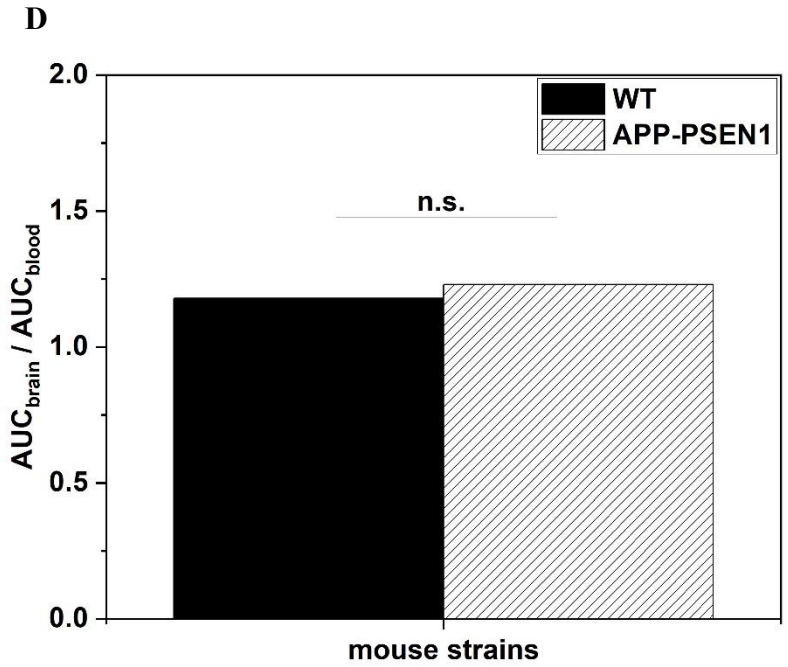

Figure 4. Comparison of (A) mean AUC ± SEM of APOB-100 mice (B) mean AUC ± SEM of APP-PSEN1 mice and (C) AUC_{brain}/AUC_{blood} values of APOB-100 animals and (D) AUC_{brain}/AUC_{blood} values of APP-PSEN1 animals compared to the wild type mice calculated from QND concentration-time curves measured in brain and in the circulation by *in vivo* microdialysis experiments. The AUC values were calculated from the individual QND concentration-time curves of each animal, then these values were averaged, and SEM was calculated. There was no statistically significant difference in either case (AUC: area under the curve, n.s. = not significant, $p < 0.05$).

1.3.2. Comparison of the cerebral cytokine levels in APOB-100, APP-PSEN1 and wild type mice

APOB-100 mice are characterized by serious cerebrovascular changes and also neurodegeneration due to the elevated serum level of ApoB-100 [26,39,67]. The change in cytokine levels caused by vascular disease in these animals compared to wild type animals was examined by ELISA cytokine microplate array.

DOI:10.15774/PPKE.ITK.2022.004

Table 1. The investigated cerebral inflammatory cytokines in the pooled samples of the two transgenic mouse strains and the wild type animals.

	1	2	3
A	**TNFα**	**IL-1α**	**PDGF-BB**
B	**IGF-1**	**IL-1β**	**β-NGF**
C	**VEGF**	**G-CSF**	**IL-17A**
D	**IL-6**	**GM-CSF**	**IL-2**
E	**FGFβ**	**MCP-1**	**IL-4**
F	**IFNγ**	**MIP-1α**	**IL-10**
G	**EGF**	**SCF**	**Resistin**
H	**Leptin**	**Rantes**	**IL-12**

Among the more than 20 different cytokines (Table 1), VEGF, Platelet-derived growth factor-BB (PDGF-BB), and interleukin-17A (IL-17A) showed a significantly upregulated level in APOB-100 mice (Table 2. Figure 5.). More than 13-fold upregulation of VEGF was observed in the samples. which plays a key role in the angiogenesis [8], because it induces the formation of new vessels. The second most upregulated cytokine was PDGF-BB, which is also involved in angiogenesis, it showed a more than 11-fold increase. Third one was IL-17A with a more than 6-fold increase, which proinflammatory cytokine has an increased level in atherosclerosis and also in Alzheimer's disease [71]. This cytokine is produced by activated T cells, and modulates the activity of Nuclear factor-κB (NF-κB), which plays an important role in the immune response [68]. Genetic modifications are thought to be responsible for the elevated levels of the last two cytokines. In contrast, no increase was observed for other cytokines, which are important in inflammation, the expression level of interleukin-1α (IL-1α), interleukin-1β (IL-1β), interleukin-2 (IL-2) and interleukin-4 (IL-4) was unchanged or slightly downregulated.

In APP-PSEN1 animals, a validated model of Alzheimer's disease, a significant increase in resistin, granulocyte-macrophage colony stimulating factor (GM-CSF) and IL-17A was detected (Table 2. Figure 5.). The largest increase of almost 10-fold compared to control animals was observed for resistin, which is produced by adipocytes, plays a role in cholesterol metabolism and in inflammatory processes, and some proinflammatory cytokines may induce its expression. Elevated levels of resistin have been studied in several patients affected with Alzheimer's disease, but their exact role in AD is not yet known [72]. For IL-17A, similar to APOB-100 mice, a nearly 6-fold increase was present. GM-CSF levels increased nearly 5-fold, which is involved in the inflammation by regulation of the number and function of macrophages

[73]. For other inflammatory cytokines (e.g. tumor necrosis factor-α (TNF-α), IL-1β, interleukin-6 (IL-6)) involved in Alzheimer's disease, no such change was observed, only a slight increase [72].

Table 2. Comparison of the extent of luminescent intensity ratio (LIR) of the measured cytokines in the two transgenic mouse strains (cytokines for both APP-PSEN1 and APOB-100 animals, which were upregulated more than 5-fold are highlighted with a pale green background).

Measured cytokines	APP-PSEN1 LIR	APOB-100 LIR	Measured cytokines	APP-PSEN1 LIR	APOB-100 LIR
TNF-α	2.71	2.04	**MCP-1**	0.65	3.15
IGF-1	0.91	1.07	**MIP-1α**	0.43	1.82
VEGF	0.82	13.63	**SCF**	1.30	1.36
IL-6	1.26	1.45	**Rantes**	0.69	1.22
FGFβ	1.76	2.97	**PDGF-BB**	2.03	11.82
IFNγ	0.66	1.63	**β-NGF**	3.69	0.88
EGF	1.53	0.61	**IL-17A**	6.31	6.38
Leptin	0.35	1.50	**IL-2**	1.33	0.46
Il-1α	1.28	0.30	**IL-4**	3.63	0.22
IL-1β	2.99	0.21	**IL-10**	2.82	1.30
G-CSF	2.19	0.58	**Resistin**	9.59	1.47
GM-CSF	5.47	1.69	**IL-12**	1.19	0.67

DOI:10.15774/PPKE.ITK.2022.004

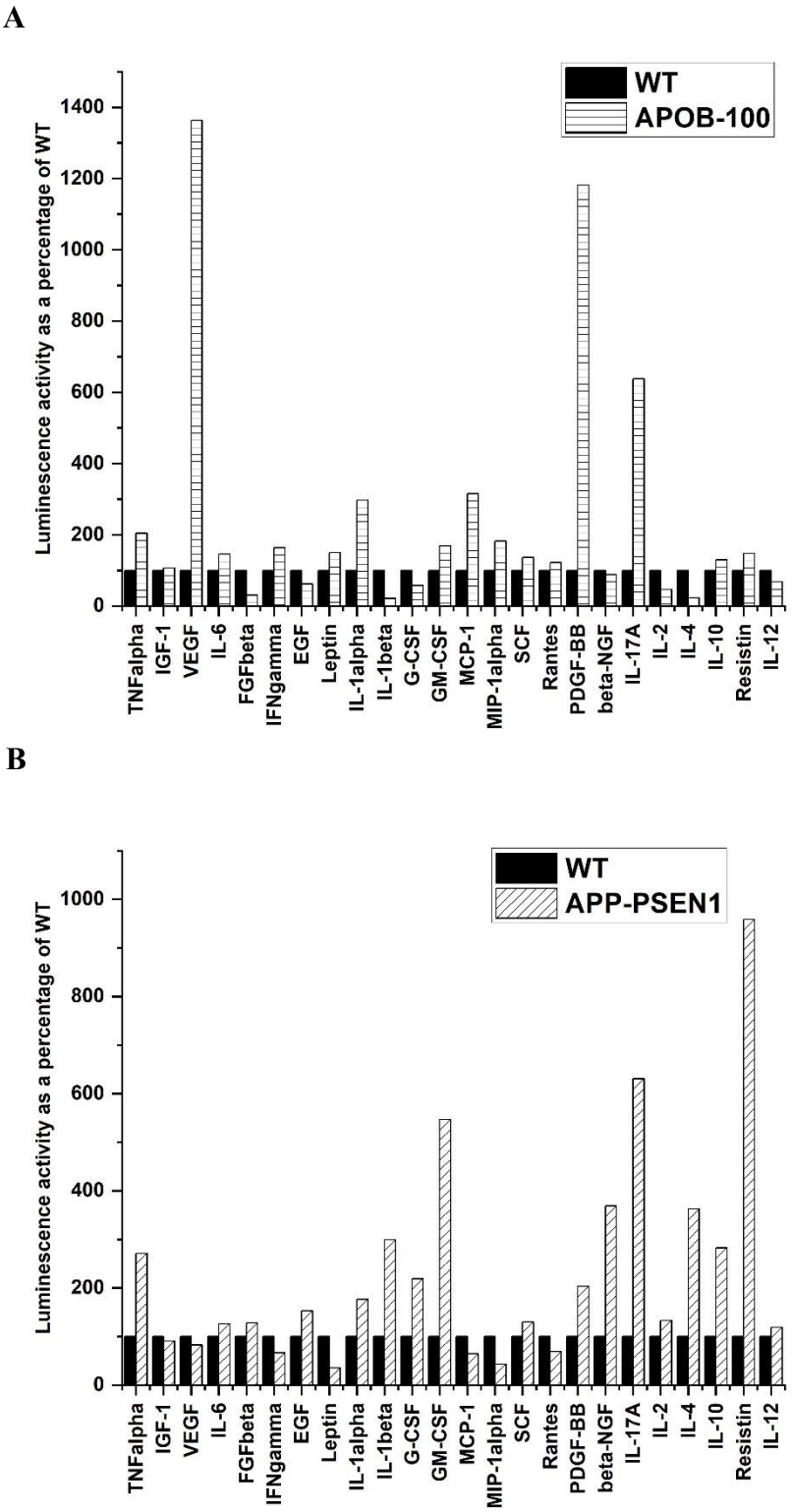

Figure 5. Comparison of LIR values of the tested cytokines compared to the wild type animals (A) APOB-100 and (B) APP-PSEN1 mice. Pooled samples were used for both transgenic mouse strains as well as wild type animals (n = 5).

DOI:10.15774/PPKE.ITK.2022.004

1.3.3. Investigation of differences in the brain morphology in both transgenic mouse strains compared to wild type animals by MRI

Magnetic resonance imaging was performed on both APOB-100 and APP-PSEN1 transgenic animal strains and the wild type mice (Figure 6.; Appendix Table 3. and Figure 1-3.). MRI scans were studied computationally and the volumes of the ventricles were segmented and calculated in case of each animal. Then, mean ventricular volume and standard deviation specific for each strain were calculated from the individual data.

Based on MRI data, several morphological changes in the brain were detected in both APOB-100 and APP-PSEN1 mice compared to the wild type animals. A notably dilated lateral and dorsal ventricles and a smaller but significantly increased aqueduct volume was observed in APOB-100 animals. In contrast, no such morphological changes were observed in APP-PSEN1 animals (Figure 6., Appendix Figure 1-3.).

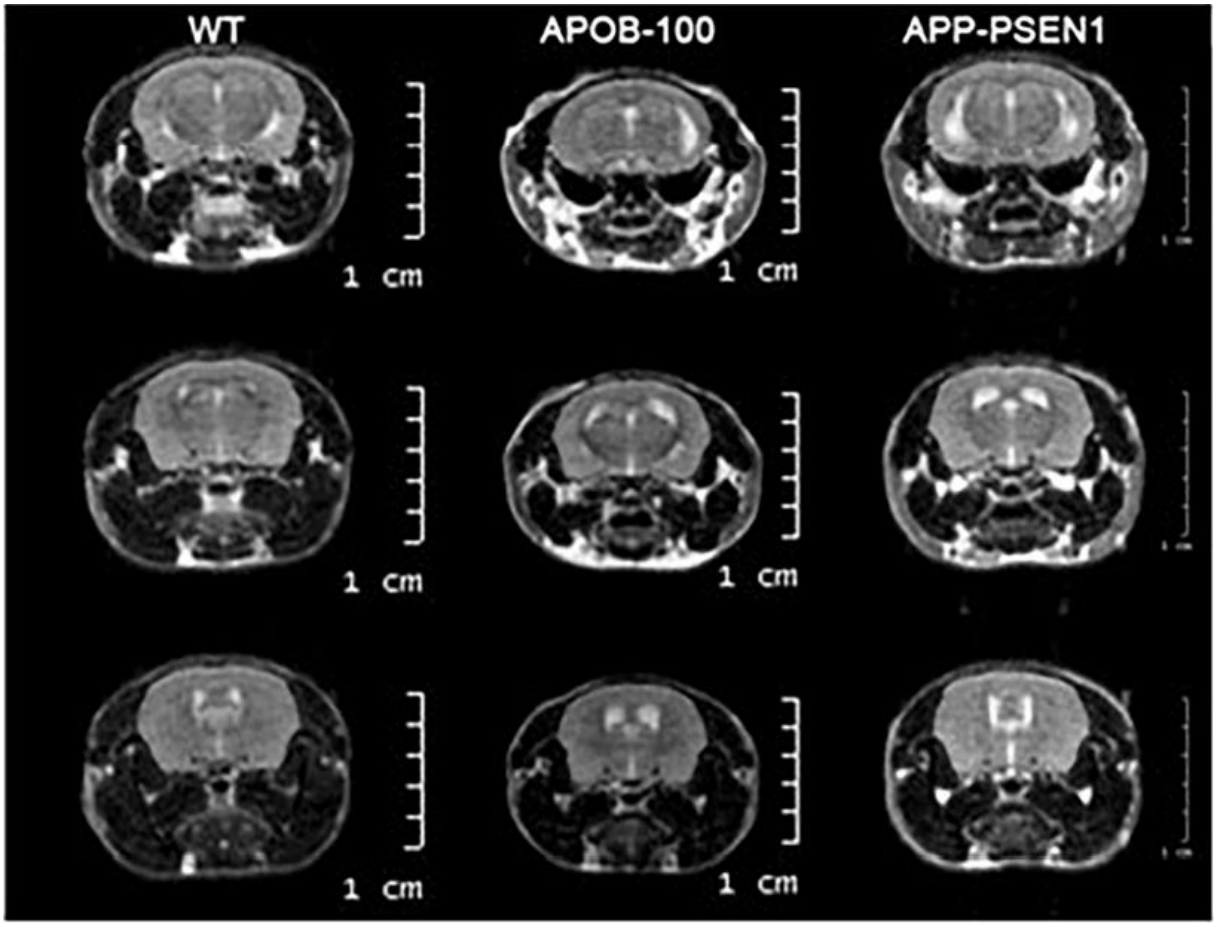

Figure 6. Comparison of anatomical MRI images of the brains of APOB-100, APP-PSEN1 and WT animals [68]

DOI:10.15774/PPKE.ITK.2022.004

1.4. Discussion

The aim of our study was to investigate two age-related neurodegenerative diseases in mice using the model of atherosclerosis, APOB-100, and the model of Alzheimer's disease, APP-PSEN1 transgenic mice. The experimental work can be divided into three main parts. First, the effect of P-gp efflux transporters in the nasal mucosa on the absorption of intranasally administered quinidine molecules was investigated by dual-probe *in vivo* microdialysis. Furthermore, different cerebral cytokines in the two animal models compared to wild type mice were examined. Finally, brain lesions and morphological changes caused by the pathological processes in the disease models were studied by MRI.

Intranasal drug delivery is a non-invasive, promising method of administration that allows each drug to enter the brain through the trigeminal and olfactory pathways, bypassing the blood-brain barrier. However, the efficiency of nasal-brain absorption may be significantly affected by several efflux transporters in the nasal mucosa, one of which is P-gp. The neurodegenerative diseases are characterized by breakdown of the blood-brain barrier and its increased permeability, moreover altered function and downregulation of P-gp has been observed in Alzheimer's disease [16], and recently demonstrated by Hoyk et al. in APOB-100 animals [26]. In order to develop new therapeutic approaches, it is important to investigate the properties of the nasal barrier in animal models of different neurodegenerative diseases. During the experimental work, a well-known P-gp substrate was administered in a gel formulation intranasally to APOB-100 and APP-PSEN1 as well as to wild type control animals [69,70]. The drug absorption was monitored by dual-probe *in vivo* microdialysis in the brain and in the periphery. After the IN administration, rapid absorption peak of quinidine was observed in each group of animals, followed by a long-lasting plateau phase, where the release and the absorption of QND was continuous. Based on the results of microdialysis experiments, unchanged function of the nasal barrier was observed, as the absorption pattern of quinidine was similar in all cases. It can be concluded that P-gp does not have any significant role in drug absorption in the nasal cavity.

Based on the results of the ELISA cytokine assay, APOB-100 mice showed significantly elevated levels of VEGF, PDGF-BB, and IL-17A, which may even be useful in detecting cerebrovascular lesions and brain dysfunction caused by hyperlipidemia. Süle et al. showed that in this transgenic mouse strain, hyperlipidemia has a serious effect on the cerebral vascular network, primarily affecting vascular network density and capillary diameter [74]. Furthermore, it is hypothesized that hyperlipidemia may inhibit the process of angiogenesis. In addition,

DOI:10.15774/PPKE.ITK.2022.004

strongly elevated levels of VEGF may even cause breakdown of the blood-brain barrier [75], experimental results confirming this claim have been described in APOB-100 animals [26]. The double-humanized, APP-PSEN1 mice showed highly elevated levels of resistin, IL-17A and GM-CSF, which may serve as important markers of AD. Demirci et al. described elevated resistin levels in the serum of AD patients [72], suggesting that this cytokine may play an important role in the pathology of AD and be useful as a marker. GM-CSF is involved in the inflammation processes by regulation of the number and function of macrophages. Significantly increased IL-17A levels were measured in both transgenic strains, which suggests the overproduction of cyclooxygenase-2 (COX-2) and nitric oxide (NO) [68].

In order to characterize the morphological consequences of the neurodegeneration in the two animal models, MRI was acquired on APOB-100, APP-PSEN1 and wild type male mice. Based on MRI data, several anatomical changes were detected in the brain in both transgenic mouse strains compared to the control animals, presumably due to pathological processes characteristic of atherosclerosis and Alzheimer's disease. Significantly enlarged lateral and dorsal ventricles and a smaller but remarkably increased fourth ventricle volume was observed in APOB-100 mice, which is in line with previous results [26,39]. We hypothesized that these changes might be the consequences of the genetic manipulation of these animals, after which enhanced production, infiltration, defected drainage of the cerebrospinal fluid (CSF) can be performed. The lower pumping and secretory function of ependymal cell in the choroid plexus of APOB-100 mice can be explained by the downregulation of the cerebral glymphatic in APOB-100 mice due to their advanced age and the reduced function of the mitochondria [39]. In contrast, no such morphological changes were observed in APP-PSEN1 animals.

DOI:10.15774/PPKE.ITK.2022.004

Part 2 – Investigation of caffeine penetration through the dermal barrier

2.1. Theoretical background – Dermal barrier

In the second half of my dissertation, I investigated the absorption of a widely used hydrophilic model compound, caffeine through the skin within the framework of two separate projects: 1) comparison of the time-course of caffeine penetration in human skin and in artificial skin substituent and 2) the study of the skin permeability in Aldara-induced psoriasiform dermatitis in three mouse strains with different genetic backgrounds by topically applied caffeine cream.

In the following subsections – in addition to a general characterization of the skin structure and a short presentation of the transdermal permeation pathways – efforts are made to develop skin substituents mimicking appropriately the physiological and pathological processes in the skin are discussed briefly. The chapter summarizes the characterization of psoriasis, a T-cell mediated inflammatory skin disease that affects many patients and severely negatively influences their quality of life.

2.1.1. Structure and function of the skin

The skin is a constantly self-renewing organ, which covers the human body and performs various essential physiological functions. It is characterized by a dual role in the relationship to the environment, because it separates the body from its surroundings, but it also helps to adapt to the different environmental conditions. Skin acts as a barrier to external, potentially harmful physical (e.g. mechanical insults, UV (ultraviolet) radiation, noxious heat or extreme cold etc.), chemical (e.g. different topically applied drugs, toxic agents etc.) and immunological (e.g. fungi, bacteria and viruses etc.) effects. In addition to the protective function, it also performs other important tasks, such as thermoregulatory, metabolic and sensory functions.

The skin is characterized by a multi-layer structure, which can be divided into three main, functionally and anatomically different layers (from the outermost to the innermost): the epidermis, the dermis and the hypodermis. This layered structure is characteristic for the two upper layers, which can be further divided. The subdivided layers (or strata) of epidermis are the stratum corneum, the stratum lucidum, the stratum granulosum, the stratum spinosum and the stratum basale. The stratum corneum plays a key role in fulfilling the protective function of the skin, as it functions as a physical, chemical and immune barrier. The epidermis is mainly composed of keratinocytes, which are nucleated between the stratum granulosum and the

DOI:10.15774/PPKE.ITK.2022.004

stratum basale. During the maturation process, keratinocytes undergo a fundamental structural transformation, thanks to which they become flat, anucleated squamous cells of the outermost layer of epidermis. Under normal conditions, the proliferation, maturation, and desquamation of keratinocyte cells are in balance, resulting in cyclic rejuvenation of the epidermis. However, for some skin diseases, this cyclic process is impaired (e.g. abnormal proliferation of keratinocytes can be witnessed in psoriasis). This outermost layer also acts as a permeability layer, protecting the body from dehydration, excessive loss of water and solutes. Other cell types (e.g. Langerhans cells, lymphocytes, Merkel cells, melanocytes) can also be found in the epidermis in significantly smaller portions, which are involved in the immune and sensory functions.

The two main main layers of the skin, the epidermis and the dermis, are separated by a basement membrane, which is built up mainly from type IV and VII collagens and laminin besides other proteins. The dermis can be subdivided into two layers: papillary and reticular dermis. This layer is made up mainly of collagen and elastin fibers, and it is characterized by proper vascularization, lymphatics and the presence of various appendages (e.g. hair follicles, arector pili muscle, sebaceous and eccrine glands, nerves, apocrine glands etc.). There are many different cell types (e.g. fibroblasts, macrophages, lymphocytes, mast cells etc.) in the dermis. This layer takes part in immunological defense, sensation, thermoregulation, and also provides elasticity and mechanical support against the external insults.

The third main layer of skin is the hypodermis (subcutaneous tissue), which is made up mainly of adipocytes, and like the dermis, this layer is also innervated and highly vascularized. Hypodermis mainly provides mechanical and thermal protection, furthermore it acts as an energy and nutrients storage [76–78].

2.1.2. Drug delivery through the dermal barrier

Transdermal drug delivery is a common non-invasive drug administration method not only for therapeutic purposes for the treatment of various skin diseases and injuries, but also in the cosmetic industry. Topical formulations primarily are applied to treat local problems. The undoubted advantage of the method over oral administration is that the active ingredient avoids the GI tract, as a result of which the first pass-effect is not to be expected, thus a lower dose is sufficient and the number of undesirable side effects is significantly lower. In addition, the skin is easily accessible and the various topical formulations (e.g. creams, ointments, gels etc.) are easy to self-administer [79].

Topically applied drugs can pass through the epidermis through three different pathways, via the appendageal, the transcellular and the intercellular route. Absorption by the appendages is negligible, molecules being absorbed mainly through the hair follicles, sweat and sebaceous glands. The transcellular pathway is chosen mainly by small, hydrophilic molecules, while lipophilic molecules are absorbed primarily through the intercellular pathway between cells [80].

2.1.3. Attempts to replace human skin samples

There is a growing medical, pharmaceutical and cosmetic need to develop different skin surrogates, which can be recapitulate the physiology of the human skin due to the ethical concerns of using animals, the limited availability of human skin samples and the differences in the physiology between the animal and human skin [78,81]. This is further exacerbated by the growing social pressure due to the use of animals, which is why the development and use of systems that do not require the use of animals under the "3R" rule is increasingly being promoted [78]. Furthermore, in 2013 the experimental use of animals for cosmetic purposes was banned in the EU [82].

Nowadays, various two-dimensional (2D) and three-dimensional (3D) culture systems are also available, which focus mostly just on the two upper layers of the skin. The great advantage of 2D systems, which are built up by 2D epidermal cell monolayers or dermo-epidermal bilayers using keratinocytes and fibroblasts, is that they are less expensive to produce than 3D systems, but they cannot fully reproduce the spatial structure of the skin [81]. Various natural or artificial polymers (polycaprolactone, poly(vinyl alcohol), chitosan, fibrin, alginate etc.) as a scaffold are applied in the design of these substituents, and collagen is often used in addition to the polymers to provide better mechanical and structural properties [78].

3D models already better mimic skin *in vivo* properties, but there are also a number of difficulties during the development due to the anatomical complexity of the skin, as this organ is densely interwoven with the blood vessels and lymphatics, innervated, and contains a number of appendages that play an important role in performing various biological functions. One of the biggest challenges is to design a continuous perfusable vascular network, however, proper innervation, pigmentation, incorporation of appendages and the formation of a third layer of skin, the hypodermis are also difficult [83]. In order to mimic the physiological properties of the skin as accurately as possible, 3D co-culture also requires modeling of different immune processes. This can be accomplished in different ways, either by adding cytokines to the system or by co-culturing the immune cells in the model [81].

DOI:10.15774/PPKE.ITK.2022.004

2.1.4. Characterization of psoriasis

In the following subsections, a chronic inflammatory skin disease, psoriasis, is briefly described. In addition to presenting the symptoms and histological changes, the immunopathogenetic model of the disease as well as possible therapies are described. The chapter concludes with a presentation of the properties of the TRPV1 and TRPA1 receptors studied in the experimental work, as well as a mouse model of Aldara-induced psoriasis-like inflammation.

2.1.4.1. Etiology, clinical manifestation and histological properties of psoriasis

Psoriasis is a chronic, polygenic, T lymphocyte-mediated disease affecting about 2-3% of the whole population of the world. The root cause of this inflammatory disorder is still unknown, but the research on the etiology of psoriasis suggest that in addition to genetic factors, various environmental factors (eg. physical trauma or infections etc.) may play an important role, and even may exacerbate the appearance and symptoms of this disease [3,84,85].

Psoriasis causes a number of marked histological changes affecting both epidermis and dermis. It is characterized primarily by abnormal hyperproliferation of epidermal keratinocytes, leading to acanthosis, which means the thickening of the epidermis. Psoriatic lesions are accompanied by a reduction in the thickness of the stratum granulosum or even complete disappearance of this layer (hypogranulosis) and thickening of the stratum corneum (hyperkeratosis). These processes lead to the parakeratosis, appearance of nucleated keratinocytes in the epidermis. Moreover, histopathological stainings showed Munro microabscesses, infiltration of immune cells into the epidermis and dermis, dilated microvessels of dermal papillae and elongated rete ridges [3,85–87].

Several phenotypes of the disease are known, of which plaque-type psoriasis (psoriasis vulgaris) is the most prevalent, which appear as a well-demarcated, mostly circular patches of indurated and pruritic plaques covered by white-silvery scales under which the skin is red and erythematous. The second most common phenotype is guttate psoriasis, which usually appears in a small, tear-shaped form. In addition to these, pustular psoriasis, erythrodermic psoriasis and inverse psoriasis are also known. Although each phenotype has a slightly different appearance, but all of them are accompanied by itching, burning and pain. The most common area of appearance are limbs (knees and elbows), trunk and scalp, but they can also affect other areas of the body (e.g. inverse psoriasis typically affects in the first line in intertriginous areas

and body folds). Depending on what percentage of the patient's body surface area (BSA) is involved by this inflammatory disease, mild (less than 3%), moderate (3-10%), and severe (more than 10%) conditions are distinguished by the National Psoriasis Foundation [3]. The size of the affected skin surface area may vary from individual to individual, and patients also may experience difficulties caused by multiple phenotypes at the same time.

Although psoriasis mainly affects skin and joints (in some cases also the nails are involved as special skin appendages), other comorbidities (e.g. psychiatric, cardiovascular or rheumatological diseases) are also very common. Psoriatic arthritis (PsA) occurs with the highest incidence of comorbidities, which is typically preceded by the onset of cutaneous symptoms. Psoriasis is associated with various comorbidities, like cardiovascular diseases, metabolic syndrome, chronic kidney disease, inflammatory bowel disease (Crohn's disease) and also mental illnesses [3,86].

Depending on the severity of psoriasis, it has a significant impact on patients' quality of life, which in many cases affects not only their daily lives, but also their long-term goals. Pain, itching, social judgment and stigmatization caused by psoriasis can have a strong negative impact on their lives, causing serious psychological problems, like anxiety, depression or even suicidal ideation [3,86]. Treating the disease is a major burden for both patients and the health care system [85].

2.1.4.2. Prevalence and incidence of psoriasis

Psoriasis is a chronic inflammatory disease affecting approximately 125 million people worldwide (2-3% of the population), in the development of which, in addition to genetic factors, environmental factors also play a significant role. Presumably, the geographical location, the so-called 'equator effect', may also be a factor in the development of the disease, as the incidence of psoriasis is higher in countries at higher latitudes, while far fewer cases have been found in areas close to the Equator. The disease affects both women and men, and can develop at any age, but it typically affects children less than adults [3,84,88].

2.1.4.2. Immunopathogenesis of psoriasis

In addition to genetic factors, environmental triggers play a role in the development of this chronic inflammatory disease. The pathogenesis of psoriasis is a cascade of complex processes involving both the innate and adaptive immune systems, in which three cellular elements play a prominent role: keratinocytes, dendritic cells (DCs) and T cells. The disease

DOI:10.15774/PPKE.ITK.2022.004

has been thought to be the result of abnormal proliferation of epidermal keratinocytes, although the disease causes histopathological changes not only in the epidermis but also in the dermis. The role of the immune system in psoriasis was discovered after immunosuppressants (e.g. cyclosporine) successfully used to relieve symptoms [3,85,89,90].

The exact mechanism of the disease is not yet known, but one of its putative mechanisms is the dysfunction of the immune response to some external environmental effects (eg. trauma (Koebner phenomenon), injury, infection, medication etc.) on the skin particularly in genetically susceptible people. In response, epidermal keratinocytes begin to produce antimicrobial peptides (AMPs), several of which (cathelicidin (LL-37), β-defensins, S100 [3,85,86,91]) are typically upregulated in psoriasis. After the secretion of LL-37, it forms complexes with self-nucleotides. The LL-37-Deoxyribonucleic acid (DNA) complex binds to Toll-like receptor 9 (TLR9) on the surface of the plasmacytoid dendritic cell (pDC) [86,91,92], which is an antigen-presenting cell (APC), which in response initiates stimulation of various antigens. In parallel, LL-37-Ribonucleic acid (RNA) complexes bind to TLR7 of pDCs and stimulates dendritic, furthermore LL-37 bound to RNA exert their stimulatory effect through the TLR8 receptor on the surface of myeloid dendritic cells (mDCs). Activation of dendritic cells is a key step in the development of psoriasis, followed by the production of type I interferons (IFN; IFN-α, INF-β), which affects the formation of myeloid dendritic cells, the activation, differentiation and function of T helper 1 (Th1) and T helper 17 (Th17) cells, furthermore IFN-γ and IL-17 secretion. Activated myeloid dendritic cells migrate into the lymphatic circulation where they secrete interleukin-23 (IL-23), interleukin-12 (IL-12) and TNF-α. IL-12 and IL-23 regulate Th1 and Th17 cells of the immune system. The adaptive immune system is involved in the maintenance of inflammation by activation of different subsets of T cells, of which Th1, Th17 and T helper 22 (Th22) are the most important. These T cells produce different cytokines and chemokines (IL-12, IL-17, interleukin-21 (IL-21), interleukin-22 (IL-22) and IL-23, TNF-α, IFN-γ etc.), which activates the proliferation of epidermal keratinocytes, which is one of the main characteristics of this inflammatory disease. Initially, the important role of INF-γ produced by Th1 cells was highlighted, so the first treatments focused on the IL-12/IFN-γ/Th1 axis, but these were unsuccessful [85,89,93]. Subsequently, the polarizing effect of IL-23 on Th17 cells became known, leading to a deeper understanding of the role of Th17 cells in psoriasis. IL-17, IL-21 and IL-22 produced by Th17 cells act primarily on the proliferation of keratinocytes. A number of therapies targeting the IL-23/IL-17 axis are available nowadays [3,85,86,89,90].

DOI:10.15774/PPKE.ITK.2022.004

2.1.4.3. Available therapeutic treatment options

Although the cause of psoriasis is still unknown, and the disease is still incurable, but various available therapeutic approaches are able to manage the symptoms successfully. Suitable treatment must be selected in each case according to the severity of psoriasis and the patient's needs, as age (children and women in child-bearing age or during pregnancy and breastfeeding need special attention, because some of the therapeutics are teratogenic) and other possible diseases and/or comorbidities (e.g. PsA or cardiovascular diseases) should also be taken into account [3,86,87]. In the following subsections, the therapies used nowadays are briefly described.

2.1.4.3.a Topical treatments

Topical treatments are one of the most commonly used therapies for the treatment of patients with mild to moderate psoriasis. During the treatment, corticosteroids and vitamin D analogues are used primarily. Corticosteroids act by binding to glucocorticoid receptors, they are available in a variety of formulations and doses depending on the steroid-sensitivity of the area of application. Many different vitamin D analogs (e.g. calcitriol, calcipotriene etc.) have been used successfully in the treatment of psoriasis, because by binding to the vitamin D receptor they play a role in the regulation of the immune process and in the normal proliferation of keratinocytes. These therapeutics are less effective than corticosteroids, but the number of side effects is also significantly lower. Both monotherapy and concomitant use with corticosteroids have also been applied. In addition to these therapeutics, anthralin, coal tar, calcineurin inhibitors and tazarotene are also used, but the frequency of their use is lower as topical treatments in management of psoriasis [3,87].

2.1.4.3.b Phototherapy

Phototherapy, like topical therapy, is a method used in patients with mild to moderate psoriatic lesions, especially when the disease affects a large area of the body surface, so the use of topical treatments is no longer beneficial. The mechanism of action of phototherapy is complex, it acts through T cells as well as through the modulation of inflammatory processes, which take place in psoriasis [3,87].

DOI:10.15774/PPKE.ITK.2022.004

2.1.4.3.c Systemic treatments

Systemic therapies are used in patients with moderate to severe psoriasis. Methotrexate, cyclosporine, acitretin, fumaric acid esters and apremilast are most commonly prescribed. These drugs are typically administered orally, with the exception of methotrexate, which is also administered as a subcutaneous injection. The mechanisms of action of systemic therapies are involved in the modulation of the inflammatory immune response, which varies from drug to drug. These therapeutics typically have many adverse effects and can cause severe damage to the liver and kidneys, therefore they should only be used under continuous medical supervision. Methotrexate and acitretin are also teratogenic, therefore they are not recommended for women in child-bearing age [3,87].

2.1.4.3.d Biologic treatments

Nowadays, various targeted biologic therapies (e.g. infliximab, adalimumab, ustekinumab etc.) are also available for patients, who suffer from moderate to severe psoriasis. These therapies primarily target one of the main steps in the complex immune response characteristic of psoriasis, acting through TNF-α signaling pathway or target the IL-23/Th17 axis (IL-23, IL-17 inhibitors). These medications are usually given by injection on a weekly basis [3,87].

2.1.4.4. Models for the study of psoriasis

Psoriasis, as we have seen in previous subsections, is a complex, multigenic immune-mediated disease whose exact pathogenesis has not yet been fully elucidated. The understanding of the complex pathological processes and histopathological alterations due to psoriasis is limited by the fact that the disease has so far only been identified in humans (apart from a few data in monkeys [94–96]) [97]. Psoriasis-like model systems are needed to discover the importance of the immunological, molecular and genetic processes behind this disease [3,86,87,98].

Although *in vitro* 2D and 3D models are already available [81,83], various *in vivo* murine models are mostly used. The model used is expected to mimic the characteristic histopathological abnormalities of psoriasis (e.g. abnormal proliferation of epidermal keratinocytes, acanthosis, hyperparakeratosis, changes in the granular layer, papillomatosis and the presence of inflammatory cells (different subsets of T cell, dendritic cells etc.)) and to

DOI:10.15774/PPKE.ITK.2022.004

respond well to therapies used to treat this inflammatory disease [99,100]. Animal models based on the method of the induction of psoriasis are divided into different groups: spontaneous, acute (inducible), xenotransplantation and genetically engineered animal (overexpressing or knock out) models [97,98,101]. In the next subsection, the mouse model of acute (inducible) psoriasis used in the experimental work is presented briefly.

2.1.4.4.a Mouse model of Aldara-induced psoriasis-like inflammation

In this murine model of psoriasis, topically applied Aldara cream containing 5% imiquimod (IMQ) is applied to induce skin inflammation. The active ingredient of the Aldara cream, imiquimod, is an imadazoquinoline derivative, which its physical properties, small size and hydrophobicity make it suitable for topical administration [102]. The cream was originally used to treat genital and perianal warts, actinic keratoses, squamous cell carcinomas and superficial basal cell carcinomas [102–104], however, psoriasis-like inflammatory side effects have been observed in susceptible individuals when applying the cream [103,105,106].

In 2009, van der Fits and colleagues proposed a mouse model for investigating of the pathological processes underlying psoriasis in which psoriasis-like symptoms – acanthosis, parakeratosis, epidermal thickening, erythema, scaling, vascular alterations and cellular infiltrates – were induced by repeated topical application of the 5% IMQ-containing cream. In their model, they also demonstrated the dependence on the IL-17/IL-23 axis, since the genetic knockout of these molecules prevents the onset of the psoriasis-like symptoms despite repeated daily IMQ treatment [100,102].

This model has enjoyed great popularity since its first appearance because, in addition to reflecting well the properties of the human phenotype of psoriasis, it is an easy-to-use model, which is relatively inexpensive [107]. Although the model has been used successfully in different mouse strains (eg. C57BL/6J, Balb/cJ, DBA/1 etc.), local and systemic responses to treatment showed strain-dependent aspects [102,108]. Furthermore, the comparability of the results is further complicated by the fact that in most experiments, different animals were used not only from different genetic backgrounds but also from different sexes [85,108,109].

The treatments usually involve the ears or a properly prepared, shaved back of the animals [102]. The first symptoms appear relatively early, 24 hours after the first treatment, but these changes are not thought to be due to imiquimod but to the biologically active isostearic acid, which is the major component of the vehicle in Aldara cream. Isostearic acid stimulates the activation of inflammasomes in keratinocytes, induces the production of proinflammatory

DOI:10.15774/PPKE.ITK.2022.004

cytokines and is also responsible for early changes in the epidermis (e.g. hyperproliferation and deaths of keratinocytes) [85,102–104,110]. However, most research focuses on the investigation of changes from day 2-3 onward, when symptoms of acute inflammation characteristic of psoriasis also began to appear [85,102].

Aldara cream exerts its psoriasis-inducing effect through several pathways. Imiquimod is a TLR7-agonist that exerts its effect primarily through the activation of TLR7 in mice and TLR7/8 in humans, which induce the NF-κB and myeloid differentiation primary response 88 (MyD88) signaling pathways. Furthermore, other mechanisms of action have also been hypothesized. On the one hand, IMQ may activate inflammasomes through the NLR family pyrin domain containing 3 (NALP3) pathway, and on the other hand, thought to act on adenosine receptors independently from the ligation of TLR [102]. This hypothesis is also confirmed by the fact that cells (e.g. keratinocytes) that do not express TLR7/8 can respond to imiquimod [102,103]. Activation of TLR by ligation and the MyD88 signaling pathway, as well as isostearic acid-induced changes, are essential for the development of a complete inflammatory response [102].

The undoubted advantage of this method is that it is simple, fast (most treatment protocols take 5-7 days), cost-effective and induces reproducible skin response. Moreover, unlike xenograft models, animals do not require special, pathogen free animal housing conditions [107,111]. The models well reflect the characteristic alterations caused by psoriatic inflammation, are suitable for examining the pathological processes underlying the disease, and mimic the dependence of the disease development on the IL-17/IL-23 axis [100,112]. The applicability of the model is limited by dehydration and severe systemic inflammation in animals due to the topical treatment of Aldara [107]. Common side effects include weight loss, splenomegaly (spleen enlargement), malaise and fever, which could potentially lead to death of mice [111,113]. It is also problematic that a large area of the dorsal skin of animals has to be treated, resulting in a higher use of animals, because separate groups of animals are needed to compare treated and untreated animals [107,111]. In addition to the large treatment area, unintended ingestion of the Aldara cream is thought to cause systemic inflammation. Oral uptake can influence the production of type I IFN, and may induce changes in the gut microbiome, which may affect the immune processes. Several solutions have been developed to eliminate all these phenomenons [107]. Grine and coworkers used a small plastic Elisabethan collar, preventing the treatment material from being licked [110]. Horváth and colleagues developed a treatment procedure using Finn chambers, in which, significantly smaller area is treated thanks to which a reduced amount of Aldara is needed to induce psoriasis-like

inflammation. However, this protocol makes it possible to reduce inter-animal differences, because it creates the opportunity to investigate the psoriasiform lesions and control skin areas within the same animal [107,111].

2.1.4.5. Role of TRPV1 and TRPA1 cation channels in skin

In mammals, at least 28 different transient receptor potential (TRP) ion channels are known, which can be classified into six different subfamilies, which are the transient potential receptor vanilloid (TRPV), transient receptor potential ankyrin (TRPA), transient receptor potential melastatin (TRPM), transient receptor potential mucolipin (TRPML), transient receptor potential canonical (TRPC) and transient receptor potential polycystin (TRPP) cation channels [114–116]. TRP ion channels are mostly built up from six transmembrane domains, a pore region and amino (N) and carboxyl (C) termini extending into the cytoplasm, which are assembled into tetramers [117,118]. These ion channels are selective for cations, but their degree of selectivity varies from cation to cation. Most channels are permeable non-selectively to both monovalent (Na^+) and divalent cations (Ca^{2+}, Mg^{2+}) [115], however, some TRP channels are highly selective for calcium or sodium ions [119]. The involvement of TRP ion channels in various physiological (e.g. thermosensation, mechanosensation etc.) and pathological processes has been supported by several studies [115,118–120]. In addition to cutaneous sensory neurons in the skin, the expression of TRP channels has been described in other non-neural cells which, although closely involved in certain cutaneous functions, could be associated with a number of pathological skin conditions [115,119,121].

The transient receptor potential of vanilloid 1 is mainly known to be activated by capsaicin, which is responsible for the pungent taste of hot peppers. The TRPV1 channels exhibit polymodal chemical and thermal sensitivity, they can be activated by both chemical (e.g. many different endo- and exogenous compounds, acidification) and physical stimulation (e.g. temperature >42 °C). The expression of TRPV1 ion channels are not confined just to cutaneous sensory neurons, because they are observed in a number of other cells in the skin, like in epidermal keratinocytes, in Langerhans cell, in sebocytes or in immune cells [119,121].

TRPA1 ion channels, like TRPV1 ion channels, can be activated in several ways, as in addition to the various compounds (e.g. cinnamaldehyde, mustard oil, cooling agents, cannabinoids, etc.), thermal and mechanical stimuli are also known as activators. It is mainly expressed in sensory neurons, but has also been shown to be present in non-neural cells (e.g. in epidermal keratinocytes, melanocytes and mast cells) [115,118,122].

DOI:10.15774/PPKE.ITK.2022.004

In many cases, these two TRP ion channels are expressed on cells simultaneously and play a very diverse role in the physiological processes of the skin [85,123]. Their role in various pathological processes affecting the skin (e.g. atopic dermatitis, psoriasis, contact dermatitis, pruritus etc.) has also been studied [5,6,115,124–127]. Riol-Blanco and her colleagues investigated the effect of resiniferatoxin (RTX) pretreatment on $TRPV1^+$ neurons in a model of imiquimod-induced psoriasiform inflammation, which resulted in a significant reduction in the inflammatory response [7]. Kemény and her colleagues investigated the role of the TRPA1 ion channel in psoriasis, and their results showed a positive regulatory role for TRPA1 [5].

2.2. Materials and methods

2.2.1. Development and evaluation of an artificial human skin substituent in a skin-on-a-chip device

2.2.1.1. Construction of artificial skin equivalent in a sample holder device

Cell-free polycaprolactone (PCL) membrane-covered collagen samples (mesh) and artificial skin equivalents used for the study the caffeine penetration were prepared and provided by members of the research group led by András Czirok (Eötvös Loránd University, Budapest). Both types of samples are based on an electrospun membrane stretched into a 3D printed sample holder.

To prepare the membranes, polycaprolactone pellets (Mw 70,000–90,000, 2-Oxepanone homopolymer, 6-Caprolactone polymer, Cat No.: 440744-500G, Sigma-Aldrich, Budapest, Hungary) were dissolved in a 1:1 (v/v) mixture of formic acid (88%, Cat No.: A118P-500, Fisher Chemical) and acetic acid (glacial, Cat. No.: BP2401-500, Fisher Chemical) to have 10 mL of a 15 w/v% solution [128], then stirred for at least 3 hours with a magnetic stirrer to completely dissolve the PCL pellets and to obtain a homogeneous solution. The prepared PCL solution was used within 3 hours and filled into a 6 mL syringe with a 18G needle gauge of 1.20 mm, then 26 kV electrospinning voltage was applied to the needle at room temperature. Electrospun membranes were collected on an aluminum foil (Reynolds Wrap, heavy duty) placed 23 cm from the needle.

The 3D printed sample holders consisted of two parts: a base and a ring element made of polylactic acid (PLA) filament by an Ultimaker Original+ printer. The base part contains a cylinder (6 mm wide and 2.5 mm tall), which was open at both ends, and which was joined to a 0.5 mm tall and 12 mm wide concentric disk with a 5.5 mm diameter inner hole. The other element of the sample holder is the cone shaped ring element (3 mm tall, with a 6.2 mm bottom

DOI:10.15774/PPKE.ITK.2022.004

and with a 6 mm top diameters) was devoted to tie down the stretched electrospun membrane (8 mm wide) on the top of the sample holder. Disinfection of the sample holder was performed with 70% ethanol for 20 minutes, then dried in a sterile hood.

The core of the 3D printed sample holder device was filled with 75 µL collagen-I gel (1.7 mg/mL, Corning, New York, NY, USA, Cat. No: 354236), the preparation of which was performed according to the manufacturer's instructions. Gelation of collagen-I occurred at 37°C for 30 minutes. In the next step, the electrospun membranes were coated by 5 µg/mL fibronectin (Sigma, St. Louis, MO, USA, Cat. No: F1141), which was followed by incubation in phosphate-buffered saline (PBS) for 5 hours at room temperature. The prepared sample holder device was incubated in cell culture medium 37 °C in a humidified incubator with 5% CO_2 atmosphere for 2 hours before use.

HaCaT immortalized human keratinocytes (Cell Lines Service GmbH., Eppelheim, Germany) were seeded on the surface of some cell-free PCL electrospun membranes, in order to model the outermost layer of the skin, the epidermis, for resulting contiguous cell layers. Dulbecco's Modified Eagle Medium (DMEM; Lonza, Basel, Switzerland, Cat. No.: 12-604F) medium supplemented with 10% fetal bovine serum (FBS; Gibco Thermo Fisher, Waltham, MA, USA) was used to culture HaCaT cells. The samples with HaCaT cell culture were maintained at 37°C and 5% CO_2. After the confluent layer was formed, the monolayers were washed twice with PBS, incubated in trypsin-ethylenediaminetetraacetic acid (EDTA; Lonza, Basel, Switzerland), resuspended in culture medium, and transferred to the 3D printed sample holder device. The cells adhered to the fibronectin-coated mesh and formed a confluent monolayer [129].

2.2.1.2. Human skin samples

Human abdominal skin samples removed by a plastic surgery used in the experiments were provided by Révész Plasztika (Budapest, Hungary). Experimental use of human tissue was performed in accordance with permission No. 6501-6/2019/EKU. After human abdominal samples were made available, they were prepared for transdermal studies by removing subcutaneous adipose tissue and stored at -80 ° C until use. Prior to the start of the experiments, the samples were thawed and then mechanically sensitized using 30-fold tape stripping. The samples were then cut to size and placed on the donor cell of the skin-on-a-chip device.

DOI:10.15774/PPKE.ITK.2022.004

2.2.1.3. Permeability studies in a skin-on-a-chip device

2.2.1.3.a Materials and solutions

Two types of perfusion fluids were used during the experimental work, aPPF for human samples and DMEM for cell-free PCL membrane-covered collagen samples (mesh) and HaCaT cell cultures. The composition of aPPF was the same as described previously (Subsection 1.2.1.). In the other experiments, DMEM was perfused in the microfluidic device.

2.2.1.3.b Topical caffeine cream formulation

A suspension cream containing 2% (w/w) of caffeine (Sigma-Aldrich, St. Louis, MO, United States) was used for skin equivalent, human abdominal skin samples and mesh. The ingredients of the cream are as follows: paraffin oil (Semmelweis University, University Pharmacy, Budapest, Hungary) 4.1%, vaseline ointment 47%, (which consists of polysorbate (Hungaropharma, Budapest, Hungary) 4%, paraffin oil 8%, vaselinum album (Hungaropharma, Budapest, Hungary) 26%, alcohol cetylstearylicum (Molarchemicals, Halásztelek, Hungary) 12%, propylene glycol 10% and purified water 40%.), propylene glycol (Hungaropharma, Budapest, Hungary) 10%, 0.547%-citric acid solution 14% and purified water 22.9% [129,130].

2.2.1.3.c Skin-on-a-chip diffusion study

In our laboratory, a polydimethylsiloxane (PDMS)-based microfluidic diffusion chamber has been developed for transdermal penetration studies [130–132]. The three main components of the device are the upper donor compartment, the middle sample compartment and the lower receptor compartment. Tissue sample, human skin equivalent or even membrane could be tested in this microfluidic device (skin-on-a-chip), one of these diffusion sample was placed in the middle compartment, and then on the top of that, the donor cell is fixed which is designed for holding the cream or gel containing the active ingredient to be tested. The diffusion surface of the donor cell was 0.5 cm^2, onto which 1000 μL of 2% caffeine cream was applied with a Microman E piston positive replacement gel pipette (Gilson, Middleton, WI, USA). During each experiment, the system was perfused at a flow rate of 4 uL/min and a collection vial placed at the outlet of the microfluidic channel was changed every 30 minutes. Samples were stored at -80 °C until spectrophotometric measurement.

During the penetration studies of human skin samples, aPPF was filled into a 5 mL syringe and was perfused through the microfluidic device, which was connected to a

DOI:10.15774/PPKE.ITK.2022.004

programmable syringe pump (NE-1000, New Era, Framingdale, NY, USA) through a Teflon tube.

In the case of the human skin equivalent, a different experimental design was used, which was justified by keeping the cells cultured on the surface of the mesh alive during the measurements. Cell-free PCL membranes were also measured in this changed system so that the properties of the mesh could be tested easily before working with the HaCaT cells. Cell culture medium (DMEM) was used as the perfusion fluid in the experiments to provide essential nutrients to the cells. DMEM was filled into a 10 mL programmable syringe, and similarly to the original experimental setup, it was connected to the microfluidic device via a Teflon tube. The system was placed in an incubator box providing a 5% CO_2 atmosphere at 37°C (Figure 7.). After the system was filled with DMEM, air bubbles were removed and a stable flow was established through the system, cell-free PCL mesh or artificial skin equivalents were carefully placed above the receptor cell of the skin-on-a-chip system. In the next step, the system was sealed with the donor cell, and then the cream formulation was placed over the sample (Figure 7.).

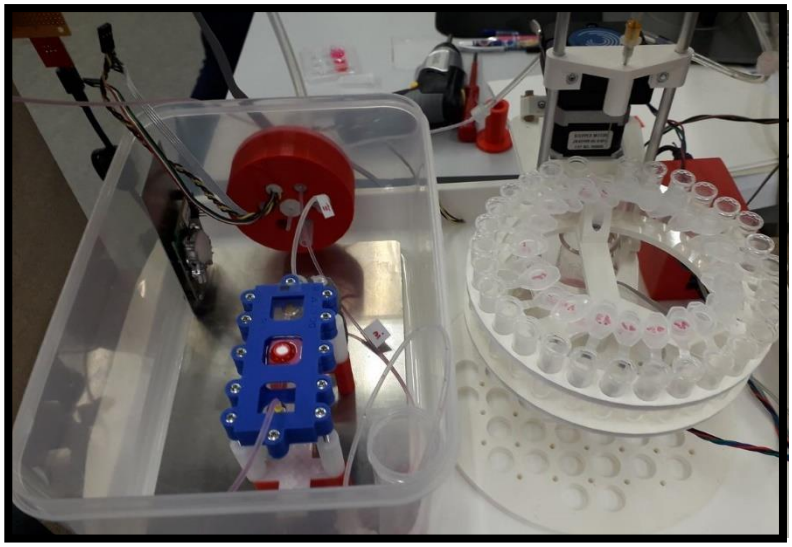

Figure 7. Demonstration of the experimental setup in which the permeability properties of cell-free PCL membrane and human skin equivalent were investigated. On the left of the image is the incubator box in which the microfluidic device was placed. On the right, the sample collection vials into which the caffeine-containing samples were collected.

2.2.1.3.d Spectrophotometric analysis

The absorbance of 2 µL of caffeine-containing samples was determined by spectrophotometric measurements at 273 nm by NanoDrop™ 2000 Spectrophotometer

DOI:10.15774/PPKE.ITK.2022.004

(ThermoFisher Scientific, Budapest, Hungary), which was followed by the calculation of the caffeine concentration based on a calibration curve.

2.2.2. Evaluation of imiquimod-induced psoriasiform inflammation in an *in vivo* mouse model

2.2.2.1. Materials, solutions and topical caffeine cream formulation

All animal experiments were performed under anesthesia using ketamine (Richter, Budapest, Hungary)/xylazine (Lavet, Kistarcsa, Hungary) anesthesia. In the *ex vivo* permeability studies of Aldara (5% IMQ; Meda Pharma, Budapest, Hungary) and vaseline treated dorsal skin samples were investigated, which was originated from C57BL/6J, TRPV1 KO, TRPA1 KO mice, for the transdermal penetration of topically applied caffeine cream with the same composition as described in Subsection 2.2.1.3.b.. Artificial peripheral perfusion fluid was used for perfusion of the microfluidic device. The composition of aPPF was described previously in Subsection 1.2.1..

2.2.2.2. Animals and treatments

Three different mouse strains were used for *in vivo* experiments: C57BL/6J (Jackson Laboratories, USA), TRPV1 KO (Jackson Laboratories, USA) and TRPA1 KO (the heterozygous breeding pair provided by Pierangelo Geppetti, University of Firenze, Italy) mice, which were provided by a research group led by Professor Dr. Gyulai Rolland at Pécs, where the animals were bred, housed and treated with vaseline or Aldara cream by his colleagues. The experiments were typically performed on 8-10 week old female animals weighing 20-25 g. Animals were bred and maintained under temperature-controlled (24-25 °C) standard pathogen-free conditions in the Laboratory Animal House of the Department of Pharmacology and Pharmacotherapy of the University of Pécs. Mice received food and water *ad libitum*. All procedures were carried out according to the 1998/XXVIII Act of the Hungarian Parliament on Animal Protection and Consideration Decree of Scientific Procedures of Animal Experiments (243/1988). Protocol was approved by the Ethics Committee on Animal Research of the University of Pécs, in full accordance with the Ethical Codex of Animal Experiments (license number: BA 02/2000-36/2017).

Every experimental intervention on the animals was performed under anesthesia using the anesthetic ketamine (100 mg/kg IP)/xylazine (5 mg/kg IP) solution. The day before the topical treatments, the hair was removed from the dorsal skin of the animals of all three mouse strains (C57BL/6J, TRPV1 and TRPA1) first with an electric shaver and then with depilatory

DOI:10.15774/PPKE.ITK.2022.004

cream (Veet, Slough, UK). The skin surface thus prepared was then treated with 62.5 mg Aldara (5% IMQ) cream on a daily basis for 4 consecutive days. Mice in the control group were prepared and treated in the same way, but here vaseline was applied on the shaved back skin instead of Aldara cream. The applied amount of the vaseline was the same as in the case of Aldara. 24 and 96 hours after the animals received their first treatment (Aldara or vaseline) were sacrificed by cervical dislocation to collect the dorsal skin samples for permeability [4,107,111].

2.2.2.3. *Ex vivo* drug penetration studies in a skin-on-a-chip device

The design and construction of the skin-on-a-chip device used for penetration testing of the dorsal skin samples of the three mouse stains (C57BL/6J, TRPV1 KO and TRPA1 KO) was the same as described in Subsection 2.2.1.3.c. The difference in the experimental setup was that aPPF solution was flowed through the device, which was used at laboratory temperature without a CO_2 atmosphere. The device was connected via a Teflon tube to a 5 mL syringe pre-filled with aPPF. During the experiments, a programmable syringe pump (NE-1000, New Era, Framingdale, NY, USA), which controlled the flow rate, which was continuous and constant at 4 µL/min. Samples passing through the device were collected into plastic sample collection tubes, which were replaced every 30 minutes and immediately placed on dry ice. Samples were stored in an ultra-freezer for spectrophotometric analysis at -80°C.

2.2.2.4. Spectrophotometric analysis

The caffeine content of the samples in the permeability studies was examined at 273 nm using NanoDrop™ 2000 Spectrophotometer (ThermoFisher Scientific, Budapest, Hungary). From the measured absorbance values the caffeine concentrations were determined based on a calibration curve.

2.2.2.5. Data analysis

Data analysis was performed by Microsoft Excel 2016 (Microsoft Corporation) and results are expressed as means ± SEM. Graphs showing the results of the diffusion studies were prepared in OriginPro 2022 Software (OriginLab Corporation).

DOI:10.15774/PPKE.ITK.2022.004

2.3. Results

2.3.1. Comparison of time-course of caffeine penetration of human abdominal skin samples, cell-free electrospun PCL membrane and artificial skin substituents

The drug penetration patterns of three different samples (I refer to these as diffusion samples in the dissertation) – human abdominal skin, cell-free electrospun PCL membrane (mesh) and HaCaT cell culture on electrospun membrane (human skin substituent) – were compared with topically applied 2% caffeine cream in a skin-on-a-chip-device.

The human skin equivalent developed by the research group led by András Czirok was a greatly minimized model of the dermal barrier, which was focused on the outermost layer of the skin. HaCaT cells corresponding to the epidermal layer of the skin were cultured on the surface of the fibronectin-coated electrospun PCL nanomesh in order to provide appropriate mechanical properties, which were required for the experimental investigation of the samples. After reaching a confluent monolayer, the mesh was placed in the 3D printed sample holder, and secured tightly with the ring element.

Cell-free PCL nanomeshes were used as a control sample and similarly to the human skin equivalents, their transdermal transport measurements were performed in a humidified incubator with 5% CO_2 at 37°C, so that the role of cells in the artificial human skin substituent could be measured exclusively. The caffeine content of the samples was examined by spectrophotometric analysis. A similar penetration pattern was observed for all three samples, with the maximum penetration (C_{max}) measured 1 h after the onset of caffeine exposure (Figure 8.). Thereafter, by the end of the experiment, the caffeine concentration-time curves of human skin equivalent and human abdominal skin showed the same course. In contrast, a continuous decrease in caffeine concentration was observed for the cell-free PCL membrane, which can be explained by the fact that during the experiment, the close contact between the caffeine cream placed in the donor cell and the membrane was disrupted by dissolving the cream in the perfused medium. This process resulted in a gradually decreasing contact between the topically applied cream and the diffusion sample thanks to which a reduced amount of caffeine could pass through the membrane by passive diffusion. This phenomenon was not observed in the case of human skin substituents, because the cells were actively involved in the penetration of caffeine, thus preventing the formation of gaps separating the cream from their surface.

DOI:10.15774/PPKE.ITK.2022.004

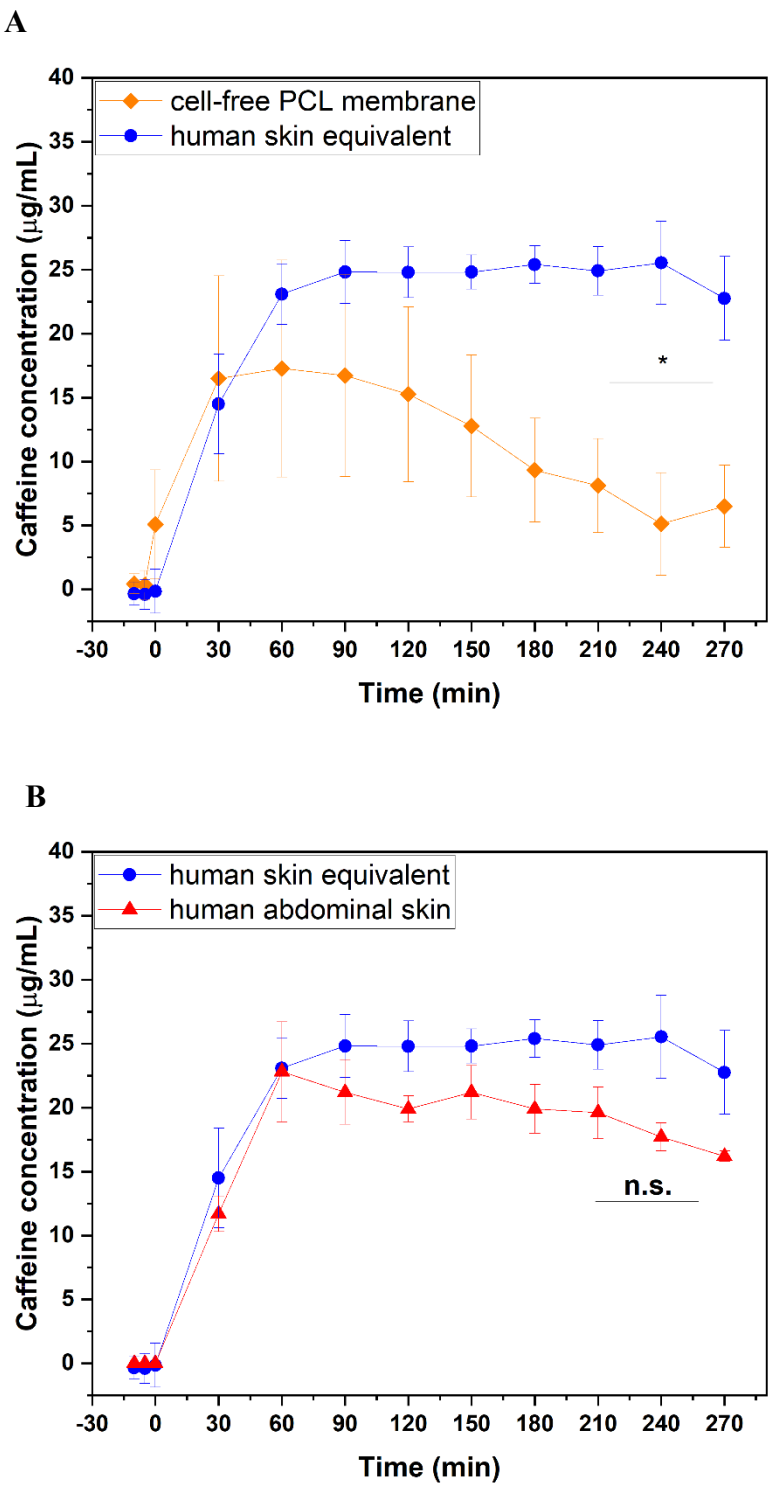

Figure 8. After assembling the device, the flow in the microfluidic channel was checked for obstruction and the presence of caffeine contamination was ruled out by analytical analysis of the sample. The caffeine cream was placed in the donor cell at time $t = 0$, then samples were taken every 30 min after caffeine exposure for all three different diffusion samples (human abdominal skin, cell-free electrospun PCL membrane and human skin equivalent). Comparison of caffeine penetration pattern of (A) cell-free PCL membrane and human skin equivalent (B)

DOI:10.15774/PPKE.ITK.2022.004

human skin equivalent and human abdominal skin. For each sample, at least three parallel measurements (n = 3) were performed, results are expressed as mean ± SEM, $p < 0.05$ indicates statistically significant difference between caffeine penetration in mesh or human skin equivalent. Statistical analysis was performed in Microsoft Excel 2016 Software.

2.3.2. Comparison of the degree of caffeine penetration during the progression of imiquimod-induced psoriasiform inflammation in C57BL/6J (WT), TRPA1 KO and TRPV1 KO mouse strains

Permeability of a hydrophilic model drug, caffeine was examined in a skin-on-a-chip device using the dorsal skin of three different mouse strains (C57BL/6J, TRPV1 KO and TRPA1 KO) treated with Aldara or vaseline for 24 hours or 96 hours. The pattern of caffeine penetration in each mouse strain was significantly different between the two treatments, since the permeability of healthy (vaseline-treated) skin was significantly lower than that of psoriatic (Aldara-treated) skin which is due to impairment of skin barrier function due to the psoriasiform inflammation (Figure 9.). Furthermore, the two observation time points allowed us to examine the time progression of the disease. No significant differences in the time-characteristics of caffeine penetration were seen for the three strains, just a moderate reduction of the caffeine absorption was observed in case of TRPA1 KO and C57BL/6J animals between the two observation points. However, no remarkable difference was seen between the Aldara treatments for 24 hours and 96 hours in TRPV1 KO animals, which is in accordance with the results published by Zhou et al. [6].

DOI:10.15774/PPKE.ITK.2022.004

A

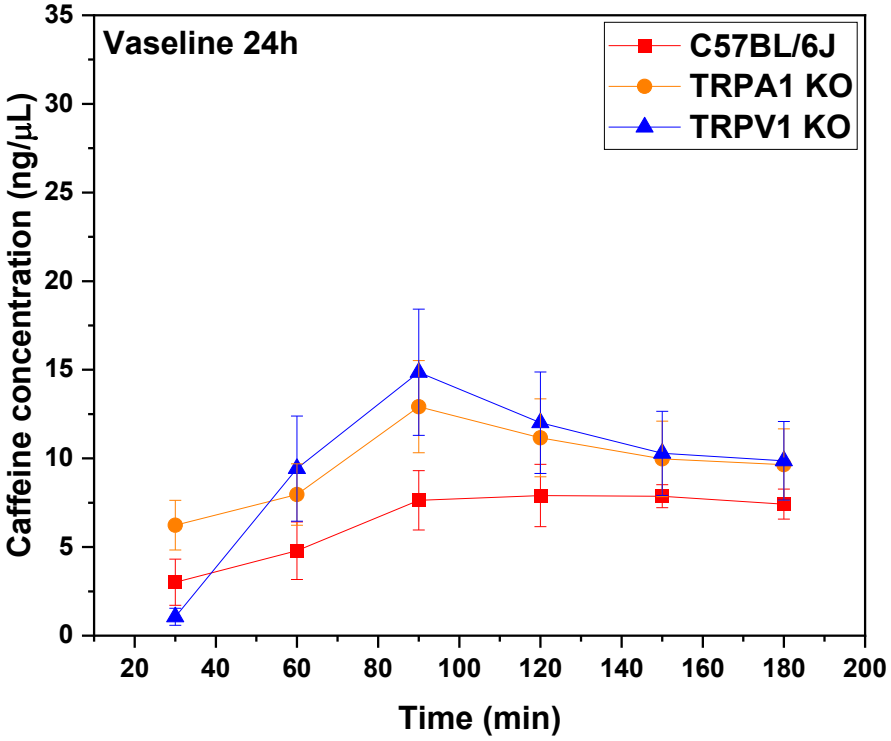

B

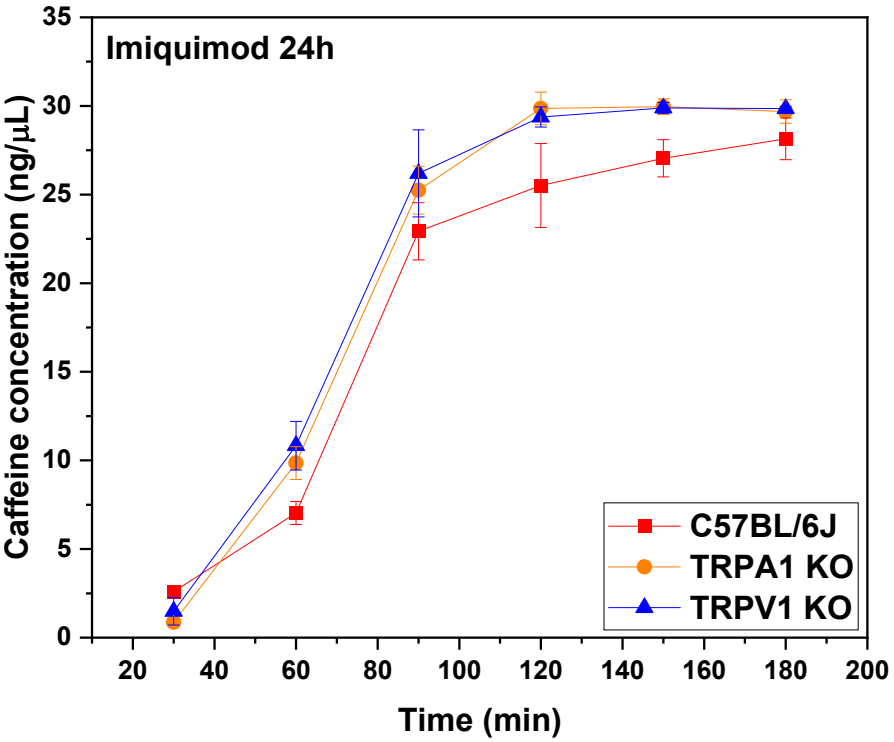

DOI:10.15774/PPKE.ITK.2022.004

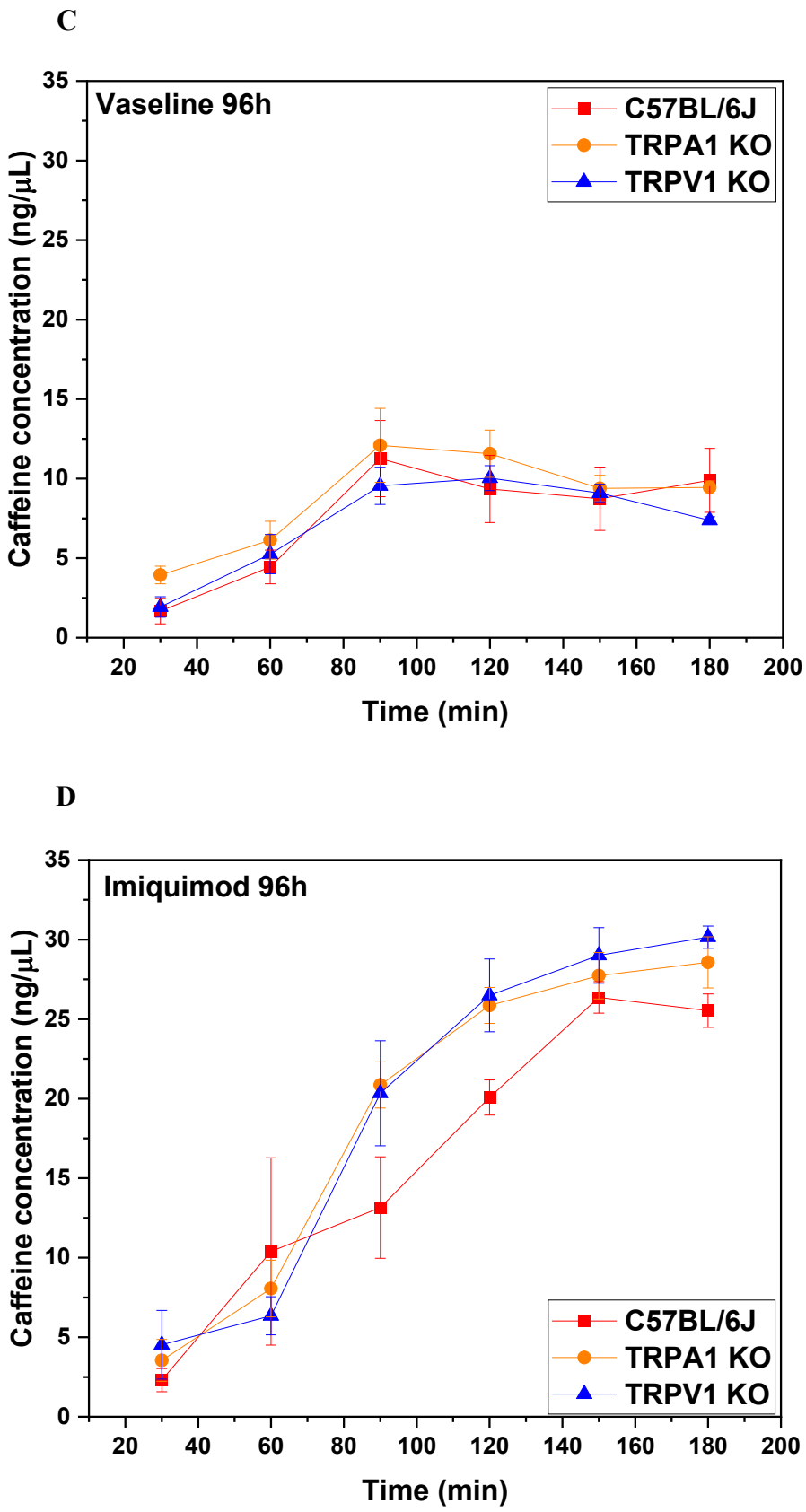

Figure 9. Concentration-time profiles of caffeine penetration using the dorsal skin samples of three different mouse strains (A) after 24 hours vaseline-treatment, (B) after 24 hours

DOI:10.15774/PPKE.ITK.2022.004

imiquimod-treatment, (C) after 96 hours vaseline-treatment and (D) after 96 hours imiquimod treatment. Red, orange and blue symbols represent the average concentration of caffeine obtained from C57BL6/J (WT), TRPA1 KO, TRPV1 KO mice. In each case, at least three independent measurements were performed (n = 3), results are expressed as means ± SEM.

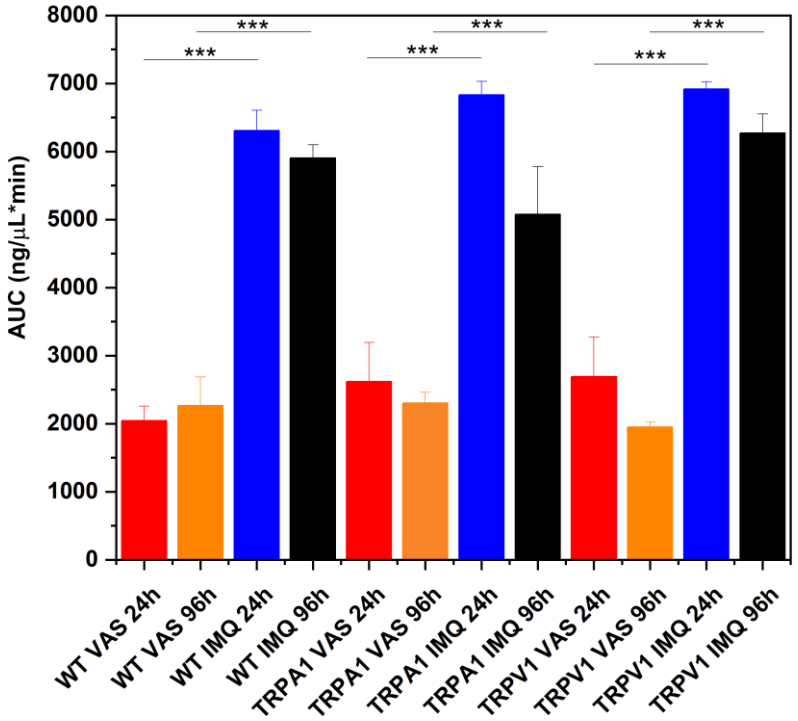

Figure 10. The AUC values were calculated from caffeine concentration-time profiles and are presented as means ± SEM (***: $p < 0.001$). Statistical analysis was performed in Microsoft Excel 2016 Software.

2.4. Discussion

2.4.1. Comparison of time-course of caffeine penetration of human abdominal skin samples, cell-free electrospun PCL membrane and artificial skin substituents

There is a growing demand in the pharmaceutical and cosmetics industries for different skin models that can mimic the physiological properties of the skin and can be used in various drug testing, toxicology and penetration studies. There have been a number of attempts to meet this need, however, due to the structural and functional differences of the layers of the skin, it remains difficult to develop suitable models in which the physiological or pathological processes of the skin can be adequately examined. In addition to the many macrostructures in the skin (the skin tissue is densely interwoven with blood and lymphatic vessels, it contains

DOI:10.15774/PPKE.ITK.2022.004

various appendages, and is innervated), that are very difficult to form in these models, and providing adequate mechanical strength is also a problem in many cases.

During the experimental work, an artificial skin substituent was developed, and its properties and utility was compared to human abdominal skin excised during plastic surgery by permeability studies in a skin-on-a-chip device. The developed skin equivalents focused on mimicking only the properties of the outermost main layer, the epidermis (stratum corneum). To ensure adequate mechanical stability for the skin equivalents, an electrospun PCL membrane was used as the scaffold of the model, which was coated with fibronectin, and on the surface of which HaCaT cells were cultured. I compared the permeability properties of the cell-free PCL membranes, the skin equivalents and the excised human abdominal skin samples in a skin-on-a-chip device by applying 2% caffeine containing gel. Although the time-course of caffeine concentration determined by spectrophotometric analysis confirmed the similarity of the human abdominal skin samples and the artificial human skin equivalents, this model has a number of limitations that can be refined and improved. This human skin equivalent can be supplemented with additional layers of skin, primarily the dermis, using fibroblast cells and type I collagen. Further, in the present work, permeability of a single hydrophilic model drug, caffeine, was investigated, so in order to fully characterize the model, it would be worthwhile to investigate the penetration profile of additional (more lipophilic) molecules.

2.4.2. Comparison of the degree of caffeine penetration during the progression of imiquimod-induced psoriasiform inflammation in C57BL/6J (WT), TRPA1 KO and TRPV1 KO mouse strains

Psoriasis is an inflammatory skin disease with many unpleasant symptoms, but nowadays various treatment options are available, which can be used as a monotherapy or in combination. In addition to systemic therapy, phototherapy and topical treatments are also available, furthermore, biological therapies that inhibit the TNF-α or IL-17/IL-23 axis are gaining ground [3,86]. However, despite all the advances so far, topical treatment is also required in many cases, which makes the study of the penetration of topically applied therapeutics important.

The skin is not only a kind of physical barrier in the epidermis (mainly localized in the stratum corneum), but also a (bio)chemical and immunological barrier against various effects, for which its molecular structure and the cells present in each layer are responsible. Psoriasis is an immune-mediated disease of unknown origin. Genetic and environmental factors play a crucial role in its pathogenesis. This chronic inflammatory disease causes lesions not only in

DOI:10.15774/PPKE.ITK.2022.004

the outermost layer of the skin, in the epidermis (e.g. abnormal proliferation of epidermal keratinocytes, acanthosis, hypogranulosis, hyperkeratosis, parakeratosis etc.), but also affects the proper functionality of the dermis due to the immunological processes. As a result of the disease, the barrier function of the skin deteriorates significantly, the degree of permeability increases, which is a novel observation of our research group and is discussed in the dissertation.

The role of TRPA1 and TRPV1 ion channels in the pathogenesis of psoriasis was investigated in permeability studies by topically applied caffeine cream in a skin-on-a-chip device. The involvement of both ion channels in the pathomechanism of psoriasis has been extensively studied by other authors. These studies were mostly performed using imiquimod-induced psoriasiform inflammation in mice, that described the protective role of TRPA1 and the active role in the inflammation of TRPV1 [5–7]. Genetic deletion of TRPA1 and TRPV1 ion channels did not result in a significant change in the skin permeability compared to wild type control animals (C57BL/6J). For TRPA1 and C57BL/6J animals, a moderate decrease in permeability was observed comparing the two observation points. These results may indicate that both physical and immunological barriers are damaged during the psoriasiform inflammation, but the thickening of the skin due to hyperproliferation of keratinocytes leads to the inhibition of the transappendageal penetration of caffeine in the late phase of the disease. These results were supported by plaque formation and intense exfoliation due to psoriasiform inflammation on electron micrographs. From these results, it can be concluded that in the early stages of the development of this disease, topical formulations can be used more effectively to treat and improve dermatological symptoms.

DOI:10.15774/PPKE.ITK.2022.004

3. Summary

The following two subsections present the new scientific results as thesis points separately for each research project.

3.1. New scientific results

In the first part of the dissertation, the results related to the investigation of the nasal barrier were presented, where the central research question was the further characterization of pathological aging processes in two neurodegenerative disease models. The research was divided into three main parts: investigation of the alterations in the nasal barrier function, the cerebral levels of different cytokines and the cerebro-morphological status of the APOB-100 and APP-PSEN1 mice.

Thesis 1: *In our experiments (dual-probe in vivo microdialysis in APOB-100, APP-PSEN1 and wild type mice), it was demonstrated that nasal barrier function is unchanged in the transgenic models, and no significant role of P-gp can be seen in the process of cerebral absorption of intranasally administered quinidine. In addition, I showed that an inflammatory balance shift is present in the brain of transgenic animals, increased cerebral levels of VEGF, PDGF-BB and IL-17A were demonstrated in APOB-100 mice and upregulation of resistin, IL-17A and GM-CSF in APP-PSEN1 mice were shown. These cytokines can be relevant biomarkers of the pathological processes.*

Related publication: [J1]

In the second part, I presented some new results of two research topics related to the dermal barrier. The first research topic was the investigation of the permeability of human abdominal skin and a human skin substituent with a topically applied caffeine cream in a skin-on-a-chip-device. It was followed by the presentation of the second research topic, which was connected to the altered properties of the dermal barrier due to psoriasis. The involvement of different TRP ion channels in this chronic immune-mediated disease has been confirmed recently, thus the genetic deletion of TRPA1 and TRPV1 cation channels on the permeability was studied in a mouse model of Aldara-induced psoriasis-like inflammation using topically applied caffeine cream in a microfluidic device.

DOI:10.15774/PPKE.ITK.2022.004

Thesis 2: *I compared the time-course of caffeine on three different diffusion samples – human abdominal skin, cell-free electrospun PCL membrane (mesh) and HaCaT cell culture on electrospun membrane (human skin substituent) – with a topically applied 2% caffeine cream in a skin-on-a-chip-device. The time-course of caffeine concentration determined by spectrophotometric analysis confirmed the similarity of the human skin substituent and the human abdominal skin, demonstrating that the skin equivalent is, although greatly simplified, a sufficient model system for studying transdermal absorption.*

Related publication: [J2]

Thesis 3: *I compared the degree and kinetics of the penetration of topically applied 2% caffeine cream during the time-progression of Aldara-induced psoriasiform inflammation in C57BL/6J (WT), TRPA1 KO and TRPV1 KO mouse skins in a skin-on-a-chip device. Based on the caffeine content of the samples of the vaseline-treated and Aldara-treated groups determined by spectrophotometric analysis, it can be concluded that psoriasiform inflammation significantly disintegrated the dermal barrier, resulting in a significant increase in the permeability of psoriasiform-inflamed skin.*

Related publication: [J3]

3.2. Új tudományos eredmények

A disszertáció első részében a nazális barrier vizsgálatával kapcsolatos eredmények kerültek bemutatásra, amelynek középpontjában a két, a vascularis és az Alzheimer-típusú neurodegenerációt kísérő patológiás öregedési folyamatok jellemzése állt. A kísérleti munkát három fő részre lehetett osztani: az APOB-100 és APP-PSEN1 állatok nazális barrier funkciójának, a különböző citokinek agyi szintjének és agyi morfológiai állapotának vizsgálatára.

1. tézis: *APOB-100, APP-PSEN1 és vad típusú egereken végzett kétpróbás in vivo mikrodialízis kísérleteink eredményei alátámasztották, hogy a nazális barrier funkciója változatlan a transzgenikus modellekben, valamint a P-gp szerepe nem szignifikáns az intranazális kezeléssel adott kinidin agyi felszívódásának folyamatában. Kimutattam továbbá, hogy a transzgenikus állatok agyában gyulladásos egyensúlyeltolódás tapasztalható, APOB-100 egerekben a VEGF,*

DOI:10.15774/PPKE.ITK.2022.004

PDGF-BB és IL-17A, míg az APP-PSEN1 állatokban a rezisztin, IL-17A és GM-CSF agyi szintje emelkedett. Ezek a citokinek a patológiás folyamatok releváns biomarkerei lehetnek.

Kapcsolódó publikáció: [J1]

A dolgozat második részében a dermális barrier vizsgálatával kapcsolatos két kutatási téma új eredményei kerültek bemutatásra. Először az újonnan fejlesztett humán bőrekvivalens és a humán hasi bőr permeabilitási tulajdonságait hasonlítottam össze topikálisan alkalmazott koffein krém penetrációjának vizsgálatával egy mikrofluidikai eszközben. Ezt követte a dermális barrier pikkelysömör következtében megváltozott tulajdonságainak vizsgálata. A közelmúltban több kutatás is igazolta a különböző TRP ioncsatornák szerepét ebben a krónikus immunmediált betegségben. A TRPA1 és a TRPV1 kationcsatornák genetikai deléciójának permeabilitásra gyakorolt hatását vizsgáltam Aldara-indukált psoriasiform dermatitis modellben transzdermálisan alkalmazott koffein krémmel, mikrofluidikai készülékben.

2. tézis: *Összehasonlítottam a koffein penetrációs mintázatát három különböző diffúziós mintán – humán hasi bőrön, elektroszövéssel előállított sejtmentes PCL membránon és elektroszövéssel előállított membránon tenyésztett HaCaT sejtkultúrán (humán bőrszubsztituens) – topikálisan alkalmazott 2%-os koffein krém felvitelét követően mikrofluidikai eszközben. A spektrofotometriás analízissel meghatározott koffeinkoncentráció időbeli lefutása megerősítette a humán bőrszubsztituens és a humán hasi bőr permeabilitási tulajdonságainak hasonlóságát, bizonyítva, hogy a felhasznált bőrekvivalens, bizonyos esetekben elégséges, bár nagymértékben leegyszerűsített modellrendszer a transzdermális felszívódás tanulmányozására.*

Kapcsolódó publikáció: [J2]

3. tézis: *Összehasonlítottam a topikálisan alkalmazott 2%-os koffeintartalmú krém penetrációjának mértékét és kinetikáját az Aldara-indukált pikkelysömörszerű gyulladás időbeli kialakulása során C57BL/6J (WT), TRPA1 KO és TRPV1 KO egérbőrökben skin-on-a-chip eszközben. A vazelinnel kezelt és az Aldara-kezelt csoportok mintáinak spektrofotometriás analízissel meghatározott koffeintartalma alapján megállapítható, hogy a pikkelysömörszerű gyulladás jelentősen károsította a dermális barriert, ami a pikkelysömörrel érintett, gyulladt bőr permeabilitásának jelentős mértékű növekedését eredményezte.*

DOI:10.15774/PPKE.ITK.2022.004

Kapcsolódó publikáció: [J3]

4. References

4.1. List of publications related to the thesis points

[J1] Varga-Medveczky, Zs.; Kovács, N.; Tóth, M.E.; Sántha, M.; Horváth, I.; Bors, L.A.; Fónagy, K.; Imre, T.; Szabó, P.; Máthé, D.; et al. Age-Related Inflammatory Balance Shift, Nasal Barrier Function, and Cerebro-Morphological Status in Healthy and Diseased Rodents. *Front Neurosci 2021, 15, 700729*, doi:10.3389/fnins.2021.700729

[J2] Tarnoki-Zach, J.*; Mehes, E.*; Varga-Medveczky, Z.*; Isai, D. G.; Barany, N.; Bugyik, E.; Revesz, Z.; Paku, S.; Erdo, F.; Czirok, A. Development and Evaluation of a Human Skin Equivalent in a Semiautomatic Microfluidic Diffusion Chamber. *Pharmaceutics 2021*, 13, 910. https://doi.org/10.3390/pharmaceutics13060910
* These authors contributed equally to this work.

[J3] Kocsis, D.; Horváth, S.; Kemény, Á.; Varga-Medveczky, Z.; Pongor, C.; Molnár, R.; Mihály, A.; Farkas, D.; Naszlady, B.M.; Fülöp, A.; et al. Drug Delivery through the Psoriatic Epidermal Barrier—A "Skin-On-A-Chip" Permeability Study and Ex Vivo Optical Imaging. *Int. J. Mol. Sci. 2022*, 23, 4237. https://doi.org/10.3390/ijms23084237

4.2. Other publications related to the topic of the doctoral dissertation

- D. Kocsis, V. Klang, E.-M. Schweiger, Zs. Varga-Medveczky, A. Mihály, Cs. Pongor, Zs. Révész, Z. Somogyi, F. Erdő: Characterization and *ex vivo* evaluation of excised skin samples as substitutes for human dermal barrier in pharmaceutical and dermatological studies, *Skin Res Technol. 2022,* 1-13. 10.1111/srt.13165

- Varga-Medveczky, Z.; Kocsis, D.; Naszlady, M.B.; Fónagy, K.; Erdő, F. Skin-on-a-Chip Technology for Testing Transdermal Drug Delivery—Starting Points and Recent Developments. *Pharmaceutics 2021*, 13, 1852. https://doi.org/10.3390/ pharmaceutics13111852

- Ponmozhi, J.; Dhinakaran, S.; Varga-Medveczky, Z.; Fónagy, K.; Bors, L.A.; Iván, K.; Erdő, F. Development of Skin-On-A-Chip Platforms for Different Utilizations: Factors to Be Considered. *Micromachines 2021*, 12, 294. https://doi.org/10.3390/mi12030294

4.3. In Annual Issues of the Doctoral School Faculty of Information Technology and Bionics

- Zs. Varga-Medveczky: Comparative evaluation of permeability properties of a human skin equivalent and *ex vivo* human skin tissue in skin-on-a-chip microfluidic device, *PhD Proceeding Annual Issues of the Doctoral School Faculty of Information Technology and Bionics,* (in press) (2022)

- Zs. Varga-Medveczky: Characterization of age-related neurodegenerative disease models in transgenic animals, *PhD Proceeding Annual Issues of the Doctoral School Faculty of Information Technology and Bionics,* vol. 16:2021 pp. 115-118., 4 p. (2021)

- Zs. Varga-Medveczky: Drug delivery through physiological barriers: investigation of the permeability of blood-brain barrier, nasal- and dermal-barriers, *PhD Proceeding Annual Issues of the Doctoral School Faculty of Information Technology and Bionics,* vol. 15:2020 pp. 117-119., 3 p. (2020)

- Zs. Varga-Medveczky: 3D two-photon imaging of putative visual cortical functional modules, *PhD Proceeding Annual Issues of the Doctoral School Faculty of Information Technology and Bionics,* vol. 14:2019 pp. 159-161., 3 p. (2019)

4.4. Other publications related to other previous research activity of the author

- Y. Miele, Y..; Medveczky, Zs.; Holló, G.; Tegze, B.; Derényi, I.; Hórvölgyi, Z.; Altamura, E.; Lagzi, I.; Rossi, F.: Self-division of giant vesicles driven by an internal enzymatic reaction, *Chem. Sci., 2020*,11, 3228-3235, https://doi.org/10.1039/C9SC05195C

- Szabó, Z.; Volk, J.; Horváth, Zs. E.; Medveczky, Zs.; Czigány, Zs.; Vad, K.; Baji, Zs.: Atomic layer deposition and annealing of Ga doped ZnO films, *Material Science In Semiconductor Processing, 2019,* 101 pp. 95-102, 8p., https://doi.org/10.1016/j.mssp.2019.05.028

- Miele, Y.; Medveczky, Z.; Lagzi, I.; Budroni, M.A.; Rossi, F.: (2019) The Relevance of Inorganic Nonlinear Chemical Reactions for the Origin of Life Studies. In: Cagnoni S., Mordonini M., Pecori R., Roli A., Villani M. (eds) *Artificial Life and Evolutionary Computation. WIVACE 2018. Communications in Computer and Information Science, vol 900.* Springer, Cham., https://doi.org/10.1007/978-3-030-21733-4_11

DOI:10.15774/PPKE.ITK.2022.004

- Tóth-Szeles, E.; Medveczky, Zs.; Holló, G.; Horváth, J.; Szűcs, R.; Nakanishi, H.; Lagzi, I.: pH mediated kinetics of assembly and disassembly of molecular and nanoscopic building blocks, *Reac Kinet Mech Cat, 2018*, 123, 323–333., https://doi.org/10.1007/s11144-017-1312-x

DOI:10.15774/PPKE.ITK.2022.004

Acknowledgements

First and foremost, I would like to thank my supervisor, Franciska Erdő, who gave me the opportunity to work in her lab during my PhD studies. I would like to thank the careful supervision, her ideas, guidance, and advice she has provided over the years.

Many thanks to Luca Bors for her support, I received from her at the beginning of my experimental work so that I could always turn to her not only during her PhD studies but also thereafter. I am deeply grateful to the senior researchers, Ágnes Bajza and Katalin Fónagy, to whom I could turn at any time with any questions, to whom I thank very much for the joint work and for helping me at all times. I thank Dorottya Kocsis for her cheerful work together, her precision and her dedication. In addition, I would like to thank all the students at the Laboratory of Microdialysis and Pharmacological Techniques with whom I could work together in various projects.

I would like to thank all the senior researchers with whom I had the opportunity to work together on various research topics during my PhD studies. First of all, I would like to thank Pál Szabó and Tímea Imre for their dedicated work and expertise in the bioanalysis of the microdialysis samples.

I am very grateful to András Czirok for giving me the opportunity to work with his laboratory, and I am very grateful for his guidance during the joint experimental work. I would especially like to thank Júlia Tárnoki-Zách for her patience and perseverance in developing a system, in which the permeability measurements of human skin equivalents could be performed. I would like to acknowledge Előd Méhes for his work with HaCaT cells. I really enjoyed working together with all of them.

I would like to express my gratitude to all the members of the research team led by Prof. Rolland Gyulai for their joint work. I am grateful to Ágnes Kemény, Erika Pintér and Rolland Gyulai for their joint strict opinion and the precision with which the manuscript made from the results of joint work was prepared. Special thanks to Szabina Horváth for her precise work in preparing the psoriatic dorsal skin samples used in the permeability measurements. I would like to thank Csaba Pongor for his help with the electron microscopic measurements.

I am grateful to Zoltán Gáspári and Bálint Péterfia for allowing me to perform spectrophotometric measurements in their laboratory at any time.

I would like to thank Márton Bese Naszlady and Kristóf Iván for the continuous post-production of the microchips used in permeability studies.

DOI:10.15774/PPKE.ITK.2022.004

I would like to take this opportunity to thank the management of the Doctoral School for all the help they have given me in recent years. I am very grateful to Gábor Szederkényi for always finding solutions to any questions I have during my doctoral studies. I would also like to thank the University for its financial support (KAP and ÚNKP-21-3 New National Excellence Program of the Ministry for Innovation and Technology from the source of the National Research, Development and Innovation Fund), which I received in the last years.

I would like to express my deep gratitude to the head of the Doctoral Office, Katinka néni, for all the kindness, precision and encouragement with which she has continuously supported me during my PhD studies, and I am grateful for her precise administrative work.

I am grateful to my previous supervisors for all their contributions to learning about the beauties of the research. I would like to express my gratitude to my very first supervisor, Zsófia Baji, who introduced me to the world of research.

Thank you to my friends, Rita, Dóri, Noémi and Emil, for their support in recent years in times of difficulty and those who have been delighted with my success.

Last but not least, I owe it to my family with the greatest gratitude. Thank you to my parents for giving me the opportunity to learn what I really want. I am deeply grateful, my aunt, Ildikó, and my uncle, Győző, for always being able to turn to them. Finally, thanks to my husband, Tamás, for always standing by me and supporting me.

DOI:10.15774/PPKE.ITK.2022.004

List of figures

Appendix

DOI:10.15774/PPKE.ITK.2022.004

List of tables

Appendix

DOI:10.15774/PPKE.ITK.2022.004

Appendix

Table 1. Age and weight of animals used for microdialysis

Group of mice (n = 5)	Age (month) (mean ± SD)	Body weight (g) (mean ± SD)
Wild type	7 ± 0.00	29.85 ± 2.36
ApoB-100	9.2 ± 0.45	30.00 ± 2.92
APP-PSEN1	13 ± 0.00	28.78 ± 2.32

Table 2. Age, weight, weight of left hemispheres and amounts of total protein measured in animals used for ELISA cytokine assay

Group of mice (n = 5)	Age (month) (mean ± SD)	Body weight (g) (mean ± SD)	Weight of the pool of homogenized hemispheres (g)	Total protein (µg/mL)
Wild type	10.5 ± 0.00	30.88 ± 1.86	0.1556 ± 0.0139	586.45
ApoB100	7.8 ± 2.08	31.90 ± 5.17	0.1381 ± 0.0090	557.70
APP-PSEN1	10.6 ± 0.22	31.11 ± 2.07	0.1540 ± 0.0152	638.35

Table 3. Age of animals used for MRI

Group of mice	Number of used animals	Age (day) (mean ± SD)
Wild type	4	301.8 ± 44.0
ApoB-100	4	345.5 ± 5.50
APP-PSEN1	2	398.5 ± 0.50

Table 4. Parameters of venous microdialysis probe parameters

Catalogue number	Microbiotech MAB 1.4.3. PES
Membrane	PES
Cut off	6 kD
Lot number	20-014

Table 5. Parameters of brain microdialysis probe parameters

Catalogue number	Microbiotech MAB 8.4.3. PES
Membrane	PES
Cut off	6 kD
Lot number	20-013

DOI:10.15774/PPKE.ITK.2022.004

Table 6. Location of 24 different cytokines in Mouse Cytokine ELISA Plate Array I (EA-4003)

	1	2	3	4	5	6	7	8	9	10	11	12
A	TNFα	IL-1α	PDGF-BB	TNFα	IL-1α	PDGF-BB	TNFα	IL-1α	PDGF-BB	TNFα	IL-1α	PDGF-BB
B	IGF-1	IL-1β	β-NGF	IGF-1	IL-1β	β-NGF	IGF-1	IL-1β	β-NGF	IGF-1	IL-1β	β-NGF
C	VEGF	G-CSF	IL-17A	VEGF	G-CSF	IL-17A	VEGF	G-CSF	IL-17A	VEGF	G-CSF	IL-17A
D	IL-6	GM-CSF	IL-2	IL-6	GM-CSF	IL-2	IL-6	GM-CSF	IL-2	IL-6	GM-CSF	IL-2
E	FGFβ	MCP-1	IL-4	FGFβ	MCP-1	IL-4	FGFβ	MCP-1	IL-4	FGFβ	MCP-1	IL-4
F	IFNγ	MIP-1α	IL-10	IFNγ	MIP-1α	IL-10	IFNγ	MIP-1α	IL-10	IFNγ	MIP-1α	IL-10
G	EGF	SCF	Resistin	EGF	SCF	Resistin	EGF	SCF	Resistin	EGF	SCF	Resistin
H	Leptin	Rantes	IL-12	Leptin	Rantes	IL-12	Leptin	Rantes	IL-12	Leptin	Rantes	IL-12

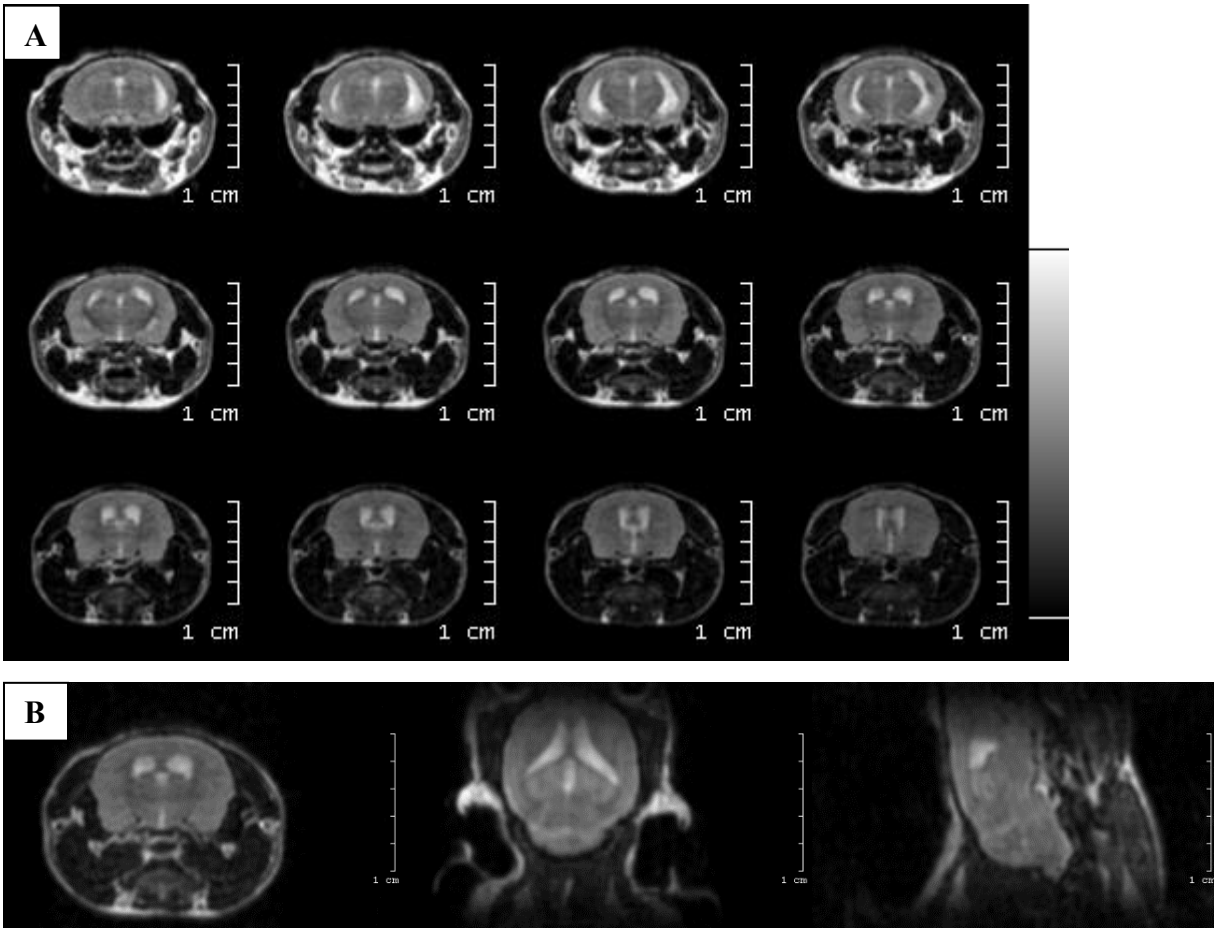

Figure 1. (A) Coronal MR images of APOB-100 transgenic mice in different slice (B) MR images of APOB-100 transgenic mice in different positions of the skull (coronal, axial and sagittal planes)

DOI:10.15774/PPKE.ITK.2022.004

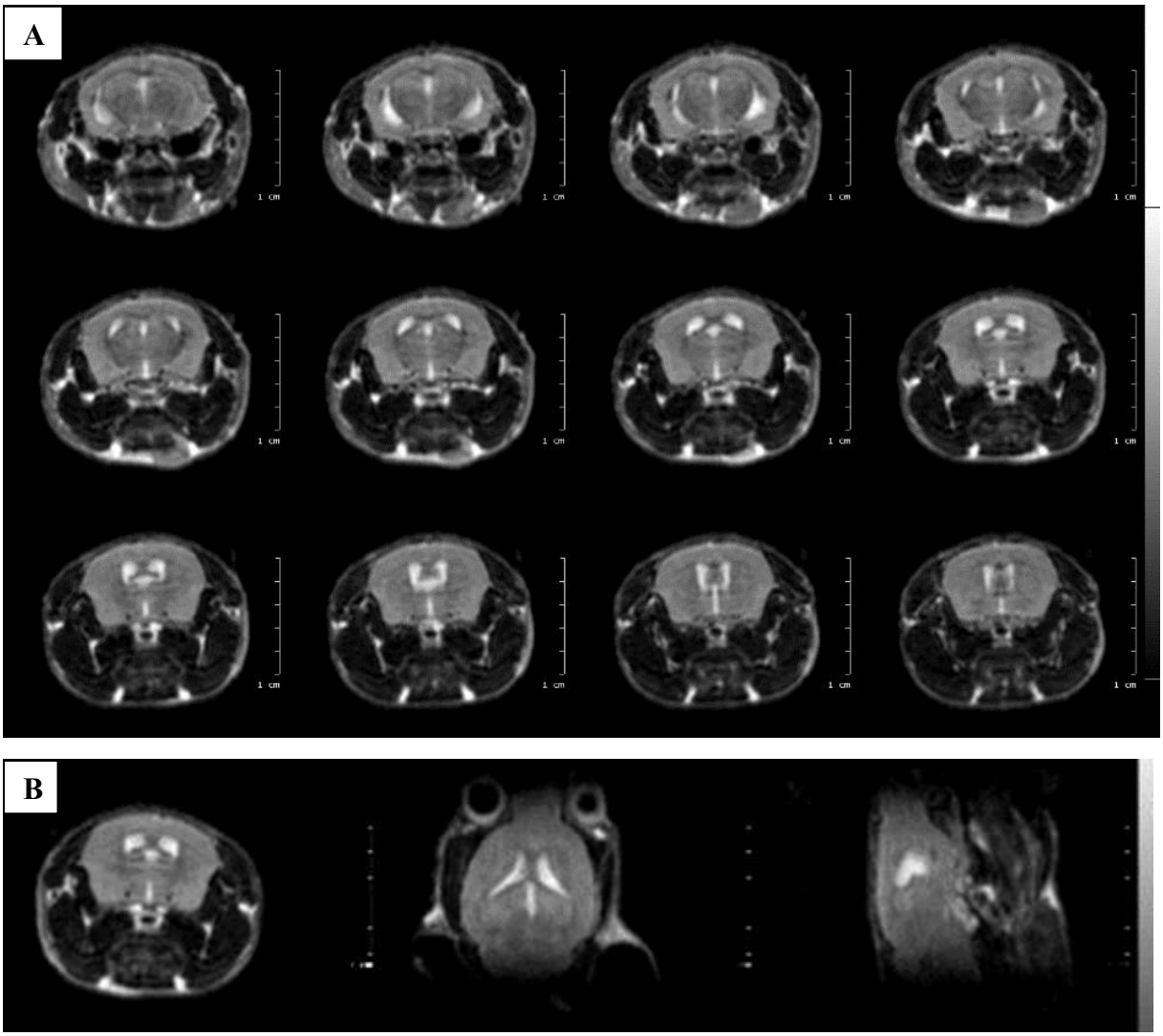

Figure 2. (A) Coronal MR images of APP-PSEN1 transgenic mice in different slice (B) MR images of APP-PSEN1 transgenic mice in different positions of the skull (coronal, axial and sagittal planes)

DOI:10.15774/PPKE.ITK.2022.004

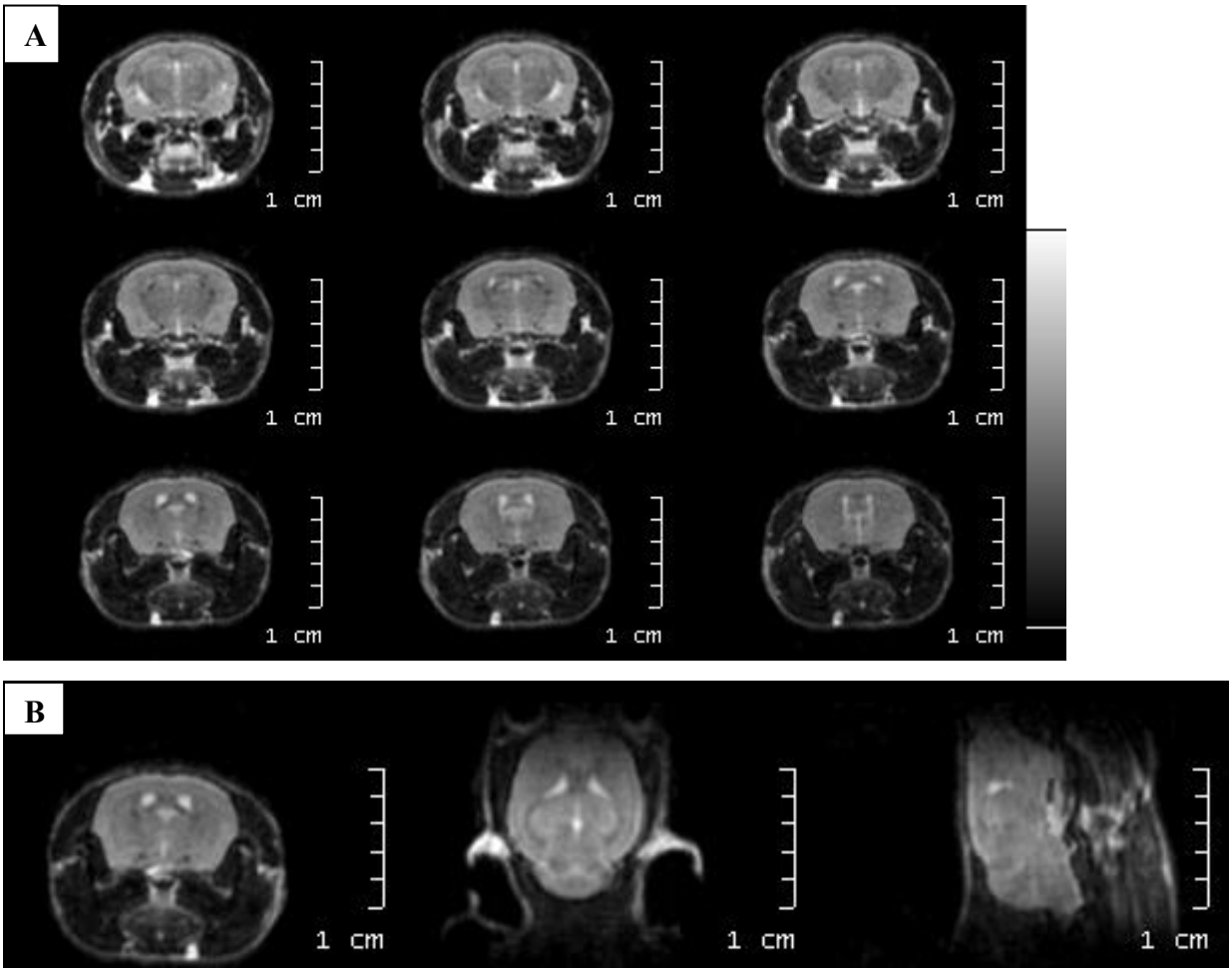

Figure 3. (A) Coronal MR images of WT transgenic mice in different slice (B) MR images of WT transgenic mice in different positions of the skull (coronal, axial and sagittal planes)

Bibliography

1. Bors, L.; Tóth, K.; Tóth, E.Z.; Bajza, Á.; Csorba, A.; Szigeti, K.; Máthé, D.; Perlaki, G.; Orsi, G.; Tóth, G.K.; et al. Age-Dependent Changes at the Blood-Brain Barrier. A Comparative Structural and Functional Study in Young Adult and Middle Aged Rats. *Brain Research Bulletin* **2018**, *139*, 269–277, doi:10.1016/j.brainresbull.2018.03.001.
2. Bors, L.A.; Bajza, Á.; Mándoki, M.; Tasi, B.J.; Cserey, G.; Imre, T.; Szabó, P.; Erdő, F. Modulation of Nose-to-Brain Delivery of a P-Glycoprotein (MDR1) Substrate Model Drug (Quinidine) in Rats. *Brain Research Bulletin* **2020**, *160*, 65–73, doi:10.1016/j.brainresbull.2020.04.012.
3. Greb, J.E.; Goldminz, A.M.; Elder, J.T.; Lebwohl, M.G.; Gladman, D.D.; Wu, J.J.; Mehta, N.N.; Finlay, A.Y.; Gottlieb, A.B. Psoriasis. *Nat Rev Dis Primers* **2016**, *2*, 16082, doi:10.1038/nrdp.2016.82.
4. Kocsis, D.; Horváth, S.; Kemény, Á.; Varga-Medveczky, Z.; Pongor, C.; Molnár, R.; Mihály, A.; Farkas, D.; Naszlady, B.M.; Fülöp, A.; et al. Drug Delivery through the Psoriatic Epidermal Barrier—A "Skin-On-A-Chip" Permeability Study and Ex Vivo Optical Imaging. *International Journal of Molecular Sciences* **2022**, *23*, 4237, doi:10.3390/ijms23084237.
5. Kemény, Á.; Kodji, X.; Horváth, S.; Komlódi, R.; Szőke, É.; Sándor, Z.; Perkecz, A.; Gyömörei, C.; Sétáló, G.; Kelemen, B.; et al. TRPA1 Acts in a Protective Manner in Imiquimod-Induced Psoriasiform Dermatitis in Mice. *J Invest Dermatol* **2018**, *138*, 1774–1784, doi:10.1016/j.jid.2018.02.040.
6. Zhou, Y.; Follansbee, T.; Wu, X.; Han, D.; Yu, S.; Domocos, D.T.; Shi, Z.; Carstens, M.; Carstens, E.; Hwang, S.T. TRPV1 Mediates Inflammation and Hyperplasia in Imiquimod (IMQ)-Induced Psoriasiform Dermatitis (PsD) in Mice. *J Dermatol Sci* **2018**, *92*, 264–271, doi:10.1016/j.jdermsci.2018.11.009.
7. Riol-Blanco, L.; Ordovas-Montanes, J.; Perro, M.; Naval, E.; Thiriot, A.; Alvarez, D.; Paust, S.; Wood, J.N.; von Andrian, U.H. Nociceptive Sensory Neurons Drive Interleukin-23-Mediated Psoriasiform Skin Inflammation. *Nature* **2014**, *510*, 157–161, doi:10.1038/nature13199.
8. Obermeier, B.; Daneman, R.; Ransohoff, R.M. Development, Maintenance and Disruption of the Blood-Brain Barrier. *Nat Med* **2013**, *19*, 1584–1596, doi:10.1038/nm.3407.
9. Daneman, R.; Agalliu, D.; Zhou, L.; Kuhnert, F.; Kuo, C.J.; Barres, B.A. Wnt/Beta-Catenin Signaling Is Required for CNS, but Not Non-CNS, Angiogenesis. *Proc Natl Acad Sci U S A* **2009**, *106*, 641–646, doi:10.1073/pnas.0805165106.
10. Zhao, Z.; Nelson, A.R.; Betsholtz, C.; Zlokovic, B.V. Establishment and Dysfunction of the Blood-Brain Barrier. *Cell* **2015**, *163*, 1064–1078, doi:10.1016/j.cell.2015.10.067.
11. Winkler, E.A.; Bell, R.D.; Zlokovic, B.V. Central Nervous System Pericytes in Health and Disease. *Nat Neurosci* **2011**, *14*, 1398–1405, doi:10.1038/nn.2946.
12. Abbott, N.J.; Rönnbäck, L.; Hansson, E. Astrocyte-Endothelial Interactions at the Blood-Brain Barrier. *Nat Rev Neurosci* **2006**, *7*, 41–53, doi:10.1038/nrn1824.
13. Erdő, F.; Bors, L.A.; Farkas, D.; Bajza, Á.; Gizurarson, S. Evaluation of Intranasal Delivery Route of Drug Administration for Brain Targeting. *Brain Res Bull* **2018**, *143*, 155–170, doi:10.1016/j.brainresbull.2018.10.009.
14. Anderson, K.D.; Pan, L.; Yang, X.; Hughes, V.C.; Walls, J.R.; Dominguez, M.G.; Simmons, M.V.; Burfeind, P.; Xue, Y.; Wei, Y.; et al. Angiogenic Sprouting into Neural Tissue Requires Gpr124, an Orphan G Protein-Coupled Receptor. *Proc Natl Acad Sci U S A* **2011**, *108*, 2807–2812, doi:10.1073/pnas.1019761108.
15. Daneman, R. The Blood-Brain Barrier in Health and Disease. *Ann Neurol* **2012**, *72*, 648–672, doi:10.1002/ana.23648.

16. Erdő, F.; Denes, L.; de Lange, E. Age-Associated Physiological and Pathological Changes at the Blood-Brain Barrier: A Review. *J Cereb Blood Flow Metab* **2017**, *37*, 4–24, doi:10.1177/0271678X16679420.
17. Tietz, S.; Engelhardt, B. Brain Barriers: Crosstalk between Complex Tight Junctions and Adherens Junctions. *J Cell Biol* **2015**, *209*, 493–506, doi:10.1083/jcb.201412147.
18. Sorokin, L. The Impact of the Extracellular Matrix on Inflammation. *Nat Rev Immunol* **2010**, *10*, 712–723, doi:10.1038/nri2852.
19. Agrawal, S.; Anderson, P.; Durbeej, M.; van Rooijen, N.; Ivars, F.; Opdenakker, G.; Sorokin, L.M. Dystroglycan Is Selectively Cleaved at the Parenchymal Basement Membrane at Sites of Leukocyte Extravasation in Experimental Autoimmune Encephalomyelitis. *J Exp Med* **2006**, *203*, 1007–1019, doi:10.1084/jem.20051342.
20. Sá-Pereira, I.; Brites, D.; Brito, M.A. Neurovascular Unit: A Focus on Pericytes. *Mol Neurobiol* **2012**, *45*, 327–347, doi:10.1007/s12035-012-8244-2.
21. Lindahl, P.; Johansson, B.R.; Levéen, P.; Betsholtz, C. Pericyte Loss and Microaneurysm Formation in PDGF-B-Deficient Mice. *Science* **1997**, *277*, 242–245, doi:10.1126/science.277.5323.242.
22. Zlokovic, B.V. The Blood-Brain Barrier in Health and Chronic Neurodegenerative Disorders. *Neuron* **2008**, *57*, 178–201, doi:10.1016/j.neuron.2008.01.003.
23. Daneman, R.; Zhou, L.; Kebede, A.A.; Barres, B.A. Pericytes Are Required for Blood-Brain Barrier Integrity during Embryogenesis. *Nature* **2010**, *468*, 562–566, doi:10.1038/nature09513.
24. Gee, J.R.; Keller, J.N. Astrocytes: Regulation of Brain Homeostasis via Apolipoprotein E. *Int J Biochem Cell Biol* **2005**, *37*, 1145–1150, doi:10.1016/j.biocel.2004.10.004.
25. Bendayan, R.; Ronaldson, P.T.; Gingras, D.; Bendayan, M. In Situ Localization of P-Glycoprotein (ABCB1) in Human and Rat Brain. *J Histochem Cytochem* **2006**, *54*, 1159–1167, doi:10.1369/jhc.5A6870.2006.
26. Hoyk, Z.; Tóth, M.E.; Lénárt, N.; Nagy, D.; Dukay, B.; Csefová, A.; Zvara, Á.; Seprényi, G.; Kincses, A.; Walter, F.R.; et al. Cerebrovascular Pathology in Hypertriglyceridemic APOB-100 Transgenic Mice. *Front Cell Neurosci* **2018**, *12*, 380, doi:10.3389/fncel.2018.00380.
27. Erdő, F. Microdialysis Techniques In Pharmacokinetic and Biomarker Studies. Past, Present and Future Directions. A Review. *Journal of Clinical & Experimental Pharmacology* **2015**, *5*, 1–11, doi:10.4172/2161-1459.1000180.
28. de Lange, E.C.; de Boer, A.G.; Breimer, D.D. Methodological Issues in Microdialysis Sampling for Pharmacokinetic Studies. *Adv Drug Deliv Rev* **2000**, *45*, 125–148, doi:10.1016/s0169-409x(00)00107-1.
29. Törnqvist, E.; Annas, A.; Granath, B.; Jalkesten, E.; Cotgreave, I.; Öberg, M. Strategic Focus on 3R Principles Reveals Major Reductions in the Use of Animals in Pharmaceutical Toxicity Testing. *PLoS One* **2014**, *9*, e101638, doi:10.1371/journal.pone.0101638.
30. Hammarlund-Udenaes, M. The Use of Microdialysis in CNS Drug Delivery Studies. Pharmacokinetic Perspectives and Results with Analgesics and Antiepileptics. *Adv Drug Deliv Rev* **2000**, *45*, 283–294, doi:10.1016/s0169-409x(00)00109-5.
31. Leng, S.X.; McElhaney, J.E.; Walston, J.D.; Xie, D.; Fedarko, N.S.; Kuchel, G.A. ELISA and Multiplex Technologies for Cytokine Measurement in Inflammation and Aging Research. *J Gerontol A Biol Sci Med Sci* **2008**, *63*, 879–884, doi:10.1093/gerona/63.8.879.
32. Engvall, E.; Perlmann, P. Enzyme-Linked Immunosorbent Assay, Elisa. 3. Quantitation of Specific Antibodies by Enzyme-Labeled Anti-Immunoglobulin in Antigen-Coated Tubes. *J Immunol* **1972**, *109*, 129–135.
33. Hegedűs, G. Development and application of enzyme-linked immunosorbent assay (ELISA) systems, PhD thesis (in Hungarian).; Budapest, Hungary, 2003.

34. Guo, H.; Siu, W.; D'Arcy, R.C.; Black, S.E.; Grajauskas, L.A.; Singh, S.; Zhang, Y.; Rockwood, K.; Song, X. MRI Assessment of Whole-Brain Structural Changes in Aging. *Clin Interv Aging* **2017**, *12*, 1251–1270, doi:10.2147/CIA.S139515.
35. Park, J.-H.; Seo, S.W.; Kim, C.; Kim, G.H.; Noh, H.J.; Kim, S.T.; Kwak, K.-C.; Yoon, U.; Lee, J.M.; Lee, J.W.; et al. Pathogenesis of Cerebral Microbleeds: In Vivo Imaging of Amyloid and Subcortical Ischemic Small Vessel Disease in 226 Individuals with Cognitive Impairment. *Ann Neurol* **2013**, *73*, 584–593, doi:10.1002/ana.23845.
36. Prins, N.D.; Scheltens, P. White Matter Hyperintensities, Cognitive Impairment and Dementia: An Update. *Nat Rev Neurol* **2015**, *11*, 157–165, doi:10.1038/nrneurol.2015.10.
37. Nicolakakis, N.; Hamel, E. Neurovascular Function in Alzheimer's Disease Patients and Experimental Models. *J Cereb Blood Flow Metab* **2011**, *31*, 1354–1370, doi:10.1038/jcbfm.2011.43.
38. Tóth, M.E.; Dukay, B.; Hoyk, Z.; Sántha, M. Cerebrovascular Changes and Neurodegeneration Related to Hyperlipidemia: Characteristics of the Human ApoB-100 Transgenic Mice. *Curr Pharm Des* **2020**, *26*, 1486–1494, doi:10.2174/1381612826666200218101818.
39. Bereczki, E.; Bernát, G.; Csont, T.; Ferdinandy, P.; Scheich, H.; Sántha, M. Overexpression of Human Apolipoprotein B-100 Induces Severe Neurodegeneration in Transgenic Mice. *J Proteome Res* **2008**, *7*, 2246–2252, doi:10.1021/pr7006329.
40. Caramelli, P.; Nitrini, R.; Maranhão, R.; Lourenço, A.C.; Damasceno, M.C.; Vinagre, C.; Caramelli, B. Increased Apolipoprotein B Serum Concentration in Alzheimer's Disease. *Acta Neurol Scand* **1999**, *100*, 61–63, doi:10.1111/j.1600-0404.1999.tb00724.x.
41. Sabbagh, M.; Zahiri, H.R.; Ceimo, J.; Cooper, K.; Gaul, W.; Connor, D.; Sparks, D.L. Is There a Characteristic Lipid Profile in Alzheimer's Disease? *J Alzheimers Dis* **2004**, *6*, 585–589; discussion 673-681, doi:10.3233/jad-2004-6602.
42. Asaad, M.; Lee, J.H. A Guide to Using Functional Magnetic Resonance Imaging to Study Alzheimer's Disease in Animal Models. *Dis Model Mech* **2018**, *11*, dmm031724, doi:10.1242/dmm.031724.
43. Tanifum, E.A.; Dasgupta, I.; Srivastava, M.; Bhavane, R.C.; Sun, L.; Berridge, J.; Pourgarzham, H.; Kamath, R.; Espinosa, G.; Cook, S.C.; et al. Intravenous Delivery of Targeted Liposomes to Amyloid-β Pathology in APP/PSEN1 Transgenic Mice. *PLOS ONE* **2012**, *7*, e48515, doi:10.1371/journal.pone.0048515.
44. Zlokovic, B.V. Neurovascular Pathways to Neurodegeneration in Alzheimer's Disease and Other Disorders. *Nat Rev Neurosci* **2011**, *12*, 723–738, doi:10.1038/nrn3114.
45. Sagare, A.P.; Bell, R.D.; Zlokovic, B.V. Neurovascular Dysfunction and Faulty Amyloid β-Peptide Clearance in Alzheimer Disease. *Cold Spring Harb Perspect Med* **2012**, *2*, a011452, doi:10.1101/cshperspect.a011452.
46. Gyires, K.; Fürst, Z. *Basics of Pharmacology (in Hungarian)*; 2011th ed.;
47. Bartels, A.L.; Willemsen, A.T.M.; Kortekaas, R.; de Jong, B.M.; de Vries, R.; de Klerk, O.; van Oostrom, J.C.H.; Portman, A.; Leenders, K.L. Decreased Blood-Brain Barrier P-Glycoprotein Function in the Progression of Parkinson's Disease, PSP and MSA. *J Neural Transm (Vienna)* **2008**, *115*, 1001–1009, doi:10.1007/s00702-008-0030-y.
48. Garbuzova-Davis, S.; Rodrigues, M.C.O.; Hernandez-Ontiveros, D.G.; Louis, M.K.; Willing, A.E.; Borlongan, C.V.; Sanberg, P.R. Amyotrophic Lateral Sclerosis: A Neurovascular Disease. *Brain Res* **2011**, *1398*, 113–125, doi:10.1016/j.brainres.2011.04.049.
49. Zhong, Z.; Deane, R.; Ali, Z.; Parisi, M.; Shapovalov, Y.; O'Banion, M.K.; Stojanovic, K.; Sagare, A.; Boillee, S.; Cleveland, D.W.; et al. ALS-Causing SOD1 Mutants Generate Vascular Changes Prior to Motor Neuron Degeneration. *Nat Neurosci* **2008**, *11*, 420–422, doi:10.1038/nn2073.

50. Greenway, M.J.; Andersen, P.M.; Russ, C.; Ennis, S.; Cashman, S.; Donaghy, C.; Patterson, V.; Swingler, R.; Kieran, D.; Prehn, J.; et al. ANG Mutations Segregate with Familial and "sporadic" Amyotrophic Lateral Sclerosis. *Nat Genet* **2006**, *38*, 411–413, doi:10.1038/ng1742.
51. Lambrechts, D.; Storkebaum, E.; Morimoto, M.; Del-Favero, J.; Desmet, F.; Marklund, S.L.; Wyns, S.; Thijs, V.; Andersson, J.; van Marion, I.; et al. VEGF Is a Modifier of Amyotrophic Lateral Sclerosis in Mice and Humans and Protects Motoneurons against Ischemic Death. *Nat Genet* **2003**, *34*, 383–394, doi:10.1038/ng1211.
52. Kooij, G.; van Horssen, J.; de Lange, E.C.M.; Reijerkerk, A.; van der Pol, S.M.A.; van Het Hof, B.; Drexhage, J.; Vennegoor, A.; Killestein, J.; Scheffer, G.; et al. T Lymphocytes Impair P-Glycoprotein Function during Neuroinflammation. *J Autoimmun* **2010**, *34*, 416–425, doi:10.1016/j.jaut.2009.10.006.
53. Kirk, J.; Plumb, J.; Mirakhur, M.; McQuaid, S. Tight Junctional Abnormality in Multiple Sclerosis White Matter Affects All Calibres of Vessel and Is Associated with Blood-Brain Barrier Leakage and Active Demyelination. *J Pathol* **2003**, *201*, 319–327, doi:10.1002/path.1434.
54. van Horssen, J.; Bö, L.; Vos, C.M.P.; Virtanen, I.; de Vries, H.E. Basement Membrane Proteins in Multiple Sclerosis-Associated Inflammatory Cuffs: Potential Role in Influx and Transport of Leukocytes. *J Neuropathol Exp Neurol* **2005**, *64*, 722–729, doi:10.1097/01.jnen.0000173894.09553.13.
55. Reijerkerk, A.; Kooij, G.; van der Pol, S.M.A.; Khazen, S.; Dijkstra, C.D.; de Vries, H.E. Diapedesis of Monocytes Is Associated with MMP-Mediated Occludin Disappearance in Brain Endothelial Cells. *FASEB J* **2006**, *20*, 2550–2552, doi:10.1096/fj.06-6099fje.
56. Deli, M.A. Potential Use of Tight Junction Modulators to Reversibly Open Membranous Barriers and Improve Drug Delivery. *Biochim Biophys Acta* **2009**, *1788*, 892–910, doi:10.1016/j.bbamem.2008.09.016.
57. Crowe, T.P.; Greenlee, M.H.W.; Kanthasamy, A.G.; Hsu, W.H. Mechanism of Intranasal Drug Delivery Directly to the Brain. *Life Sci* **2018**, *195*, 44–52, doi:10.1016/j.lfs.2017.12.025.
58. Kapoor, M.; Cloyd, J.C.; Siegel, R.A. A Review of Intranasal Formulations for the Treatment of Seizure Emergencies. *J Control Release* **2016**, *237*, 147–159, doi:10.1016/j.jconrel.2016.07.001.
59. Illum, L. Transport of Drugs from the Nasal Cavity to the Central Nervous System. *Eur J Pharm Sci* **2000**, *11*, 1–18, doi:10.1016/s0928-0987(00)00087-7.
60. Gizurarson, S. Anatomical and Histological Factors Affecting Intranasal Drug and Vaccine Delivery. *Curr Drug Deliv* **2012**, *9*, 566–582, doi:10.2174/156720112803529828.
61. Keverne, E.B. The Vomeronasal Organ. *Science* **1999**, *286*, 716–720, doi:10.1126/science.286.5440.716.
62. Stoyanov, G.S.; Sapundzhiev, N.R.; Tonchev, A.B. The Vomeronasal Organ: History, Development, Morphology, and Functional Neuroanatomy. *Handb Clin Neurol* **2021**, *182*, 283–291, doi:10.1016/B978-0-12-819973-2.00020-4.
63. Monti-Bloch, L.; Jennings-White, C.; Berliner, D.L. The Human Vomeronasal System. A Review. *Ann N Y Acad Sci* **1998**, *855*, 373–389, doi:10.1111/j.1749-6632.1998.tb10595.x.
64. Bors, L.A. Investigation of the Effect of Intravenous and Intranasal P-Glycoprotein Modulation on the Blood-Brain Barrier in Young and Old Rats, PhD Thesis (in Hungarian).; Budapest, Hungary, 2020.
65. Gartziandia, O.; Egusquiaguirre, S.P.; Bianco, J.; Pedraz, J.L.; Igartua, M.; Hernandez, R.M.; Préat, V.; Beloqui, A. Nanoparticle Transport across in Vitro Olfactory Cell Monolayers. *Int J Pharm* **2016**, *499*, 81–89, doi:10.1016/j.ijpharm.2015.12.046.

66. Arora, P.; Sharma, S.; Garg, S. Permeability Issues in Nasal Drug Delivery. *Drug Discov Today* **2002**, *7*, 967–975, doi:10.1016/s1359-6446(02)02452-2.
67. Bjelik, A.; Bereczki, E.; Gonda, S.; Juhász, A.; Rimanóczy, A.; Zana, M.; Csont, T.; Pákáski, M.; Boda, K.; Ferdinandy, P.; et al. Human ApoB Overexpression and a High-Cholesterol Diet Differently Modify the Brain APP Metabolism in the Transgenic Mouse Model of Atherosclerosis. *Neurochem Int* **2006**, *49*, 393–400, doi:10.1016/j.neuint.2006.01.026.
68. Varga-Medveczky, Z.; Kovács, N.; Tóth, M.E.; Sántha, M.; Horváth, I.; Bors, L.A.; Fónagy, K.; Imre, T.; Szabó, P.; Máthé, D.; et al. Age-Related Inflammatory Balance Shift, Nasal Barrier Function, and Cerebro-Morphological Status in Healthy and Diseased Rodents. *Front Neurosci* **2021**, *15*, 700729, doi:10.3389/fnins.2021.700729.
69. Sziráki, I.; Erdo, F.; Beéry, E.; Molnár, P.M.; Fazakas, C.; Wilhelm, I.; Makai, I.; Kis, E.; Herédi-Szabó, K.; Abonyi, T.; et al. Quinidine as an ABCB1 Probe for Testing Drug Interactions at the Blood-Brain Barrier: An in Vitro in Vivo Correlation Study. *J Biomol Screen* **2011**, *16*, 886–894, doi:10.1177/1087057111414896.
70. Sziráki, I.; Erdő, F.; Trampus, P.; Sike, M.; Molnár, P.M.; Rajnai, Z.; Molnár, J.; Wilhelm, I.; Fazakas, C.; Kis, E.; et al. The Use of Microdialysis Techniques in Mice to Study P-Gp Function at the Blood-Brain Barrier. *J Biomol Screen* **2013**, *18*, 430–440, doi:10.1177/1087057112468156.
71. Asby, D.; Boche, D.; Allan, S.; Love, S.; Miners, J.S. Systemic Infection Exacerbates Cerebrovascular Dysfunction in Alzheimer's Disease. *Brain* **2021**, *144*, 1869–1883, doi:10.1093/brain/awab094.
72. Demirci, S.; Aynalı, A.; Demirci, K.; Demirci, S.; Arıdoğan, B.C. The Serum Levels of Resistin and Its Relationship with Other Proinflammatory Cytokines in Patients with Alzheimer's Disease. *Clin Psychopharmacol Neurosci* **2017**, *15*, 59–63, doi:10.9758/cpn.2017.15.1.59.
73. Lotfi, N.; Thome, R.; Rezaei, N.; Zhang, G.-X.; Rezaei, A.; Rostami, A.; Esmaeil, N. Roles of GM-CSF in the Pathogenesis of Autoimmune Diseases: An Update. *Front Immunol* **2019**, *10*, 1265, doi:10.3389/fimmu.2019.01265.
74. Süle, Z.; Mracskó, E.; Bereczki, E.; Sántha, M.; Csont, T.; Ferdinandy, P.; Bari, F.; Farkas, E. Capillary Injury in the Ischemic Brain of Hyperlipidemic, Apolipoprotein B-100 Transgenic Mice. *Life Sci* **2009**, *84*, 935–939, doi:10.1016/j.lfs.2009.04.011.
75. Lange, C.; Storkebaum, E.; de Almodóvar, C.R.; Dewerchin, M.; Carmeliet, P. Vascular Endothelial Growth Factor: A Neurovascular Target in Neurological Diseases. *Nat Rev Neurol* **2016**, *12*, 439–454, doi:10.1038/nrneurol.2016.88.
76. Randall, M.J.; Jüngel, A.; Rimann, M.; Wuertz-Kozak, K. Advances in the Biofabrication of 3D Skin in Vitro: Healthy and Pathological Models. *Front Bioeng Biotechnol* **2018**, *6*, 154, doi:10.3389/fbioe.2018.00154.
77. Baroni, A.; Buommino, E.; De Gregorio, V.; Ruocco, E.; Ruocco, V.; Wolf, R. Structure and Function of the Epidermis Related to Barrier Properties. *Clin Dermatol* **2012**, *30*, 257–262, doi:10.1016/j.clindermatol.2011.08.007.
78. Risueño, I.; Valencia, L.; Jorcano, J.L.; Velasco, D. Skin-on-a-Chip Models: General Overview and Future Perspectives. *APL Bioeng* **2021**, *5*, 030901, doi:10.1063/5.0046376.
79. Prausnitz, M.R.; Langer, R. Transdermal Drug Delivery. *Nat Biotechnol* **2008**, *26*, 1261–1268, doi:10.1038/nbt.1504.
80. Shaker, D.S.; Ishak, R.A.H.; Ghoneim, A.; Elhuoni, M.A. Nanoemulsion: A Review on Mechanisms for the Transdermal Delivery of Hydrophobic and Hydrophilic Drugs. *Scientia Pharmaceutica* **2019**, *87*, 17, doi:10.3390/scipharm87030017.
81. Moon, S.; Kim, D.H.; Shin, J.U. In Vitro Models Mimicking Immune Response in the Skin. *Yonsei Med J* **2021**, *62*, 969–980, doi:10.3349/ymj.2021.62.11.969.

82. *Directive 2003/15/EC of the European Parliament and of the Council of 27 February 2003 Amending Council Directive 76/768/EEC on the Approximation of the Laws of the Member States Relating to Cosmetic Products (Text with EEA Relevance)*; 2003; Vol. 066;
83. Abaci, H.E.; Guo, Z.; Doucet, Y.; Jacków, J.; Christiano, A. Next Generation Human Skin Constructs as Advanced Tools for Drug Development. *Exp Biol Med (Maywood)* **2017**, *242*, 1657–1668, doi:10.1177/1535370217712690.
84. Parisi, R.; Symmons, D.P.M.; Griffiths, C.E.M.; Ashcroft, D.M.; Identification and Management of Psoriasis and Associated ComorbidiTy (IMPACT) project team Global Epidemiology of Psoriasis: A Systematic Review of Incidence and Prevalence. *J Invest Dermatol* **2013**, *133*, 377–385, doi:10.1038/jid.2012.339.
85. Horváth, S. Methodological Refinement of the Psoriasis Animal Model and the Role of Transient Receptor Potential (TRP) Ion Channels in Psoriasiform Dermatitis, PhD Thesis (in Hungarian).; Pécs, Hungary, 2020.
86. Rendon, A.; Schäkel, K. Psoriasis Pathogenesis and Treatment. *Int J Mol Sci* **2019**, *20*, E1475, doi:10.3390/ijms20061475.
87. Gudjonsson, J.E.; Elder, J.T. Chapter 18. Psoriasis. In *Fitzpatrick's Dermatology in General Medicine*; Goldsmith, L.A., Katz, S.I., Gilchrest, B.A., Paller, A.S., Leffell, D.J., Wolff, K., Eds.; The McGraw-Hill Companies: New York, NY, 2012.
88. Griffiths, C.E.M.; van der Walt, J.M.; Ashcroft, D.M.; Flohr, C.; Naldi, L.; Nijsten, T.; Augustin, M. The Global State of Psoriasis Disease Epidemiology: A Workshop Report. *Br J Dermatol* **2017**, *177*, e4–e7, doi:10.1111/bjd.15610.
89. Harden, J.L.; Krueger, J.G.; Bowcock, A.M. The Immunogenetics of Psoriasis: A Comprehensive Review. *J Autoimmun* **2015**, *64*, 66–73, doi:10.1016/j.jaut.2015.07.008.
90. Di Meglio, P.; Villanova, F.; Nestle, F.O. Psoriasis. *Cold Spring Harb Perspect Med* **2014**, *4*, a015354, doi:10.1101/cshperspect.a015354.
91. Morizane, S.; Gallo, R.L. Antimicrobial Peptides in the Pathogenesis of Psoriasis. *J Dermatol* **2012**, *39*, 225–230, doi:10.1111/j.1346-8138.2011.01483.x.
92. Morizane, S.; Yamasaki, K.; Mühleisen, B.; Kotol, P.F.; Murakami, M.; Aoyama, Y.; Iwatsuki, K.; Hata, T.; Gallo, R.L. Cathelicidin Antimicrobial Peptide LL-37 in Psoriasis Enables Keratinocyte Reactivity against TLR9 Ligands. *J Invest Dermatol* **2012**, *132*, 135–143, doi:10.1038/jid.2011.259.
93. Harden, J.L.; Johnson-Huang, L.M.; Chamian, M.F.; Lee, E.; Pearce, T.; Leonardi, C.L.; Haider, A.; Lowes, M.A.; Krueger, J.G. Humanized Anti-IFN-γ (HuZAF) in the Treatment of Psoriasis. *J Allergy Clin Immunol* **2015**, *135*, 553–556, doi:10.1016/j.jaci.2014.05.046.
94. Lowe, N.J.; Breeding, J.; Kean, C.; Cohn, M.L. Psoriasiform Dermatosis in a Rhesus Monkey. *J Invest Dermatol* **1981**, *76*, 141–143, doi:10.1111/1523-1747.ep12525484.
95. Zanolli, M.D.; Jayo, M.J.; Jayo, J.M.; Blaine, D.; Hall, J.; Jorizzo, J.L. Evaluation of Psoriatic Plaques That Spontaneously Developed in a Cynomolgus Monkey (Macaca Fascicularis). *Acta Derm Venereol Suppl (Stockh)* **1989**, *146*, 58.
96. Jayo, M.J.; Zanolli, M.D.; Jayo, J.M. Psoriatic Plaques in Macaca Fascicularis. *Vet Pathol* **1988**, *25*, 282–285, doi:10.1177/030098588802500406.
97. Gudjonsson, J.E.; Johnston, A.; Dyson, M.; Valdimarsson, H.; Elder, J.T. Mouse Models of Psoriasis. *J Invest Dermatol* **2007**, *127*, 1292–1308, doi:10.1038/sj.jid.5700807.
98. Horváth S.; Gyulai R. Animal models of psoriasis. *BVSZ* **2018**, *94*, 168–171, doi:10.7188/bvsz.2018.94.4.1.
99. Nestle, F.; Nickoloff, B. Animal Models of Psoriasis: A Brief Update. *Journal of the European Academy of Dermatology and Venereology* **2006**, *20*, 24–27, doi:10.1111/j.1468-3083.2006.01769.x.
100. van der Fits, L.; Mourits, S.; Voerman, J.S.A.; Kant, M.; Boon, L.; Laman, J.D.; Cornelissen, F.; Mus, A.-M.; Florencia, E.; Prens, E.P.; et al. Imiquimod-Induced Psoriasis-

like Skin Inflammation in Mice Is Mediated via the IL-23/IL-17 Axis. *J Immunol* **2009**, *182*, 5836–5845, doi:10.4049/jimmunol.0802999.
101. Schön, M.P. Animal Models of Psoriasis - What Can We Learn from Them? *J Invest Dermatol* **1999**, *112*, 405–410, doi:10.1046/j.1523-1747.1999.00538.x.
102. Flutter, B.; Nestle, F.O. TLRs to Cytokines: Mechanistic Insights from the Imiquimod Mouse Model of Psoriasis. *Eur J Immunol* **2013**, *43*, 3138–3146, doi:10.1002/eji.201343801.
103. Walter, A.; Schäfer, M.; Cecconi, V.; Matter, C.; Urosevic-Maiwald, M.; Belloni, B.; Schönewolf, N.; Dummer, R.; Bloch, W.; Werner, S.; et al. Aldara Activates TLR7-Independent Immune Defence. *Nat Commun* **2013**, *4*, 1560, doi:10.1038/ncomms2566.
104. Grine, L.; Dejager, L.; Libert, C.; Vandenbroucke, R.E. Dual Inhibition of TNFR1 and IFNAR1 in Imiquimod-Induced Psoriasiform Skin Inflammation in Mice. *J Immunol* **2015**, *194*, 5094–5102, doi:10.4049/jimmunol.1403015.
105. Gilliet, M.; Conrad, C.; Geiges, M.; Cozzio, A.; Thürlimann, W.; Burg, G.; Nestle, F.O.; Dummer, R. Psoriasis Triggered by Toll-like Receptor 7 Agonist Imiquimod in the Presence of Dermal Plasmacytoid Dendritic Cell Precursors. *Arch Dermatol* **2004**, *140*, 1490–1495, doi:10.1001/archderm.140.12.1490.
106. Fanti, P.A.; Dika, E.; Vaccari, S.; Miscial, C.; Varotti, C. Generalized Psoriasis Induced by Topical Treatment of Actinic Keratosis with Imiquimod. *Int J Dermatol* **2006**, *45*, 1464–1465, doi:10.1111/j.1365-4632.2006.02980.x.
107. Horváth, S.; Komlódi, R.; Perkecz, A.; Pintér, E.; Gyulai, R.; Kemény, Á. Methodological Refinement of Aldara-Induced Psoriasiform Dermatitis Model in Mice. *Sci Rep* **2019**, *9*, 3685, doi:10.1038/s41598-019-39903-x.
108. Swindell, W.R.; Michaels, K.A.; Sutter, A.J.; Diaconu, D.; Fritz, Y.; Xing, X.; Sarkar, M.K.; Liang, Y.; Tsoi, A.; Gudjonsson, J.E.; et al. Imiquimod Has Strain-Dependent Effects in Mice and Does Not Uniquely Model Human Psoriasis. *Genome Med* **2017**, *9*, 24, doi:10.1186/s13073-017-0415-3.
109. Kong, B.Y.; Haugh, I.M.; Schlosser, B.J.; Getsios, S.; Paller, A.S. Mind the Gap: Sex Bias in Basic Skin Research. *J Invest Dermatol* **2016**, *136*, 12–14, doi:10.1038/JID.2015.298.
110. Grine, L.; Steeland, S.; Van Ryckeghem, S.; Ballegeer, M.; Lienenklaus, S.; Weiss, S.; Sanders, N.N.; Vandenbroucke, R.E.; Libert, C. Topical Imiquimod Yields Systemic Effects Due to Unintended Oral Uptake. *Sci Rep* **2016**, *6*, 20134, doi:10.1038/srep20134.
111. Horváth, S.; Kemény, Á.; Pintér, E.; Gyulai, R. A Localized Aldara (5% Imiquimod)-Induced Psoriasiform Dermatitis Model in Mice Using Finn Chambers. *Curr Protoc Pharmacol* **2020**, *90*, e78, doi:10.1002/cpph.78.
112. Yoshiki, R.; Kabashima, K.; Honda, T.; Nakamizo, S.; Sawada, Y.; Sugita, K.; Yoshioka, H.; Ohmori, S.; Malissen, B.; Tokura, Y.; et al. IL-23 from Langerhans Cells Is Required for the Development of Imiquimod-Induced Psoriasis-like Dermatitis by Induction of IL-17A-Producing Γδ T Cells. *J Invest Dermatol* **2014**, *134*, 1912–1921, doi:10.1038/jid.2014.98.
113. Alvarez, P.; Jensen, L.E. Imiquimod Treatment Causes Systemic Disease in Mice Resembling Generalized Pustular Psoriasis in an IL-1 and IL-36 Dependent Manner. *Mediators Inflamm* **2016**, *2016*, 6756138, doi:10.1155/2016/6756138.
114. Clapham, D.E.; Julius, D.; Montell, C.; Schultz, G. International Union of Pharmacology. XLIX. Nomenclature and Structure-Function Relationships of Transient Receptor Potential Channels. *Pharmacol Rev* **2005**, *57*, 427–450, doi:10.1124/pr.57.4.6.
115. Caterina, M.J.; Pang, Z. TRP Channels in Skin Biology and Pathophysiology. *Pharmaceuticals (Basel)* **2016**, *9*, E77, doi:10.3390/ph9040077.

116. Caterina, M.J.; Julius, D. The Vanilloid Receptor: A Molecular Gateway to the Pain Pathway. *Annu Rev Neurosci* **2001**, *24*, 487–517, doi:10.1146/annurev.neuro.24.1.487.
117. Gunthorpe, M.J.; Chizh, B.A. Clinical Development of TRPV1 Antagonists: Targeting a Pivotal Point in the Pain Pathway. *Drug Discov Today* **2009**, *14*, 56–67, doi:10.1016/j.drudis.2008.11.005.
118. Lumpkin, E.A.; Caterina, M.J. Mechanisms of Sensory Transduction in the Skin. *Nature* **2007**, *445*, 858–865, doi:10.1038/nature05662.
119. Caterina, M.J. TRP Channel Cannabinoid Receptors in Skin Sensation, Homeostasis, and Inflammation. *ACS Chem Neurosci* **2014**, *5*, 1107–1116, doi:10.1021/cn5000919.
120. Nilius, B.; Owsianik, G. Transient Receptor Potential Channelopathies. *Pflugers Arch* **2010**, *460*, 437–450, doi:10.1007/s00424-010-0788-2.
121. Ho, J.-C.; Lee, C.-H. TRP Channels in Skin: From Physiological Implications to Clinical Significances. *Biophysics (Nagoya-shi)* **2015**, *11*, 17–24, doi:10.2142/biophysics.11.17.
122. Zhou, Y.; Han, D.; Follansbee, T.; Wu, X.; Yu, S.; Wang, B.; Shi, Z.; Domocos, D.T.; Carstens, M.; Carstens, E.; et al. Transient Receptor Potential Ankyrin 1 (TRPA1) Positively Regulates Imiquimod-Induced, Psoriasiform Dermal Inflammation in Mice. *J Cell Mol Med* **2019**, *23*, 4819–4828, doi:10.1111/jcmm.14392.
123. Akopian, A.N. Regulation of Nociceptive Transmission at the Periphery via TRPA1-TRPV1 Interactions. *Curr Pharm Biotechnol* **2011**, *12*, 89–94, doi:10.2174/138920111793937952.
124. Oh, M.-H.; Oh, S.Y.; Lu, J.; Lou, H.; Myers, A.C.; Zhu, Z.; Zheng, T. TRPA1-Dependent Pruritus in IL-13-Induced Chronic Atopic Dermatitis. *J Immunol* **2013**, *191*, 5371–5382, doi:10.4049/jimmunol.1300300.
125. Nattkemper, L.A.; Tey, H.L.; Valdes-Rodriguez, R.; Lee, H.; Mollanazar, N.K.; Albornoz, C.; Sanders, K.M.; Yosipovitch, G. The Genetics of Chronic Itch: Gene Expression in the Skin of Patients with Atopic Dermatitis and Psoriasis with Severe Itch. *J Invest Dermatol* **2018**, *138*, 1311–1317, doi:10.1016/j.jid.2017.12.029.
126. Fernandes, E.S.; Vong, C.T.; Quek, S.; Cheong, J.; Awal, S.; Gentry, C.; Aubdool, A.A.; Liang, L.; Bodkin, J.V.; Bevan, S.; et al. Superoxide Generation and Leukocyte Accumulation: Key Elements in the Mediation of Leukotriene B_4-Induced Itch by Transient Receptor Potential Ankyrin 1 and Transient Receptor Potential Vanilloid 1. *FASEB J* **2013**, *27*, 1664–1673, doi:10.1096/fj.12-221218.
127. Liu, B.; Escalera, J.; Balakrishna, S.; Fan, L.; Caceres, A.I.; Robinson, E.; Sui, A.; McKay, M.C.; McAlexander, M.A.; Herrick, C.A.; et al. TRPA1 Controls Inflammation and Pruritogen Responses in Allergic Contact Dermatitis. *FASEB J* **2013**, *27*, 3549–3563, doi:10.1096/fj.13-229948.
128. Van der Schueren, L.; De Schoenmaker, B.; Kalaoglu Altan, Ö.İ.; De Clerck, K. An Alternative Solvent System for the Steady State Electrospinning of Polycaprolactone. *EUROPEAN POLYMER JOURNAL* **2011**, *47*, 1256–1263, doi:10.1016/j.eurpolymj.2011.02.025.
129. Tárnoki-Zách, J.; Mehes, E.; Varga-Medveczky, Z.; Isai, D.G.; Barany, N.; Bugyik, E.; Revesz, Z.; Paku, S.; Erdo, F.; Czirok, A. Development and Evaluation of a Human Skin Equivalent in a Semiautomatic Microfluidic Diffusion Chamber. *Pharmaceutics* **2021**, *13*, 910, doi:10.3390/pharmaceutics13060910.
130. Lukács, B.; Bajza, Á.; Kocsis, D.; Csorba, A.; Antal, I.; Iván, K.; Laki, A.J.; Erdő, F. Skin-on-a-Chip Device for Ex Vivo Monitoring of Transdermal Delivery of Drugs-Design, Fabrication, and Testing. *Pharmaceutics* **2019**, *11*, E445, doi:10.3390/pharmaceutics11090445.

131. Varga-Medveczky, Z.; Kocsis, D.; Naszlady, M.B.; Fónagy, K.; Erdő, F. Skin-on-a-Chip Technology for Testing Transdermal Drug Delivery—Starting Points and Recent Developments. *Pharmaceutics* **2021**, *13*, 1852, doi:10.3390/pharmaceutics13111852.
132. Bajza, Á.; Kocsis, D.; Berezvai, O.; Laki, A.J.; Lukács, B.; Imre, T.; Iván, K.; Szabó, P.; Erdő, F. Verification of P-Glycoprotein Function at the Dermal Barrier in Diffusion Cells and Dynamic "Skin-On-A-Chip" Microfluidic Device. *Pharmaceutics* **2020**, *12*, 804, doi:10.3390/pharmaceutics12090804.